

On the Ytterbium Valence and the Physical Properties in Selected Intermetallic Phases

Stefan Engel,[§] Elias C. J. Giebelmann,[§] Maximilian K. Reimann,[§] Rainer Pöttgen,* and Oliver Janka*Cite This: *ACS Org. Inorg. Au* 2024, 4, 188–222

Read Online

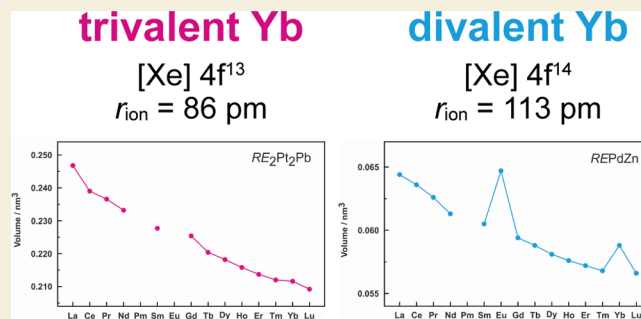
ACCESS |

Metrics & More

Article Recommendations

ABSTRACT: The present review summarizes important aspects of the crystal chemistry of ytterbium-based intermetallic compounds along with a selection of their outstanding physical properties. These originate in many cases from the ytterbium valence. Different valence states are possible here, divalent ($4f^{14}$), intermediate-valent, or trivalent ($4f^{13}$) ytterbium, resulting in simple diamagnetic, Pauli or Curie–Weiss paramagnetic, or valence fluctuating behavior. Especially, some of the Yb^{3+} intermetallics have gained deep interest due to their Kondo or heavy Fermion ground states. We have summarized their property investigations using magnetic and transport measurements, specific heat data, NMR, ESR, and Mössbauer spectroscopy, elastic and inelastic neutron scattering, and XAS data as well as detailed thermoelectric measurements.

KEYWORDS: ytterbium, intermediate valence, Kondo effect, heavy Fermion, ^{170}Yb Mössbauer spectroscopy, ^{171}Yb NMR, ESR, XAS, XPS, valence fluctuations



Ytterbium is one of the few rare earth elements that is prone to valence instabilities in intermetallic compounds. In the rare earth series, many examples are known for cerium, where the interplay between the $4f^1$ configuration for Ce^{3+} and the empty f shell for tetravalent cerium led to a huge number of compounds with broadly varying magnetic and electrical properties, such as long-range magnetic ordering (antiferro-, ferro-, or ferrimagnetism), Kondo-type behavior, heavy Fermion behavior as well as static or dynamic intermediate cerium valence. These many facets of structure–property relationships of cerium intermetallics have been summarized in review articles.^{1–6} While only a few examples are known for divalent samarium (the trivalent state is usually observed),⁷ many europium compounds have been studied with respect to their valence behavior.^{8–10} Most of these compounds exhibit the stable half-filled f shell ($4f^7$ configuration), and consequently, divalent europium is the usual case for intermetallics along with paramagnetism and long-range magnetic ordering, sometimes at comparatively high ordering temperatures. The scarce case of trivalent europium in intermetallic phases has recently been reviewed.¹⁰

The present review focuses on intermetallic ytterbium compounds. Here, the configurations $4f^{14}$ (filled f shell; divalent ytterbium; diamagnetic) and $4f^{13}$ (paramagnetic trivalent ytterbium) are the edge states, and static and dynamic ytterbium valence states are observed in-between. Especially, the trivalent ytterbium compounds have attracted high attention in solid-state chemistry and physics, since the $4f^{13}$

configuration is the $4f$ hole analogue to Ce^{3+} . Thus, the ground state properties of these ytterbium-based phases are highly sensitive to the amount of $4f$ electron (hole)–conduction electron hybridization (Kondo effect).^{11–14} This influences the Ruderman–Kittel–Kasuya–Yosida (RKKY) exchange interactions and consequently the magnetic ordering. The broad analogy to cerium intermetallics is especially interesting with respect to intermediate-valence and potential heavy Fermion materials.^{15–17}

Materials science can only work with an excellent interplay of solid-state physics and solid-state chemistry, whereby detailed phase analyses and high-quality sample preparation along with precise structure determination are the indispensable prerequisites for reliable property measurements. Herein we review these features for the field of intermetallic ytterbium compounds with a strong emphasis on the ytterbium valence behavior.

The review is written from a solid-state chemist's point of view. Bearing the enormous number of compounds¹⁸ and property measurements in mind, it is simply not possible to

Received: October 13, 2023

Revised: November 16, 2023

Accepted: November 17, 2023

Published: January 4, 2024



include all known intermetallic ytterbium compounds and all references into such an overview (e.g., > 350 references for YbRh_2Si_2 in SciFinder¹⁹). Herein we mainly concentrate on the role of the ytterbium valence in intermetallics and underpin these peculiarities with selected examples. Any missing compound or reference is unintentional.

SYNTHESES AND CRYSTAL GROWTH

The peculiar electronic structure of ytterbium has drastic effects on its physical properties, when compared with the neighboring rare earth elements. Its divalent nature already in the elemental state leads to drastically reduced melting (1097 K) and boiling (1466 K) points.²⁰ Arc-melting is a broadly used synthesis technique for intermetallic samples,²¹ however, drastic evaporation losses can occur in the cases of ytterbium-based synthesis, when reacting ytterbium with the high-melting noble metals, e.g., platinum (mp 2025 K) or iridium (mp 2683 K). To give an example, during an arc-melting synthesis of YbRh_2Si_2 ,²² the ytterbium would largely evaporate before the rhodium melts. Thus, only a few ytterbium intermetallics were prepared by arc melting. Representative examples are YbNiAl_4 ²³ or $\text{Yb}_3\text{Rh}_9\text{Si}_2\text{Sn}_3$.²⁴ For the precise reaction conditions, we refer to the individual publications. In the present chapter, we summarize the different techniques that find application.

Broader phase analytical studies were conducted by simple, direct reaction of the elements in sealed evacuated fused silica ampules. This is possible for almost all $\text{Yb}_x\text{T}_y\text{X}_z$ samples with X = elements of the group 13, 14, or 15. The inner surface of the silica ampules can be graphitized (thermal decomposition of acetone) for passivation, or alumina crucibles can be used as inert container material. The reactions and annealing sequences are usually carried out in tube or muffle furnaces. These reactions are not that far from the classical ceramic method²⁵ for the preparation of solids. Often the samples are still multiphase after the first annealing cycle. Thus, repeated grinding, pressing of pellets, and reannealing is necessary in order to obtain samples that are at least phase-pure on the level of powder X-ray diffraction. A critical feature is the repeated grinding, since the increasing surface area might lead to surface oxidation and thus Yb_2O_3 contamination (vide infra). This ceramic technique was frequently used for the synthesis of ytterbium-based ternary phosphides and arsenides.²⁶ The best way to avoid these Yb_2O_3 contaminations is the use of distilled ytterbium and working under purified inert gas.

For physical property measurements, high sample purity is required. Nowadays, the intermetallic ytterbium phases are prepared in sealed (arc-welded²⁷ under argon or helium atmosphere) high-melting metal tubes, usually niobium or tantalum, but molybdenum can also find application. This ensures largely inert crucible conditions and prevents evaporation losses of ytterbium. For the reaction, the metal tubes can be sealed in silica tubes (oxidation protection), and the annealing sequence can be run in a tube or muffle furnace. Much better results are obtained through induction melting and subsequent annealing.^{28,29} Good quantities of X-ray pure polycrystalline samples are available by this technique.

Direction-dependent property measurements can only be performed on high-quality single crystals. This deserves sophisticated crystal growth conditions. The flux growth technique^{30–33} is meanwhile well established in the field of crystal growth of intermetallic phases. Usually the low-melting p block elements aluminum, gallium, indium, tin, and bismuth

find application as flux medium. Two strategies for crystal growth are possible. The easy way is the self-flux technique (the so-called reactive flux), where the low-melting p element is a component of the product and flux medium at the same time. Otherwise, one can use an inert flux (the so-called nonreactive flux), which does not enter the product crystals. There are some prerequisites for targeted crystal growth: (i) the flux medium should be inert toward the crucible material and (ii) the excess flux should easily be separable from the product crystals.

Typical examples for flux-grown crystals are YbRh_2Si_2 and YbIr_2Si_2 ,³⁴ or Yb_2CuGe_6 and $\text{Yb}_3\text{Cu}_4\text{Ge}_4$,³⁵ which form in liquid indium. Also, Yb_2AuGe_3 crystals can be grown from liquid indium with up to 2 mm edge size.³⁶ The excess flux can be dissolved in diluted hydrochloric acid. Similar flux growth experiments are feasible with aluminum and gallium as the flux medium.³⁷ A interesting example for a nonreactive flux is the growth of YbRh_6P_4 crystals in liquid bismuth.³⁸ Besides dissolution of the flux after successful crystal growth, the liquid flux can also be separated by centrifugation at elevated temperatures. Here are two possible ways: (i) a second crucible filled with quartz wool or a quartz wool plug can be placed (reversed) on top of the one containing the starting materials³⁰ or (ii) a frit-disc crucible set (“Canfield crucible set”) can be utilized.³⁹

Finally, we turn back to the classical textbook examples for crystal growth. Due to the high vapor pressure of molten ytterbium, the Czochralski technique cannot be used. The Bridgman technique (where again sealed tubes are used) was successfully applied for crystal growth of the copper-rich ytterbium compounds $\text{YbCu}_{4.25}$ and $\text{YbCu}_{4.4}$.⁴⁰ Tantalum was used as container materials, and the crucible lowering speed at the high-frequency coil was 3 mm h^{-1} . Crystals for diffraction experiments were finally separated from different slices that were prepared from the bulk crystal via spark erosion. Further examples for the Bridgman crystal growth are the germanides $\text{Yb}_2\text{Ru}_3\text{Ge}_4$,⁴¹ YbPdGe , and YbPtGe .⁴²

CRYSTAL CHEMICAL PRINCIPLES

The present review has a higher focus on the physical properties of ytterbium intermetallics, and we therefore only give a short and concise overview on some of the basic crystal chemical principles that are important for the family of $\text{Yb}_x\text{T}_y\text{X}_z$ intermetallics. The structural chemistry is mostly driven by the ytterbium valence. As discussed above, the filled 4f shell of Yb(II) might be considered as a diamagnetic core–electron shell, and consequently, we observe a crystal chemical behavior of an alkaline earth element. This is readily understandable when comparing the ionic radii for coordination number 6 for Ca^{2+} (100 pm) and Yb^{2+} (102 pm).⁴³ We thus observe a close structural relationship of the divalent ytterbium intermetallics with their respective calcium analogues. Typical examples are the binary Zintl phases Ca_2Ge ⁴⁴ and Yb_2Ge ⁴⁵ as well as the ternary Zintl phases CaZnSn ⁴⁶ and YbZnSn ⁴⁷ with many more pairs of isotypic compounds than for $\text{Yb}^{2+}/\text{Ca}^{2+}$.⁴⁸

A similar close relationship is known for Eu^{2+} (117 pm) and Sr^{2+} (118 pm).⁴³ Some examples are EuAl_2Pt and SrAl_2Pt (MgCuAl_2 type, space group $Cmcm$),⁴⁹ EuAl_3Pt_3 ⁵⁰ and SrAl_3Pt_3 ⁵¹ (YNi_5Si_3 type, space group $Pnma$), SrAu_3Al_2 ⁵² and EuAu_3Al_2 ⁵³ (RbAu_3Ga_2 type, space group $Pnma$), EuAu_2Al_2 ⁵⁴ and SrAu_2Al_2 ^{54,55} (CaBe_2Ge_2 type, space group $P4/nmm$), $\text{Eu}_2\text{T}_2\text{In}$ ⁵⁶ and $\text{Sr}_2\text{T}_2\text{In}$ ⁵⁷ ($T = \text{Pd}, \text{Pt}; \text{Ca}_2\text{Ir}_2\text{Si}$ type, space

group $C2/c$), EuRh_2In_8 ⁵⁸ and SrRh_2In_8 ⁵⁹ (CeFe_2Al_8 type, space group $Pbam$), EuPtSi and SrPtSi (LaIrSi type, space group $Pnma$),⁶⁰ or finally EuPt_2Si_2 and SrPt_2Si_2 (ThCr_2Si_2 type, space group $I4/mmm$).⁶¹ Besides the direct comparisons $\text{Sr}^{2+}/\text{Eu}^{2+}$ and $\text{Ca}^{2+}/\text{Yb}^{2+}$, it is not always possible to directly compare an $\text{Eu}(\text{II})$ example and an $\text{Yb}(\text{II})$ example within one series of compounds, since (i) the structure type is not formed with both cations or (ii) the given ytterbium is trivalent. And even if both compounds are known and adopt the same structure type, the physical properties are significantly different due to $\text{Yb}(\text{II})$ being a diamagnetic cation while $\text{Eu}(\text{II})$ exhibits a half-filled 4f shell ($4f^7$).

In the case of trivalent ytterbium intermetallics, the ytterbium compound usually adopts the crystal structure of the neighboring compounds existing with thulium or lutetium. A first fast hint for the ytterbium valence can be gathered from the plot of the unit cell volumes of a given series of rare earth compounds, a so-called Iandelli plot. As examples, we present the series of REPdZn ^{62–64} and $\text{RE}_2\text{Pt}_2\text{Pb}$ ^{47,65} phases in Figure 1. Since divalent ytterbium has a distinctly larger radius than

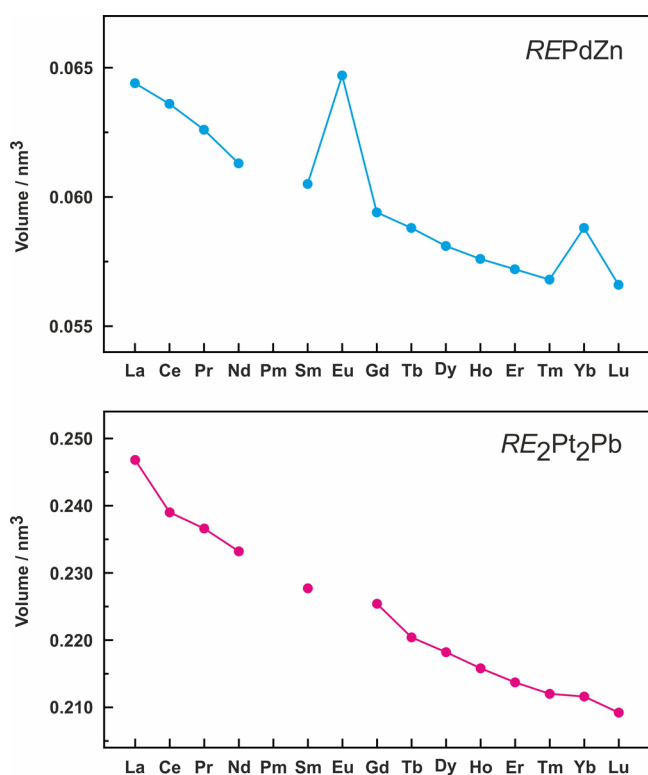


Figure 1. Plot of the unit cell volumes for the series REPdZn (per formula unit) and $\text{RE}_2\text{Pt}_2\text{Pb}$ (subcell volumes). Data was taken from the Pearson database.¹⁸

trivalent ytterbium, positive deviations in the Iandelli plot (this is the case for the REPdZn series) indicate divalent ytterbium. If the unit cell volume fits smoothly into the plot, then ytterbium is trivalent (this is the case for the $\text{RE}_2\text{Pt}_2\text{Pb}$ series). Nevertheless, one important observation needs to be mentioned at this point. Although the physical property measurements (vide infra) show stable trivalent ytterbium in $\text{Yb}_2\text{Pt}_2\text{Pb}$, the Iandelli plot shows a very small positive deviation. Such an anomaly is frequently observed for rare earth series with trivalent ytterbium. Another striking series with such a weak positive deviation is the one of REAL_3C_3 .⁶⁶

Many more examples for both cases can be found when checking structural databases like the Pearson database.¹⁸

Compounds that exhibit temperature- or pressure-dependent valence phase transitions show a discontinuity in their lattice parameters. YbPd_2Al_3 (YNi_2Al_3 type, space group $P6/mmm$), for example, exhibits a mixed valent state (Yb^{II} and Yb^{III}) at room temperature which transitions into an almost fully divalent state below $T_{\text{trans}} = 110$ K. The temperature dependence of the lattice parameters is shown in Figure 2. Here, a clear increase of the c lattice parameter is

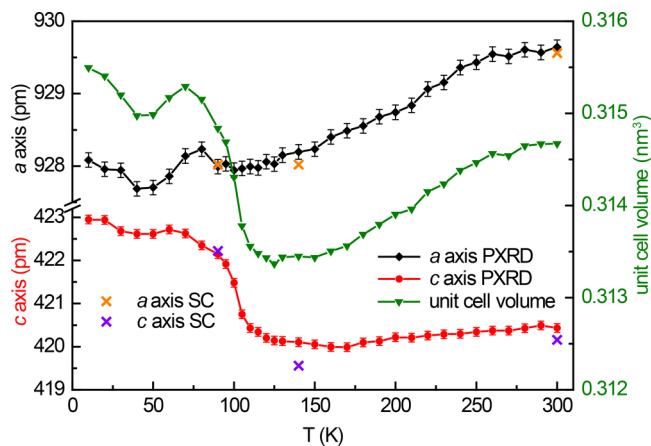


Figure 2. Lattice parameters of YbPd_2Al_3 obtained from temperature-dependent powder X-ray diffraction experiments upon cooling from 300 to 10 K and from single-crystal X-ray diffraction experiments. Reprinted with permission from ref 67.

visible (+3 pm, 0.7%). Due to the relatively high transition temperature, single crystal studies were possible, that confirmed the thermal behavior of the lattice parameters and clearly indicated that no structural phase transition takes place. However, significant distortions in the respective Yb coordination polyhedra are observed.⁶⁷

Finally, a very recent study of $\text{Yb}_2\text{Pd}_2\text{Cd}$ should be mentioned. Here, a structural phase transition at ~ 150 K was observed. The high-temperature modification adopts the $\text{Mo}_2\text{B}_2\text{Fe}$ type (space group $P4/mbm$) while below the phase transition temperature, LT- $\text{Yb}_2\text{Pd}_2\text{Cd}$ is found in a new structure type (space group $P4/mbm$) with a doubled c axis. The striking structural feature concerns the ytterbium–palladium coordination. The average Yb–Pd distances distort, forming a smaller and a larger coordination environment and enabling a charge separation for Yb^{2+} and Yb^{3+} .⁶⁸

SELECTED CRYSTAL STRUCTURES

In the present chapter, we want to selectively focus on some structural principles and refer to extended crystal chemical review articles for further reading. Some of the $\text{Yb}_x\text{T}_y\text{X}_z$ phases crystallize with their individual structure type which have all been thoroughly described in the original articles.

Many of the intermetallic ytterbium compounds belong to the so-called equiatomic phases YbTX (T = (transition) metal; X = element of group 13, 14, or 15). The most frequent structure types that occur for these phases are TiNiSi (space group $Pnma$), ZrNiAl (space group $P62m$), MgAgAs (space group $F43m$), PbFCl (space group $P4/nmm$), and other AlB_2 (space group $P6/mmm$) derived superstructures. Their crystal chemistry has been reviewed in the *Handbook on the Physics*

and Chemistry of Rare Earths.¹³ These structure types allow for a certain structural flexibility. To give an example, for the orthorhombic TiNiSi type, a manifold of ytterbium-based phases YbTX ($T = \text{Mg, Ni, Cu, Rh, Pd, Pt, Au}$; $X = \text{Al, Si, P, Ga, Ge, Sn, Sb}$) have been synthesized.^{13,18} Apart from the overview on the equiatomic YbTX phases, the crystal chemistry of these versatile structure types has repeatedly been discussed in various other review articles.^{3–6,8,69–72} We refer to these overviews for further reading.

A huge number of property studies has been conducted for the binary aluminides YbAl₂ (MgCu₂ type, cubic Laves phase, space group $Fd\bar{3}m$)⁷³ and YbAl₃ (Cu₃Au type; ordered cubic closest packing, space group $Pm\bar{3}m$).^{74,75} Both compounds crystallize with well-known basic structure types. In this context it is interesting to note that ternary ones have also been reported with the structure types of the cubic and hexagonal Laves phases. In the case of the MgCu₂ type phases, especially the solid solution members Yb_{1-x}In_xCu₂ have been studied, where the ytterbium substructure has been magnetically diluted through indium substitution. YbCu₄In⁷⁶ shows 1:1 Yb/In ordering and crystallizes with the noncentrosymmetric MgCu₄Sn type (space group $F43m$). The crystal chemical details of Laves phase superstructures have recently been reviewed.⁷⁷ Several aluminides were reported as equiatomic compounds, and the MgZn₂ type (space group $P6_3/mmc$) was assigned.¹³ Meanwhile, it is known that an equiatomic composition with complete atom ordering is not possible. The superstructure formation leads to a small deviation. The correct model was solved for Yb₆Ir₅Ga₇ (space group $P6_3/mcm$) and the series of gallides RE₆Ir₅Ga₇.^{78,79} Shortly later, also the aluminum containing RE₆T₅Al₇ phases ($RE = \text{Sc, Y, Ce–Nd, Sm, Gd–Lu}$; $T = \text{Ru, Ir}$)⁸⁰ have been structurally characterized. With respect to the physical properties, one must differentiate between the fully ordered 6–5–7 phases and solid solutions where mixed occupied sites occur. Often, disorder destroys magnetic ordering or drastically reduces the magnetic ordering temperature.

We now discuss the crystal chemistry of some selected examples. One of the striking ternary ytterbium intermetallics is YbRh₂Si₂ (ThCr₂Si₂ type, space group $I4/mmm$) originally reported in 1979 by Rossi et al.²² Due to its outstanding physical properties (vide infra), meanwhile >350 publications are listed in SciFinder.¹⁹ The YbRh₂Si₂ unit cell is presented in Figure 3. The rhodium atoms have a tetrahedral silicon coordination with Rh–Si distances of 235 pm. These [RhSi₄] tetrahedra are condensed via edge-sharing, building a dense layer in the ab plane. Adjacent layers are connected via Si–Si bonds (246 pm). The resulting network provides large cages for the ytterbium atoms which have a coordination number of 18, i.e., Yb@Si₁₀Rh₈. Due to the large cages, the shortest Yb–Yb distances are 401 pm, corresponding to the a lattice parameter. The ThCr₂Si₂ family of compounds is one of the largest among all intermetallic compounds with more than 4000 entries in the Pearson database.¹⁸ The crystal chemical details for these materials are summarized in diverse overviews.^{1,69,81,82}

Another, smaller series of tetragonal compounds concerns those with HoCoGa₅ type structure⁸⁴ (space group $P4/mmm$). This type has been observed for YbCoGa₅ and the indides YbTIn₅ ($T = \text{Co, Rh, Ir}$).^{83,85} The YbIrIn₅ unit cell⁸³ is also presented in Figure 3. The YbIrIn₅ structure is composed of two striking building units. The ytterbium atoms have slightly tetragonally distorted cuboctahedral indium coordination ($8 \times$

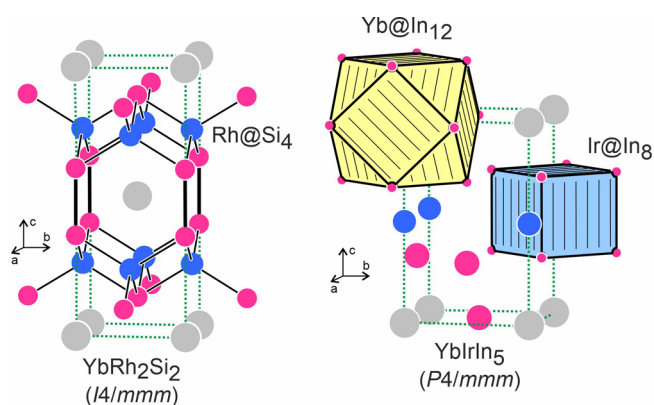


Figure 3. Crystal structures of YbRh₂Si₂²² and YbIrIn₅.⁸³ Ytterbium, rhodium (iridium), and silicon (indium) atoms are drawn as medium gray, blue, and magenta circles, respectively. The network of edge-sharing [RhSi₄] tetrahedra for YbRh₂Si₂ and the characteristic polyhedra for YbIrIn₅ are emphasized.

320 and 4×327 pm Yb–In), which can be considered as a cutout of an ordered closest fcc related packing (given the comparable size of ytterbium and indium). These cuboctahedra condense to layers via four common rectangular faces. These layers alternate with layers of condensed Ir@In₈ square prisms (275 pm Ir–In). Similar to YbRh₂Si₂ discussed above, the ytterbium atoms in YbIrIn₅ are also well separated from each other. The shortest Yb–Yb distance of 462 pm again corresponds to the lattice parameter a .

Yb₂Pt₂Pb⁴³ is one of the few ytterbium intermetallics that belong to the family of U₃Si₂ derived phases. Due to a puckering effect, one observes superstructure formation for Yb₂Pt₂Pb (space group $P4_2/mmm$) with a small distortion of the ytterbium trigonal and square prisms. For better visibility, only one layer is presented in Figure 4. A more detailed crystal

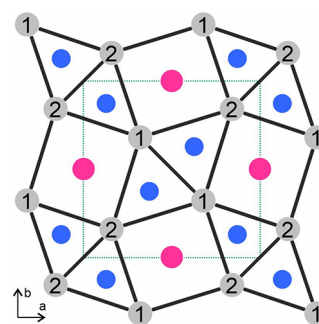


Figure 4. Cutout of the Yb₂Pt₂Pb⁴⁷ structure. Ytterbium, platinum, and lead atoms are drawn as medium gray, blue, and magenta circles, respectively. The CsCl and AlB₂ related slabs and the two crystallographically independent ytterbium sites are emphasized. Only one layer is shown for better visibility.

chemical discussion is given in references 86 and 87. The striking feature of this plumbide is the Shastry–Sutherland-like substructure of the ytterbium atoms, which gives rise to magnetic frustration (discussed in detail in the magnetic part, vide infra). Several years after the discovery of the compound,⁴⁷ this has motivated many detailed property studies, which are addressed below.

A complex cubic structure occurs for the aluminum- and zinc-rich compounds YbT₂Al₂₀ ($T = \text{Ti, V, Cr}$) and YbT₂Zn₂₀ ($T = \text{Co, Rh, Ir}$).¹⁸ They crystallize with the CeCr₂Al₂₀ type,

space group $Fd\bar{3}m$ with 184 atoms per unit cell. The main interest in these ytterbium compounds concerned their heavy-Fermion type behavior. The many facets of their physical properties have recently been summarized.⁸⁸ As an example we present the $\text{YbCo}_2\text{Zn}_{20}$ structure⁸⁹ in Figure 5. Although the

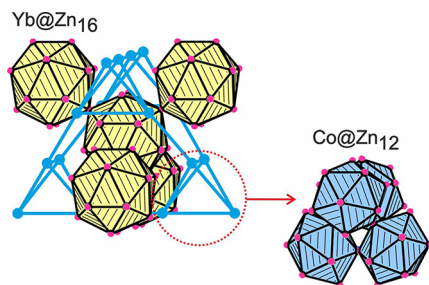


Figure 5. Cutout of the $\text{YbCo}_2\text{Zn}_{20}$ ⁸⁹ structure. Cobalt and zinc atoms are drawn as medium blue and magenta circles, respectively. The connectivity pattern of the Yb@Zn_{16} and Co@Zn_{12} polyhedra is emphasized. For details see text.

structure seems complex at first sight, it can easily be constructed from two basic building units. The ytterbium and cobalt atoms of $\text{YbCo}_2\text{Zn}_{20}$ form a substructure that is isopointal with the cubic Laves phase MgCu_2 , i.e., has the same space group symmetry. The zinc atoms now surround the ytterbium and cobalt atoms, leading to Yb@Zn_{16} and Co@Zn_{12} polyhedra which condense in a tetrahedral motif. Again, the ytterbium atoms are well separated from each other and show no bonding contacts. This “highly diluted” rare earth substructure is prone for basic property studies.

In Figure 6, we now turn to a series of ytterbium compounds with complex extended polyanionic networks which exhibit multiple ytterbium sites. Exemplarily, we present the structures of $\text{Yb}_3\text{Pd}_4\text{Ge}_4$,⁹⁰ $\text{Yb}_2\text{Pt}_3\text{Sn}_5$,²⁹ and $\text{Yb}_2\text{Au}_3\text{In}_5$.⁹¹ The common structural feature concerns the dense condensation of the transition metal and p element atoms within the polyanionic networks $[\text{Pd}_4\text{Ge}_4]$, $[\text{Pt}_3\text{Sn}_5]$, and $[\text{Au}_3\text{In}_5]$. The latter are stabilized through Pd–Ge, Pt–Sn, Au–In as well as Ge–Ge, Sn–Sn, and In–In bonding interactions. The networks then leave cavities of different sizes which are filled by the ytterbium atoms. This leads to the coordination polyhedra $\text{Yb1@Ge}_6\text{Pd}_6$ and $\text{Yb2@Ge}_6\text{Pd}_8$ for $\text{Yb}_3\text{Pd}_4\text{Ge}_4$, $\text{Yb1@Sn}_6\text{Pt}_2$ and $\text{Yb2@Pt}_5\text{Sn}_8$ for $\text{Yb}_2\text{Pt}_3\text{Sn}_5$ as well as $\text{Yb1@Au}_4\text{In}_{10}$ and $\text{Yb2@Au}_5\text{In}_8$ for $\text{Yb}_2\text{Au}_3\text{In}_5$. The three compounds tend to exhibit mixed ytterbium valences. From a crystal chemical point of view, the smaller cavities are filled by trivalent ytterbium (static mixed valency). For $\text{Yb}_2\text{Pt}_3\text{Sn}_5$, this feature was tested also from a synthetic point of view. Given the comparable size of Yb^{2+} and Ca^{2+} it was possible to synthesize the stannides $\text{CaErPt}_3\text{Sn}_5$, $\text{CaTmPt}_3\text{Sn}_5$, $\text{CaYbPt}_3\text{Sn}_5$, and $\text{CaLuPt}_3\text{Sn}_5$ with calcium site preference on the “divalent” place.⁹²

The last crystal chemical example concerns ytterbium aluminum borides. Figure 7 shows projections of the α - and β - YbAlB_4 ⁹³ and Yb_2AlB_6 ⁹⁴ structures along the short unit cell axis. The boron atoms build up planar layers with different tessellations, which are stacked in a ...AA... sequence. Between the layers, pentagonal prisms for the smaller aluminum atoms and hexagonal, respectively, heptagonal ones for the larger ytterbium atoms are formed. The two modifications of YbAlB_4 show ytterbium exclusively in the heptagonal prisms, while two prism types occur in Yb_2AlB_6 . The YbAlB_4 modifications gained high interest in recent years since they exhibit heavy

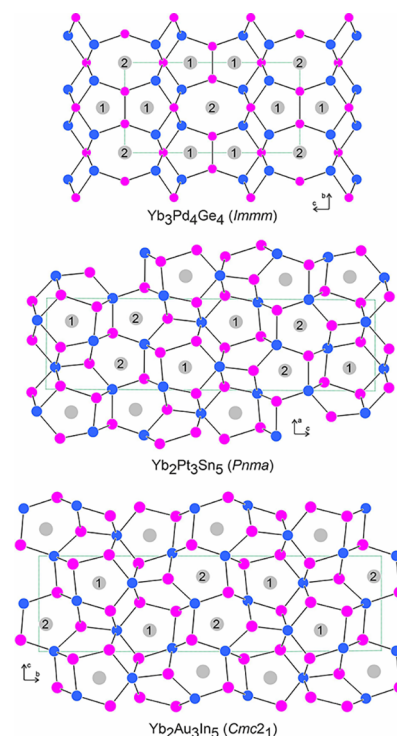


Figure 6. View of the $\text{Yb}_3\text{Pd}_4\text{Ge}_4$,⁹⁰ $\text{Yb}_2\text{Pt}_3\text{Sn}_5$,²⁹ and $\text{Yb}_2\text{Au}_3\text{In}_5$ ⁹¹ structures along the short unit cell axis. Ytterbium, palladium (platinum, gold), and germanium (tin, indium) atoms are drawn as medium gray, blue, and magenta circles, respectively. The $[\text{Pd}_4\text{Ge}_4]$, $[\text{Pt}_3\text{Sn}_5]$, and $[\text{Au}_3\text{In}_5]$ networks and the crystallographically independent ytterbium sites are emphasized.

Fermion ground state and superconductivity at low temperatures (vide infra). Already more than 120 publications appeared for this composition.¹⁹

PHYSICAL PROPERTIES AND SPECTROSCOPY

Given the large number of known phases and the fact that some of them have only been characterized with respect to their structure, the review focuses on the ytterbium valence and selected physical properties that arise from these. Thus, selected compounds with a divalent or trivalent ytterbium state are discussed to outline these properties.

Most compounds have routinely been studied with respect to their magnetic behavior in order to get a first hint for the ytterbium valence. A significantly smaller section of these studies is additionally accompanied by resistivity and specific heat measurements; however, these measurements are usually not routinely conducted. Therefore, magnetic, resistivity, and specific heat investigations are, where applicable, discussed together in the following chapter. Subsequently, separate chapters summarize the data on more sophisticated investigation techniques such as (i) inelastic neutron scattering, (ii) XANES/XAS, (iii) X-ray photoelectron spectroscopy (XPS), (iv) nuclear magnetic and electron resonance spectroscopy (NMR and ESR), (v) ^{171}Yb Mössbauer spectroscopy, and (vi) thermoelectric measurements.

Within each property chapter, the data has been summarized with respect to composition (binary or ternary) as well as structure types or structural families (e.g., Zintl phases), facilitating the comparability with respect to the valence electron count, etc.

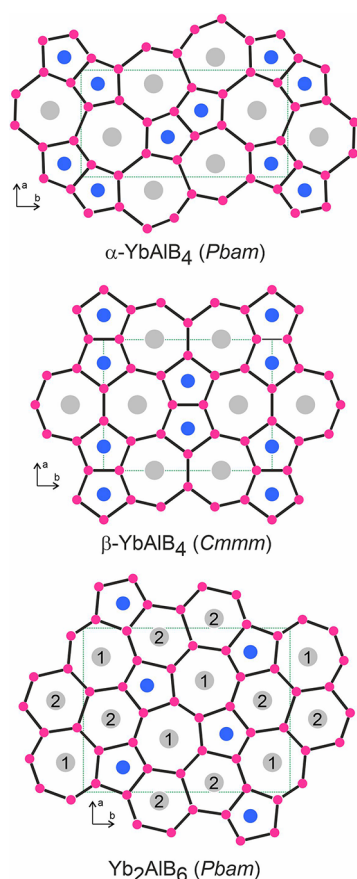


Figure 7. View of the α -YbAlB₄,⁹³ β -YbAlB₄,⁹³ and Yb₂AlB₆,⁹⁴ structures along the short unit cell axis. Ytterbium, aluminum, and boron atoms are drawn as medium gray, blue, and magenta circles, respectively. The boron nets and the crystallographically independent ytterbium sites are emphasized.

MAGNETISM, RESISTIVITY AND SPECIFIC HEAT

Before starting with a broader discussion on the magnetic properties of intermetallic ytterbium compounds, we need to comment on ytterbium sesquioxide, Yb₂O₃, the most inconvenient byproduct occurring during the synthesis of Yb intermetallics. Yb₂O₃ exhibits paramagnetism (4f¹³ configuration; $T_N = 2.3$ K⁹⁵) and can dominate the susceptibility in the low-temperature regime,⁹⁶ especially in the case of intermediate-valent or almost divalent ytterbium intermetallics. In those cases, a clear quantification of the Yb₂O₃ content is necessary along with a correction procedure.⁹⁷ If this feature is not taken into account, the interpretation of the magnetic data remains ambiguous. Since many of the ytterbium intermetallics order magnetically at very low temperature, the Yb₂O₃ impurity might overlay the intrinsic magnetism of the sample.

Divalent Ytterbium Compounds

Purely divalent ytterbium compounds have the valence electron configuration 4f¹⁴, which exhibits high stability. This filled 4f shell can be considered as a core-electron shell; therefore, no magnetic moment is observed. Such ytterbium intermetallics behave either as diamagnets or as Pauli paramagnets. Since most of these phases are metallic conductors, the observed susceptibility usually arises from an overcompensation of the intrinsic core diamagnetism by the Pauli susceptibility caused by the conduction electrons.

Exemplarily, the temperature dependences of the magnetic susceptibility of Yb₅Cu₂Zn and Yb₃Ag₄Mg₁₂ are given in Figure 8. Above 100 K, the susceptibilities are very weak and almost

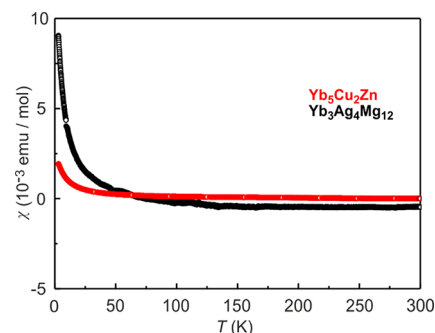


Figure 8. Temperature dependence of the magnetic susceptibility χ of Yb₃Ag₄Mg₁₂⁹⁹ and Yb₅Cu₂Zn,⁹⁸ measured at 10 kOe.

temperature-independent. The room temperature value of 7.2×10^{-6} emu mol⁻¹ for Yb₅Cu₂Zn indicates Pauli paramagnetism.⁹⁸ In contrast, in Yb₃Ag₄Mg₁₂ the intrinsic diamagnetism is not as strongly overcompensated by the Pauli contribution, leading to a room temperature value of -4.61×10^{-4} emu mol⁻¹.⁹⁹ The susceptibility increases in the low-temperature regimes (the so-called Curie tails), which originates from traces of paramagnetic impurities. Further examples of room temperature susceptibilities are given in Table 1. In these compounds, the ytterbium atoms are divalent and therefore carry no magnetic moment.

Table 1. Magnetic Susceptibilities of Selected Ytterbium Intermetallics at Room Temperature^a

| Compound | χ /emu mol ⁻¹ | Reference |
|--|-------------------------------|-----------|
| YbAgMg | $+1.2(1) \times 10^{-4}$ | 100 |
| YbAuMg | $+2.4 \times 10^{-4}$ | 101 |
| Yb ₃ Ag ₄ Mg ₁₂ | -4.61×10^{-4} | 99 |
| Yb ₅ Cu ₂ Zn | $+7.2 \times 10^{-6}$ | 98 |
| YbAgCd | $+4.8 \times 10^{-5}$ | 102 |
| YbAuCd | $+5.8 \times 10^{-5}$ | 101 |
| YbPdIn ₂ | $-4.9(2) \times 10^{-4}$ | 103 |
| YbCuSn | $+4.22 \times 10^{-4}$ | 104 |
| YbAgSn | -1.37×10^{-5} | 104 |
| YbAuSn | -2.62×10^{-5} | 104 |
| YbZnSn | $+2.0(1) \times 10^{-4}$ | 47 |
| YbCuSb | $+1.38 \times 10^{-4}$ | 104 |
| YbAgSb | -7.69×10^{-5} | 104 |
| YbAuSb | -8.47×10^{-5} | 104 |

^aStandard deviations are given in parentheses, where available.

Trivalent Ytterbium Compounds

Trivalent ytterbium cations have a 4f¹³ valence electron configuration. The g value of 8/7 and the total angular momentum of $J = 7/2$ lead to a magnetic moment of $\mu = \sqrt{g_f J(J + 1)} = 4.54 \mu_B$ per Yb³⁺.¹⁰⁵ The f electrons may play an important role in bonding/hybridization of intermetallic ytterbium compounds, leading to interesting properties, such as heavy Fermion behavior, Kondo behavior, intermediate valence, or complex magnetic structures. These properties can be influenced by different parameters, like the chemical environment, the magnetic field, temperature, or pressure.¹⁰⁶

Table 2. Magnetic Properties of Selected Ytterbium Compounds^a

| Compound | T_C/K | T_N/K | μ_{eff}/μ_B | $\gamma/\text{mJ mol}^{-1} \text{K}^{-2}$ | Reference |
|---|---------|-----------|--------------------------|---|-------------|
| YbAlB ₄ | | | | 125 | 204,222 |
| YbAl ₃ C ₃ | | | 4.66 | | 177 |
| YbFe ₂ Zn ₂₀ | | | Near 4.53 | 520 | 88,183–186 |
| YbCo ₂ Zn ₂₀ | | | Near 4.53 | 7900 | 88,183–186 |
| YbNiAl ₄ | | | 2.9 | 16 | 23,215,216 |
| YbNi ₃ Al ₉ | – | 3.4 | 4.37 | 110 | 223 |
| YbNi ₄ Si | | | 4.15 | 25 | 224 |
| YbNiGa | | 1.7, 1.9 | 4.4 | 450 | 126 |
| YbNiSn | 5.65 | – | 4.3 | 300 | 121–123,125 |
| YbCuAl | | | 4.32 | 260 | 146,147,225 |
| YbCu ₂ Si ₂ | | | 4.19 | 135 | 226 |
| YbPdCu ₄ | – | 0.8 | 4.33 | 200 | 227 |
| YbInCu ₄ | | | 4.37 | 50–400 | 228,229 |
| YbRh ₂ Si ₂ | – | 0.07 | 2×10^{-3} | | 155,161 |
| YbRhSn | – | 1.4, 1.85 | 4.3–4.5 | 1200(200) | 110,126–128 |
| YbRhSb | 2.7 | – | 1.4 | 370 | 129–131 |
| Yb ₄ Rh ₇ Ge ₆ | | | 4.55–4.65 | 0.184 | 230 |
| YbPdBi | 1 | – | 4.11(5) | 1200(100) | 110,127 |
| Yb ₄ Ir ₇ Ge ₆ | | | 4.8 | 0.281 | 230 |
| YbPtGe | 5.4 | – | 4.48 | 209 | 231 |
| YbPtIn | | 1.4, 3.4 | 4.21–4.4 | 400 | 126,232 |
| YbPtSn | 3.5(4) | – | 4.27(2) | | 127 |
| Yb ₂ Pt ₂ Pb | – | 2.07 | 4.42–4.54 | 30 | 173,233 |
| YbPtBi | – | 0.4 | | 8000 | 135–139 |

^aMagnetic properties include Néel temperature, T_N ; Curie temperature, T_C ; effective magnetic moment, μ_{eff} and specific heat capacity (Sommerfeld) coefficient (γ). Standard deviations are given in parentheses, where available.

Characteristic for heavy Fermion behavior is the large electronic specific heat coefficient γ at low temperatures, 2 or 3 orders of magnitude larger (arbitrary value of $400 \text{ mJ mol}^{-1} \text{K}^{-2}$ according to ref 107) than that of copper ($\sim 1 \text{ mJ mol}^{-1} \text{K}^{-2}$).¹⁰⁸ In addition, heavy Fermion compounds typically have large Pauli susceptibilities at low temperatures, due to the large density of states.¹⁰⁹ It is very difficult to establish the heavy Fermion behavior of ytterbium compounds, due to the challenging distinction between magnetic, crystal field, and Kondo energy scales. Thus, many compounds show both, magnetic and heavy Fermion character.¹¹⁰

The common way to fit the dependence of the magnetic susceptibility is using the Curie–Weiss law. Within the modified Curie–Weiss law, contributions of the conduction electrons are also taken into account. This makes it possible to adjust even slight curvatures of the reciprocal susceptibility. However, both laws do not consider the temperature dependency of the effective magnetic moment, which marks the only way to explain decrease of the χ^{-1} value. The ICF model (interconfiguration fluctuation model),¹¹¹ developed by Sales and Wohleben, addresses a possible mixed-valent behavior of rare earth atoms (like Yb or Ce) and is represented by

$$\chi_{\text{ICF}}(T) = \frac{N\mu_{\text{eff}}^2[1 - \nu(T)]}{3k_B(T + T_{\text{sf}})}$$

with T_{sf} as the spin fluctuation temperature and $\nu(T)$ as the temperature-dependent mean occupation of the ground state given by

$$\nu(T) = \frac{1}{1 + 8\exp[-E_{\text{ex}}/k_B(T + T_{\text{sf}})]}$$

where E_{ex} is the energy gap between the ground and the excited state. In most cases, the experimental $\chi(T)$ data can be described by

$$\chi(T) = \chi_{\text{ICF}}(T) + \chi_{\text{CW}}(T) + \chi_0$$

consisting in part of the ICF model (χ_{ICF}), the Curie–Weiss impurity (χ_{CW}), and χ_0 , the latter being a sum of temperature-independent contributions.^{111,112}

In the following paragraph, some striking examples will be briefly discussed. The magnetic properties and specific heat coefficients of these and further compounds were summarized in Table 2.

Binary Compounds

During the last 50 years, YbAl₂ (MgCu₂ type, space group $Fd\bar{3}m$) and YbAl₃ (Cu₃Au type, space group $Pm\bar{3}m$) have been extensively examined regarding their physical properties. Both compounds show Curie–Weiss behavior above 100 K, with a broad maximum of the susceptibility around 850 K for YbAl₂. The detected characteristic spin fluctuation temperatures are $T_{\text{sf}} = 200 \text{ K}$ for YbAl₂ and $T_{\text{sf}} = 125 \text{ K}$ in case of YbAl₃.^{13,114} In a hard X-ray photoemission spectroscopy study for YbAl₂, below 300 K, a ytterbium valence of ca. +2.2 was determined.^{115,116} The Kondo temperature suggested from the magnetic measurements is very high ($T_K > 2000 \text{ K}$).^{97,117} The valence of YbAl₃ (+2.75) results in a ground state with 4f occupancy of 0.75.^{118,119} In contrast, photoemission experiments revealed a valence of +2.73, whereas the determined Kondo temperature is in an order of 500–600 K, and the specific heat coefficient is $\gamma = 40 \text{ mJ/mol K}^2$. Below the Fermi-liquid temperature $T_{\text{fl}} = 50 \text{ K}$, a quadratic temperature dependence of the resistivity was found.^{118–120}

Equiatomic Ternary Compounds

Weak ferromagnetism is reported for the equiatomic compound YbNiSn (TiNiSi type, space group $Pnma$). The dense Kondo compound has a Curie-temperature of $T_C = 5.65$ K, and the magnetic moment lies along the c axis. A value of $\mu_{\text{eff}} = 4.3 \mu_B$ was determined as an effective magnetic moment close to the value of a free Yb³⁺ ion ($4.54 \mu_B$). The maximum detected magnetization is $0.85 \mu_B$ per Yb atom. Kondo fluctuations with a Kondo temperature $T_K = 2$ K lead to the reduction of the ferromagnetism.^{121–124} Further investigations by Mössbauer spectroscopy, neutron diffraction, and resistivity measurements confirm these results.^{121–125}

The susceptibility of YbRhSn with ZrNiAl type structure (space group $P62m$) follows the Curie–Weiss law at high temperatures, with a trivalent state of the Yb ions. The deduced effective magnetic moment was in a range of 4.4–4.5 μ_B , and a negative Weiss constant was observed.^{126–128} Two different magnetic transitions at $T = 1.85$ and 1.4 K were reported via heat capacity data, which shift to lower temperatures with applied magnetic fields as expected for antiferromagnetic ordering. In addition, the heat capacity data indicate a possible heavy Fermion ground state. The resistivity of YbRhSn is Kondo-like and decreases almost linearly down to 20 K, followed by a rapid decrease at 1.8 K. Below 1 K it has a Fermi-liquid-like temperature variation.^{126–128}

YbRhSb was first synthesized by Muro et al. in 2004 and crystallizes with the TiNiSi type structure. It reveals a ferromagnetic transition at $T_C = 2.7$ K. For an applied magnetic field parallel to the crystallographic b axis, a spontaneous moment of only $\sim 3.0 \times 10^{-3} \mu_B$ per Yb atom was observed, although the magnetic easy axis is the a axis. At around 2 T a metamagnetic transition occurs, and at 15 T the magnetization reaches $1.4 \mu_B/\text{Yb}$ for the $B\parallel a$ axis, somewhat reduced when compared with the theoretical saturation magnetization of $4 \mu_B$.¹⁰⁵ The specific heat coefficient was determined to be $\gamma \sim 370 \text{ mJ mol}^{-1} \text{ K}^{-2}$ in the ferromagnetically ordered state.¹²⁹ Instead of typical ferromagnets, the Curie temperature furthermore decreases with higher applied magnetic fields. Thus, the weak ferromagnetism of YbRhSb is possibly the result of a canted antiferromagnetic structure. Resistivity measurements and investigations in a p/T phase diagram revealed a minimum for $T_M(p)$ at $p_C = 1.7$ GPa. For $p \geq 2$ GPa, the canted antiferromagnetic structure changes to a ferromagnetic structure and a moment of $0.4 \mu_B/\text{Yb}$ within the bc plane.^{130–133}

YbBiPt crystallizes in the cubic MgAgAs type structure with space group $F\bar{4}3m$.¹³⁴ Antiferromagnetic ordering was detected at $T_N = 0.4$ K, while the determined Weiss constant is $\Theta_p = 0.4$ K.^{135–137} Heat capacity data (Figure 9) revealed an extremely large low-temperature specific heat coefficient of $\gamma = 8 \text{ J mol}^{-1} \text{ K}^{-2}$,^{135–137} and the also determined Kondo temperature was measured to be $T_K = 1$ K.^{134,136} Further experiments showed that the antiferromagnetism is very sensitive to magnetic field, pressure, and strain.^{137–140} In addition, below T_N very broad magnetic neutron-diffraction peaks were observed.^{141,142}

YbCuAl crystallizes with a ZrNiAl type structure^{143–145} (space group $P\bar{6}2m$), was first discovered by Dwight et al. in 1968¹⁴⁴ and shows mixed-valent character for Yb in this compound.^{146,147} Down to $T = 30$ K, the susceptibility follows the Curie–Weiss law, while at the lowest temperatures it is marked by a saturation at a high level. The observed intermediate valence is close to 3, and YbCuAl can be described as a heavy Fermion compound with a high value of

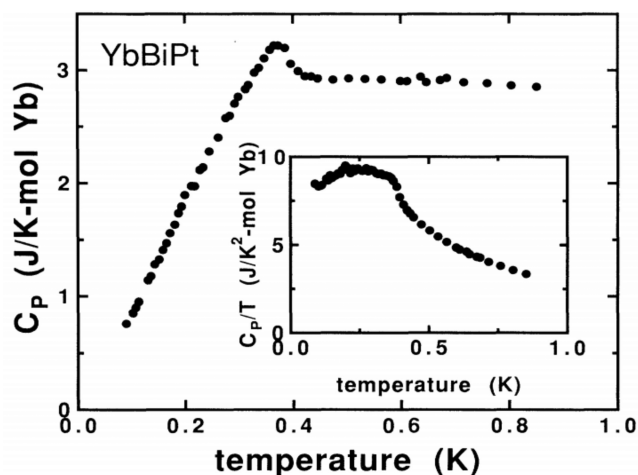


Figure 9. Low-temperature specific heat $C_p(T)$ of YbBiPt between 0.09 and 0.85 K. Inset: Same data as C_p/T vs T . Reprinted with permission from ref 136.

its specific heat coefficient ($\gamma = 260 \text{ mJ mol}^{-1} \text{ K}^{-2}$).^{148,149} For more details, we refer to the review of Bonville in 1988, who summarized the results of the different physical experiments on YbCuAl together with other ytterbium compounds.¹⁴⁹

Further Ternary Compounds

One of the most intensively studied ytterbium compounds is YbRh₂Si₂. Over the last 20 years, more than 350 publications have been published on this silicide. It was first described by Rossi et al. in 1979,²² adopts the tetragonal ThCr₂Si₂ type structure (space group $I4/mmm$), and has a (theoretically) three-dimensional Fermi surface.^{150–154} Antiferromagnetic ordering was detected at very low temperatures, with the Néel temperature being $T_N = 70$ mK. Yet, the nature of this order is still not clear and was further examined with different techniques such as neutron scattering,¹⁵⁵ static susceptibility,^{156–157} ²⁹Si NMR,¹⁵⁷ or ESR.^{158–160} (vide infra). Ferromagnetic fluctuations cause incommensurate antiferromagnetic correlations, which were detected by these investigations above 70 mK.

YbRh₂Si₂ exhibits a non-Fermi-liquid behavior. The ordered Yb³⁺ moment is very small, with only $2 \times 10^{-3} \mu_B/\text{Yb}$ atom (Figure 10). The characteristic Kondo-temperature is $T_K = 25$ K.¹⁶¹ A quantum critical point is suggested for the suppression of T_N at ambient pressure by a magnetic field of only $B_c = 60$ mT.¹⁶² The substitution of Si by Ge shifts the quantum critical point to lower fields,^{156,163} whereas Co substitution leads to ferromagnetism.^{164,165} In addition, superconductivity was reported for YbRh₂Si₂, thus leading to the assumption of a strong coupling of electronic and nuclear magnetism.^{166,167} Reasons for this superconductivity as well as the mentioned nature of ordering and the quantum critical point itself remain unclear and are the subject of further research.¹⁶⁸

One of the remarkable trivalent ytterbium compounds is the Shastry–Sutherland^{170–172} phase Yb₂Pt₂Pb, originally reported in 1999.⁴⁷ Yb₂Pt₂Pb adopts the Er₂Au₂Sn type structure (space group $P4_2/mmm$). Later property studies were performed on single crystals which were grown from lead flux (Yb:Pt:Pb = 5:4:40 starting composition).¹⁷³ Orientation-dependent magnetic susceptibility measurements showed a high anisotropy with an about 30 times larger value for $\chi_{(100)}$ as compared to $\chi_{(001)}$ (Figure 11).¹⁷⁴ The Néel temperature of Yb₂Pt₂Pb is $T_N = 2.07$ K.¹⁷³

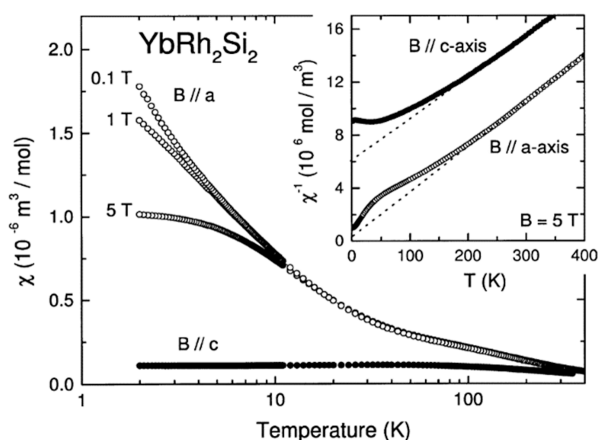


Figure 10. Temperature dependence of the magnetic and inverse magnetic susceptibility of YbRh_2Si_2 measured parallel to the a and c axis with different applied fields. Reprinted with permission from ref 169.

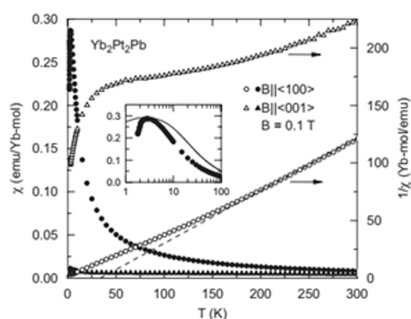


Figure 11. Temperature dependence of the magnetic and inverse magnetic susceptibility of $\text{Yb}_2\text{Pt}_2\text{Pb}$ measured parallel (100) and (001). Reprinted with permission from ref 174.

Besides, $\text{Yb}_2\text{Pt}_2\text{Pb}$ was studied by specific heat and resistivity measurements and with respect to its crystal field parameters obtained by inelastic neutron scattering data. All these property studies were supported by quantum chemical calculations for a better understanding of the structure–property relationships. The complete property data of $\text{Yb}_2\text{Pt}_2\text{Pb}$ has recently been reviewed,⁸⁷ and we refer to this broad overview for more details.

Magnetization data support the anisotropic behavior observed in the orientation-dependent susceptibility measurements. $\text{Yb}_2\text{Pt}_2\text{Pb}$ shows multiple metamagnetic steps in both the (100) and (110) directions.¹⁷⁵ The maximum magnetization observed in (100) at 5 T is around $2.4 \mu_B$ per ytterbium atom, significantly reduced when compared with the theoretical value of $4 \mu_B$ ($g \times J$). The magnetic structure of $\text{Yb}_2\text{Pt}_2\text{Pb}$ was studied from powder and single crystal neutron diffraction data.¹⁷⁶ The ordered ytterbium magnetic moments were described in a $5 \times 5 \times 1$ magnetic supercell.

YbAl_3C_3 is another example of isotropic exchange interaction and crystallizes with the hexagonal ScAl_3C_3 type structure (space group $P6_3/mmc$). The ytterbium atoms form a triangular lattice, then a structural phase transition to an orthorhombic phase (own structure type) occurs at $T_S = 80$ K.^{177–179} Above this temperature, Curie–Weiss behavior with an effective magnetic moment of $\mu_{\text{eff}} = 4.66 \mu_B$ was observed, underlining the trivalent state of the ytterbium atoms. The calculated Weiss constant of $\Theta_p = -120$ K indicates

antiferromagnetic interactions in the paramagnetic regime.^{177,178} Below T_S , no long-range magnetic order was visible by measurements of the magnetization or specific heat. It has been proposed that the anisotropic Kramers doublet of YbAl_3C_3 forms an antiferromagnetic dimer ground state with a single-triplet energy gap of about 15 K in a relatively narrow field and the 4f electrons are expected to behave as a $S = 1/2$ spin system at low temperatures, thus suggesting only weaker interdimer interaction in the ytterbium triangles.^{177,178,180–182}

$\text{YbCo}_2\text{Zn}_{20}$ is a member of the $\text{CeCr}_2\text{Al}_{20}$ type family (space group $Fd\bar{3}m$). The high temperature susceptibility follows the Curie–Weiss law with an effective magnetic moment near the value of a free Yb^{3+} ion ($\mu_{\text{eff}} = 4.54 \mu_B$). No magnetic ordering down to 20 mK was observed, while the recorded magnetization isotherms at low temperatures indicate a metamagnetic transition. At lowest temperatures, the magnetic ground state is enhanced by the Pauli susceptibility. By heat capacity measurements, a large Sommerfeld coefficient of $\gamma = 7.9 \text{ J}^{-1} \text{ mol}^{-1} \text{ K}^{-2}$ was observed. Kondo interactions were confirmed via the T^2 resistivity, resulting from the A coefficient ($A = 165 \mu\Omega \text{ K}^{-2}$). This classifies $\text{YbCo}_2\text{Zn}_{20}$ as a superheavy electron metal. For further detail, we refer to the literature and reviews.^{88,183–186}

Stoichiometric YbInCu_4 adopts the MgCuSn_4 type structure^{187,188} (cubic $C15B$, space group $F\bar{4}3m$);¹⁸⁹ however, the disordered structure (solid solution) $\text{Yb}_{1-x}\text{In}_x\text{Cu}_2$ ($C15$, MgCu_2 type, space group $Fd\bar{3}m$) has also been observed.^{190,191} It is one of the few Yb compounds (YbPd_2Al_3 is another one⁶⁷) that exhibits a first-order isostructural valence transition (VT) with the transition temperature $T_{\text{trans}} = 42$ K.^{189–191} In the high-temperature regime, the Yb valence has been reported to be +2.9 and suddenly drops to +2.74 when cooling below T_{trans} .¹⁹² At the same time, the magnetic ground state undergoes a transition from a local moment susceptibility of $4.5 \mu_B$ to temperature-independent Pauli paramagnetism below T_{trans} .¹⁹³ No change in the structure is observed during the transition, although the unit cell volume increases by $\sim 0.5\%$.^{194,195}

Furthermore, the transition was confirmed by synchrotron radiation X-ray absorption, X-ray emission spectroscopy, inelastic neutron scattering (vide infra),^{196–200} and abrupt changes in other physical properties like electrical resistivity, specific heat capacity, and nuclear spin-relaxation rate (vide infra).^{198,201,202} The transition is also accompanied by a drastic change of the Kondo temperature (T_K) from 20 to ~ 400 K in the low-temperature phase.^{199,203}

In Yb-based heavy Fermion systems, $\beta\text{-YbAlB}_4$ was the first discovered superconductor with the transition temperature $T_C = 80$ mK.^{204,205} The results of transport and thermodynamic properties suggest non-Fermi liquid behavior in the normal $\beta\text{-YbAlB}_4$ state.^{203,206} It adopts the orthorhombic ThMoB_4 type structure (space group $Cmmm$) with the Yb and Al atoms being in the ab plane between two B layers of hepta- and hexagonal boron rings (vide ultra).⁹³ This structural environment and the strong observed valence fluctuations²⁰⁷ are essential for understanding the properties of $\beta\text{-YbAlB}_4$. Within the ab plane, the Kondo hybridization was discussed to be isotropic, in contrast to the anisotropy between the crystal c axis and the ab plane.²⁰⁸ This may explain the observed T/B scaling of the magnetic susceptibility and the intrinsic quantum criticality.^{209–214}

Another example of an intermediate valence ytterbium compound is YbNiAl_4 , which adopts the YNiAl_4 type structure

(space group $Cmcm$). The temperature dependence of the magnetic susceptibility is compatible with the ICF model. At $T = 4.2$ K the determined valence of the Yb atoms is +2.1, in contrast to +3 at $T = 1000$ K. Resistivity measurements revealed a Fermi-liquid behavior, due to the observed AT^2 variation below 60 K. At room temperature, it shows a metallic-like behavior. The heat capacity measurements gave no hints for any magnetic ordering down to 1.9 K. For the electronic specific heat capacity, a value of $\gamma = 16$ mJ mol⁻¹ K⁻² was determined, so that a heavy Fermion state can be excluded.^{23,215} In addition, various transport measurements (thermal and electrical) were analyzed.²¹⁶ In-situ high-pressure studies show an increase of the ytterbium valence with increasing pressure for YbNiGa₄ and YbNiIn₄.²¹⁷

Also, the complex structure of Yb₄Ga₂₄Pt₉, a platinumide, shows intermediate ytterbium valence. Hard X-ray photoelectron spectra and magnetic susceptibility measurements point to an ytterbium valence of ~ 2.5 .²¹⁸ The stannide YbRhSn₂,²¹⁹ and the solid solution YbIn_{1-x}Au_{1+x} ($x = 0-0.3$)²²⁰ show comparable behavior.

An intermediate ytterbium valence can also be induced by isovalent substitution. The phosphide Yb₂Ni₁₂P₇ exhibits a heavy-Fermion paramagnetic ground state and switches to intermediate valence in Yb₂Ni₁₂As₇.²²¹

INELASTIC NEUTRON SCATTERING

Inelastic neutron scattering is often used to probe crystal field excitations which allow drawbacks on the crystal electric field (CEF) splitting for a certain atom and magnetic phase transitions. In contrast to elastic scattering, in this case, the energy difference of the scattered neutrons is detected. Therefore, it is a useful tool to obtain information about the ground state and the magnetic exchange interactions of, in this case, the Yb atoms.²³⁴

Binary Compounds

One of the first compounds that has been studied by inelastic neutron scattering was YbBe₁₃ (NaZn₁₃ type, space group $Fm\bar{3}c$).²³⁵ The spectra were recorded on a polycrystalline sample between 1.2 and 300 K. Since YbBe₁₃ undergoes antiferromagnetic ordering at $T_N = 1.28$ K,²³⁶ the single line observed at 1.2 K was interpreted as a magnon. The spin fluctuations associated with the magnetic ordering, however, persist for quite a large temperature range and are still observable at 10 K. At 39 K, the CEF splitting can be observed with Γ_7 being the ground state and Γ_8 (3.20 meV) and Γ_6 (4.39 meV) being the next excited states. These observations contradict the results from the literature where a different sequence was reported; however, all agree on the Γ_7 ground state.^{236,237}

For YbPd (CsCl type, space group $Pm\bar{3}m$) and Yb₃Pd₄ (Pu₃Pd₄ type, space group $R\bar{3}$), inelastic neutron scattering has been used to probe the proposed magnetic transitions in these intermediate valent compounds and to determine the CEF splitting to gain information about the ground state. For YbPd, Γ_8 was determined to be the ground state with Γ_7 being 4.75 meV and Γ_6 being 12.3 meV higher in energy. This scheme is in line with trivalent Yb in a cubic environment. At 1.3 K, an additional contribution with magnetic origin is observed for YbPd. For Yb₃Pd₄, the first excitation was shifted to lower energy (4.08 meV) and is more distinct compared to the one in YbPd. It is interesting to note that despite Yb₃Pd₄ being trigonal (26 independent CF parameters are expected—note,

the referenced paper states that Yb₃Pd₄ is triclinic; this statement has been corrected) the observed transitions still can be interpreted by a cubic site symmetry. Finally, measurements between 1.3 and 6 K revealed a strong inelastic line at low temperatures that softens toward the proposed magnetic phase transition near 3 K. An abrupt change of the line width at $T = 3.1$ K indicates that this excitation can be attributed to a magnon in the magnetically ordered state.²³⁸

Ternary Compounds

To understand the valence fluctuating behavior of YbInAu₂ (MnCu₂Al type, space group $Fm\bar{3}m$), neutron scattering experiments were conducted and compared to the results of YbAl₃ (Cu₃Au type, space group $Pm\bar{3}m$) which exhibits similar physical properties. The data obtained at temperatures near the susceptibility maxima (~ 80 K for YbInAu₂ and ~ 120 K for YbAl₃) could be fitted with a single spectral function. At 5 K, however, the data of YbAl₃ needs more components while the data of YbInAu₂ still can be fitted with a single function. The differences are also visible in the phonon scattering (high angle data). Here, a well-defined phonon mode is visible for YbAl₃ in contrast to YbInAu₂.²³⁹

As mentioned before, Yb_{1-x}In_xCu₂ (MgCu₂ type, space group $Fd\bar{3}m$) shows a temperature-dependent valence phase transition. It changes from a nearly trivalent state at high temperatures to a mixed-valent Pauli paramagnetic state at low temperatures. A sample with $x = 0.5$ was investigated at $T = 30$ and 60 K, above and below the transition temperature of $T = 40$ K. The spin dynamics in the mixed-valent phase ($T = 30$ K) can be modeled with a Lorentzian power spectrum with the center at $E = 40$ meV.²⁴⁰

Also, different YbT₂X₂ compounds were investigated by inelastic neutron scattering. Among the first investigations was the work on YbT₂Si₂ for $T = \text{Fe, Co, and Ni}$ (ThCr₂Si₂ type, space group $I4/mmm$).²⁴¹ The performed experiments showed that YbCo₂Si₂ exhibits three excited states at ~ 4 , 12.5, and 30.5 meV above the ground state, while for YbNi₂Si₂, two clear transitions at ~ 7.5 and 13.5 meV are visible alongside a shoulder at lower energy of the 7.5 meV peak. For YbFe₂Si₂, no clear inelastic signals are observed.²⁴¹ Taking the experimentally determined energies for YbCo₂Si₂ into account, the CF level scheme could be derived, indicating Γ_7 to be the ground state.²⁴² YbMn₂Si₂ (ThCr₂Si₂ type, space group $I4/mmm$) has the peculiarity that it shows two antiferromagnetic transitions at $T_{N,1} = 526$ and $T_{N,2} = 30$ K originating from the Mn atoms.²⁴³ Determination of the magnetic structure showed that, below $T_{N,1}$, the Mn atoms show a + - + - sequence, while below $T_{N,2}$, a + - - + magnetic substructure arises, which leads to a doubling of c in the magnetic unit cell. At 1.5 K also the Yb atoms are antiferromagnetically ordered, however, with their spins orthogonal to the Mn spins.²⁴⁴ Above 30 K, only one Yb site is present which exhibits a doublet ground state as well as three excited states at 4.65, 11.89, and 15.05 meV. Below 30 K, however, a second Yb site emerges due to the antiferromagnetically ordered Yb atoms. This leads to two additional signals in the inelastic neutron spectrum of YbMn₂Si₂ at 2.5 K. These transitions can be associated with a different CEF scheme for the Yb2 site with energy levels at 7.24, 8.76, and 16.4 meV.^{245,246} For the heavy Fermion compound YbRh₂Si₂ (ThCr₂Si₂ type, space group $I4/mmm$), inelastic neutron scattering experiments conducted at 1.5 K are also dominated by the CEF excitations of the Yb³⁺ ion. Besides a ground state doublet, three excited state

doublets were observed at higher energies of 17, 25, and 43 meV, in line with the CF theory for a tetragonal system.²⁴⁷ Subsequent calculations showed that the ground state is a Γ_6 Kramers doublet.²⁴⁸ For YbIr_2Si_2 , both modifications (CaBe_2Ge_2 type, $P4/nmm$, and ThCr_2Si_2 type, $I4/mmm$) were investigated by inelastic neutron scattering experiments at 1.5 K. As for YbRh_2Si_2 , a doublet ground state and three excited doublet states are expected. For the body-centered polymorph, energies of 0, 18, 25, and 36 meV were observed, while for the primitive polymorph they are slightly lower in energy at 0, 15, 22, and 33 meV.²⁴⁹ These values are in good agreement with the calculated values for both YbRh_2Si_2 and YbIr_2Si_2 .²⁵⁰

XANES/XAS

X-ray absorption spectroscopy (XAS) describes the overall measurement of the absorption spectrum of electrons, which interact with polychromatic X-ray photons and absorb characteristic wavelengths. The XA spectrum can be separated into two parts. First, the area at higher photon energy than the absorption, called extended X-ray absorption fine structure (EXAFS) which contains information about the local environment of the absorbing atom. The second area is at the absorption energy, the X-ray absorption near edge structure (XANES) or near edge X-ray absorption fine structure (NEXAFS), which gives insight into the electronic properties, e.g., the oxidation state of the absorbing atom. In the following chapter, examples of classical intermetallic Yb-compounds as well as Zintl phases will be addressed with regards to their respective valence in the XAS and XANES measurements.

Binary Compounds

The binary compounds YbAl_2 (MgCu_2 type, space group $Fd\bar{3}m$) and YbAl_3 (Cu_3Au type, space group $Pm\bar{3}m$) are among the most investigated intermetallics. Both have one crystallographic Yb position in the crystal structure. One of the earliest X-ray absorption measurements of YbAl_2 was done by Beaurepaire, Kappler, and Krill in 1986.²⁵¹ In their work, YbAl_2 was measured at room temperature under pressures of 10 and 30 kbar. At room temperature, YbAl_2 has a valence of +2.3, whereas under pressure the valence rises to +2.6 at 30 kbar (pressure-induced oxidation). Due to the width of the 2p core hole of 4.6 eV, the Yb^{2+} and Yb^{3+} L_{III} edges could not be resolved, but the two contributions are separated by about 6 eV.²⁵¹ Dallera et al. measured the pressure dependence of the Yb L_{III} edge in YbAl_2 up to 385 kbar using the partial fluorescence yield mode of the X-ray absorption (PFY-XAS), giving a higher resolution of the spectra compared to the conventional measurement mode. The absorption spectra show the valence shift from a valence in YbAl_2 of +2.25 at ambient pressure to a valence of +2.9 at 385 kbar. At pressures of 170 and 385 kbar, the spectra of YbAl_2 become similar to $\text{Yb}_{1-x}\text{In}_x\text{Cu}_2$, which has a stated valence of +2.96, indicating a valence close to +3.²⁵²

XAS spectra of YbAl_3 were measured at 10 and 300 K, showing the Yb 3d \rightarrow 4f transition and indicating an open 4f shell in the ground state. A decrease in the intensity of 11% at 10 K compared to 300 K is additionally reported by Tjeng et al., suggesting a decrease in the valence of the Yb atom, which is also shown in the photoemission spectroscopy.²⁵³ The pressure-induced valence change of YbAl_3 was measured by PFY-XAS starting at ambient pressure and the valence of +2.75 for YbAl_3 , which subsequently rises alongside the increasing

pressure. At 9 GPa, the valence is +2.82, then +2.86 at 20 GPa, and finally +2.93 at an applied pressure of 38 GPa. The incident energy for Yb^{2+} is 8.942 keV, Yb^{3+} resonates at a slightly higher energy of 8.950 keV.²⁵⁴ By changing from bulk materials to nanoparticles, the valence of YbAl_3 changes from +2.86 to +2.70 after mechanical milling in a planetary high-energy ball milling system for 120 h. The reference Yb_2O_3 indicates the Yb^{3+} peak at 8946.5 eV, and the spectra of the milled YbAl_3 shows an increase of the Yb^{2+} contribution at 8941 eV. The valences for 20 and 70 h milling time are +2.74 and +2.70, respectively. A cause of the valence change is the size effect stated. The milled YbAl_3 particles possess two types of Yb atoms, the trivalent in the bulk of the sample and the ones near the surface having a variation of their coordination number, leading to divalent Yb. Another reason is the disorder introduced in the ball milling process, which is particularly visible in the X-ray diffraction data.²⁵⁵

YbGa_2 crystallizes at ambient pressure in the hexagonal CaIn_2 type structure ($P6_3/mmc$), at higher pressures above 22 GPa a phase transition into the UHg_2 type ($P6/mmm$) occurs. XANES measurements of the Yb L_{III} -edge show a valence increase from Yb^{2+} at ambient pressure to Yb^{3+} in the high-pressure structure. At low pressures, two peaks are visible, wherein the peak at higher energy represents the Yb^{3+} and is within 1 eV to the reference Yb_2O_3 , and the second peak is 7 eV lower, corresponding to Yb^{2+} . Measurements were taken at 0.6, 4.7, and 28.8 GPa, showing a continuous increase in the intensity of Yb^{3+} and decrease of the Yb^{2+} white line until the phase transition occurs and only Yb^{3+} is present (Figure 12). In

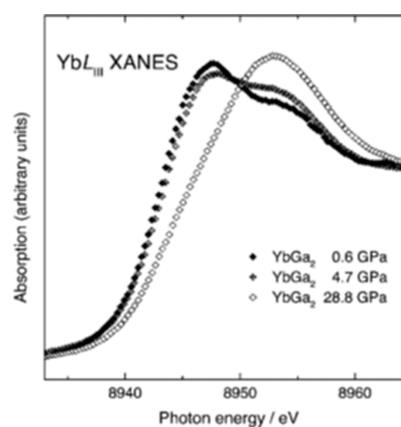


Figure 12. Yb L_{III} XANES spectra of YbGa_2 at different pressures. The white lines at low energies are attributed to Yb^{2+} , and the lines at higher energies are attributed to Yb^{3+} . Figure reproduced with permission from ref 256. Copyright 2001 John Wiley & Sons, Inc.

the high-pressure modification, YbGa_2 possesses a two-dimensional polyanion, compared to the Ga network found in the normal pressure phase. The two-dimensional arrangement can then be supported with the additional electrons from the Yb atoms.²⁵⁶

The hexagonal phase Yb_5Si_3 crystallizes in the Mn_5Si_3 type structure ($P6_3/mcm$) and possesses two distinct crystallographic Yb positions (4d and 6g). Alongside XANES, Mössbauer spectroscopic investigations and magnetic measurements were also conducted. The magnetic measurements indicated that only trivalent Yb is present, in contrast to the Mössbauer spectrum proposing 60% of Yb^{3+} . XANES measurements were performed at 10 and 300 K; these show

two white lines at 8943 and 8935 eV corresponding to Yb^{3+} and Yb^{2+} , respectively. The calculated valence from the spectra is +2.88, which is higher than the expected value of +2.6 if the Yb atoms on the 6d site were purely trivalent and the ones on the 4g site divalent. The authors suggested that a hybridization of the 4f electrons is occurring, whose strength is different for the two different crystallographic sites. The Yb atoms on the 4d site are more strongly influenced than the Yb atoms on 6g.²⁵⁷

Yb_5Ge_4 (Sm_5Ge_4 type, space group $Pnma$) is reported to be a mixed valence compound with a valence of +2.42, showing the white band at 8948 eV and a big shoulder at 8941 eV, indicating Yb^{3+} and Yb^{2+} , respectively.²⁵⁸

Equiatomic Ternary Compounds

The heavy Fermion compound YbCuAl (ZrNiAl type, space group $P\bar{6}2m$) is described with a Yb valence of nearly +3. With increasing pressure, the valence of Yb can be increased, and with lowering the temperature, the Yb becomes more divalent as shown by XES measurements.²²⁵ YbAuIn also crystallizes in the hexagonal ZrNiAl type structure with one crystallographic Yb position. X-ray absorption measurements of YbAuIn were taken at 15–18 and 300 K at ambient pressure, resulting in an intensive white line at 8941 eV corresponding to a divalent Yb, but also a weak shoulder at 8949 eV showing a small amount of trivalent Yb. By fitting the spectra and excluding Yb_2O_3 impurities, a valence of +2.17 was determined.²⁵⁹ YbGaGe possesses two crystallographically different Yb positions and crystallizes in the hexagonal YPtAs type structure ($P6_3/mmc$). The compound shows a white band at around 8940 eV and a small shoulder around 8950 eV, indicating a divalent system with oxidic impurities, which is in line with the magnetic measurements.²⁶⁰

Further Ternary Compounds

YbRh_2Si_2 (ThCr_2Si_2 type, space group $I4/mmm$) has a temperature- and magnetic-field-dependent Yb valence, which is decreasing with lower temperature and increasing alongside higher magnetic fields. To measure the influence of the two parameters, XAS measurements were conducted by Nakai et al. The Yb L_{III} absorption spectra show a shoulder at 8940 eV appearing at decreasing temperature and an intensive white line at 8946 eV, indicating the trivalent Yb, whose intensity decreases with lower temperatures. Above 200 K, the valence was determined to be +2.96, while below 25 K, a valence of +2.92 was reported. In contrast, the valence change of Yb was measured by increasing magnetic field at 2 K. At 0 T, the valence is +2.92, and it rises to +2.93 monotonically with stronger magnetic fields up to 33 T.²⁶¹

X-ray absorption spectra of YbCu_2Si_2 , YbCu_2Ge_2 (ThCr_2Si_2 type, space group $I4/mmm$), and YbPt_2 (MgCu_2 type, space group $Fd\bar{3}m$) were measured at 300 K, showing a pure trivalent Yb in YbPt_2 , divalent Yb in YbCu_2Ge_2 , and a mixed valence occurring in YbCu_2Si_2 with a higher amount of Yb^{3+} than Yb^{2+} . It was also stated that the Yb valence in YbCu_2Si_2 does not show any signs of a temperature dependency.²⁶² Similar to YbCu_2Ge_2 , YbAl_2Ga_2 possesses a white line at 8936 eV and a resulting valence of Yb^{2+} .²⁶³ YbMn_2Ge_2 (ThCr_2Si_2 type, space group $I4/mmm$) is also described as a mixed valent compound with a Yb valence of +2.40 at 300 K. This compound shows not only a negative thermal expansion, but also a temperature dependence of the Yb valence. With the increase of the temperature, the white line at 8943 eV decreases while the one at 8949 eV increases, corresponding to the Yb^{2+} and Yb^{3+}

respectively, leading to a valence of +2.82 at 700 K. Also, the valence of Yb can be influenced by applying pressure; e.g., at a pressure of 1.4 GPa, the Yb valence is +2.82.²⁶⁴

The $\text{YbT}_2\text{X}_{20}$ compounds with $T = \text{Cr, Ti, V, Co, Fe, Ir, Rh}$ and $X = \text{Al, Zn}$ all crystallize in the cubic $\text{CeCr}_2\text{Al}_{20}$ type structure (space group $Fd\bar{3}m$). These structures are heavy Fermion compounds and can possess a particularly high specific heat coefficient. XAS measurements were taken of $\text{YbRh}_2\text{Zn}_{20}$ and $\text{YbIr}_2\text{Al}_{20}$ at 2, 250, and 290 K, respectively, with additional measurements at 2 K with an applied external field of 10 T. The absorption spectra of $\text{YbRh}_2\text{Zn}_{20}$ have two peaks, the white line at 8950 eV indicating Yb^{3+} and a shoulder at 8940 eV originating from Yb^{2+} . The valence at 250 K is stated as +2.89 and is decreasing with decreasing temperature, especially below 100 K, reaching a valence of +2.87 at 20 K. The same trend is visible for $\text{YbIr}_2\text{Al}_{20}$, also having a decreasing Yb valence with decreasing temperatures below 90 K; above 100 K, the valence is nearly constant. As for the measurements under an applied field, only changes in the valence are present below 80 K.²⁶⁵ In contrast, $\text{YbCo}_2\text{Zn}_{20}$ was investigated by XAS measurements, showing no indication of temperature or magnetic field dependency.²⁶⁶ $\text{YbFe}_2\text{Zn}_{20}$ and Cd-substituted $\text{YbFe}_2\text{Zn}_{20-x}\text{Cd}_x$ with $x = 0-1.4$ were analyzed by Fahl et al. Their XANES studies of the Yb L_{III} absorption show only the white line at 8946 eV corresponding to Yb^{3+} and no additional shoulder, making all compounds formally trivalent.²⁶⁷

For the valence transition compounds $\text{Yb}_{1-x}\text{In}_x\text{Cu}_2$ ($x = 0.5$), the valence transition temperature is stated to be $T_{\text{trans}} = 42$ K where the valence changes from +2.98 to +2.85, as calculated from the XANES measurements at 300 and 7 K, respectively.²⁶⁸ Another study on $\text{Yb}_{0.5}\text{In}_{0.5}\text{Cu}_2$ by Yamaoka et al. focused on the pressure-induced valence transition. In their work, X-ray absorption spectra of $\text{Yb}_{0.5}\text{In}_{0.5}\text{Cu}_2$ were taken at 300 and 13 K under pressure. At 300 K, $\text{Yb}_{0.5}\text{In}_{0.5}\text{Cu}_2$ shows no pressure dependent valence; at 13 K on the other hand, it presents an increase of valence at pressures of 3.1 GPa and above.²⁶⁹ The XAS spectra of YbAgCu_4 (MgCu_4Sn type, space group $F\bar{4}3m$) measured at 10 and 300 K by Lawrence et al. show the white line at 8947 eV and a shoulder at 8940 eV, corresponding to Yb^{3+} and Yb^{2+} , respectively. Also, they are stating that the valence of YbAgCu_4 is nearly +3 and changes continuously with temperature.²⁷⁰ Sarrao et al. investigated the Yb valence in the YbTCu_4 series (MgCu_4Sn type, space group $F\bar{4}3m$) with $T = \text{Mg, Ag, Au, Zn, Cd, Tl}$ by XAS of the Yb L_{III} line between 20 and 300 K, showing the Mg compound with the lowest Yb valence of +2.64 at 20 K and +2.69 at 300 K, followed by YbTlCu_4 with +2.75 to +2.82, YbCdCu_4 +2.76 to +2.82, YbZnCu_4 +2.84 to +2.88, YbAgCu_4 +2.86 to +2.93, and finally YbAuCu_4 with a valence of +2.95 at 20 K and +2.96 at 300 K.²⁴⁰ XANES studies of YbPtIn_4 and YbPdIn_4 (YNiAl_4 type, space group $Cmcm$) were reported, stating both compounds containing mixed valent Yb.²⁷¹

Zintl Phases

The Zintl compounds $\text{Yb}_{14}\text{TSb}_{11}$ ($T = \text{Zn, Mn, Mg; Ca}_{14}\text{AlSb}_{11}$ type, space group $I4_1/acd$) exhibit besides intriguing magnetic also highly important thermoelectric properties (see *thermoelectric properties*). Using the Zintl counting rules, the Mn-containing compounds only have Yb^{2+} cations, while the Zn and Mg compound should also contain one Yb^{3+} . To verify the valence of the Yb atoms in these compounds, XANES measurements were taken by He et al. The absorption spectra of all three compounds indicate the

presence of both Yb^{2+} and Yb^{3+} , but the overall valence is close to Yb^{2+} . Additionally, it is visible that the Mg and Mn compounds have a constant amount of Yb^{3+} , but in the Zn compound, the valence is highly temperature-dependent. The formation of Yb^{3+} is explained by introducing disorder in the structure of $\text{Yb}_{14}\text{TSb}_{11}$.²⁷²

■ X-RAY PHOTOELECTRON SPECTROSCOPY (XPS)

X-ray photoelectron spectroscopy (XPS) describes the analysis of a (solid) material, using the photoelectric effect, meaning the emission of an electron due to absorption of X-ray radiation. Typically, Al $K\alpha$ is used as an X-ray source with a photon energy around 1486 eV. Due to the nature of the interaction between condensed matter and electrons, especially the short inelastic mean free path of, e.g., 1–2 nm for metallic systems, makes this analysis a rather surface-sensitive method.

Binary Compounds

YbAl_2 (MgCu₂ type, space group $Fd\bar{3}m$) was measured by XPS in 1985 by Oh et al. at 120, 460, and 750 K. The spectra at the two lower temperatures show the peaks of both Yb^{2+} and Yb^{3+} , with the $4f^{14} \rightarrow 4f^{13}$ and $4f^{13} \rightarrow 4f^{12}$ bands, respectively. At higher temperatures, the intensity of the peak originating from the divalent Yb atoms is reduced, while the trivalent one increases, leading to valences of +2.32 at 120 K, +2.40 at 460 K, and finally +2.53 at 750 K.²⁷³ In 2012, the valence of Yb in YbAl_2 was analyzed by HAXPES using hard X-ray radiation of 7.94 keV for excitation at 20 K, allowing the Yb 3d core levels to be shown. In the spectrum recorded at 20 K, the Yb 3d core levels can be seen at 1515–1540 eV ($3d_{5/2}$) and 1560–1585 eV ($3d_{3/2}$). The spectra at 20 and 300 K both show Yb^{2+} and Yb^{3+} species, leading to a mean valence of +2.20, staying nearly unchanged below 300 K.¹¹⁶

The valence of YbAl_3 (Cu₃Au type, space group $Pm\bar{3}m$) was analyzed using XPS by Buschow et al. in 1977. The Yb 4f spectra show a peak multiplet extending from 5 to 10 eV, corresponding to Yb^{3+} . Also, a spin doublet is visible from 0 to 3 eV, indicating divalent Yb, but no mean valence of the compound could be calculated from the measured spectra.²⁷⁴ Later, in 1996, YbAl_3 was measured by XPS, with a well-resolved doublet of divalent Yb and the multiplet of trivalent Yb. The mean valence of YbAl_3 was determined to be +2.63 based on the recorded XPS spectra.²⁷⁵ The nearly same results were reported by Joyce et al. in 2001, measuring YbAl_3 around 20 K showing both Yb valence species in the spectra with a mean valence around +2.6.²⁷⁶

YbCu_2 and YbAg_2 (both KHg₂ type, space group $Imma$), YbAu_2 (MoSi₂ type, space group $I4/mmm$), and YbNi_5 (CaCu₅ type, space group $P6/mmm$) were measured by XPS to determine the valence states of ytterbium in these compounds. The measured spectra show the 4f and the 5p levels. As expected, the trivalent Yb compound YbNi_5 has peaks only in the region of Yb^{3+} while YbCu_2 , which is purely divalent, shows the two peaks corresponding to Yb^{2+} . YbAg_2 on the other hand, exhibits a small trivalent signal due to oxidic impurities. According to the unit cell volume, YbAu_2 should possess a trivalent Yb state, but the XPS measurements showed not only the Yb^{3+} peaks, but also the more intensive peaks of divalent Yb in the spectra, indicating YbAu_2 to rather be an intermediate valence system, compared to YbCu_2 .²⁷⁷

The valence fluctuating compound YbB_{12} (UB₁₂ type, space group $Fm\bar{3}m$) was investigated at room temperature, showing the Yb^{2+} doublet at 0–3 eV and the Yb^{3+} multiplet between 5

and 12 eV. The mean valence of Yb was determined to be +2.9.²⁷⁸

Finally, Yb_4As_3 , Yb_4Sb_3 , and Yb_4SbBi_3 (all Th₃P₄ type, space group $I43d$) are also known to be valence fluctuating compounds. The XPS spectra, measured at room temperature, all show the peaks for divalent and trivalent Yb, although the Yb^{3+} peak in Yb_4Bi_3 is of low intensity. After analyzing the Yb 4f spectra, the mean Yb valences were calculated to be +2.32, +2.34, and +2.10 for Yb_4As_3 , Yb_4Sb_3 , and Yb_4Bi_3 , respectively.²⁷⁹

Equiatomic Compounds

YbAuMg crystallizes in the orthorhombic TiNiSi type structure (space group $Pnma$), and its electronic structure was investigated by XPS measurements. The spectrum was recorded at room temperature with Al $K\alpha$ excitation radiation (1486.6 eV), showing the two peaks for divalent Yb $4f_{7/2}$ and $4f_{5/2}$ at 0.5 and 1.7 eV binding energy, rendering the system purely divalent.²⁸⁰

Further Ternary Compounds

The tetrelides YbNi_2Ge_2 , YbPd_2Si_2 , and YbCu_2Si_2 all crystallize in the ThCr₂Si₂ type structure (space group $I4/mmm$). Their spectra show the 4f level and 4d core levels; in all of them, Yb^{3+} and Yb^{2+} are visible, and the divalent peaks are in the range of 0–2 eV for the 4f level and around 185 eV in the 4d spectra. The signal from the trivalent atoms forms a multiplet ranging from 5 to 12 eV and centered around 195 eV for the 4f and 4d spectra, respectively. Due to the presence of the two Yb valence species, these compounds are mixed valent.²⁸¹

The valence of Yb in YbInCu_4 was investigated by Maeda et al. in 2019 using HAXPES with an excitation energy of 8915–8965 eV at 20 and 70 K. The Yb $3d_{5/2}$ spectra show a Yb^{2+} single peak at 1520 eV and the Yb^{3+} multiplet at 1525–1540 eV. With lower temperature, the intensity of the divalent Yb increases, while the trivalent Yb decreases. The mean valence at 70 K is +2.91 and +2.67 at 20 K.²⁸² Before this, investigation on $\text{Yb}_{0.5}\text{In}_{0.5}\text{Cu}_2$ via XPS measurements at 20 K and excitation energies of 90 to 500 eV also showed both species present in the spectra. A valence of +2.6 was calculated from the data.²⁷⁶ The series of YbInCu_4 , YbCdCu_4 , and YbMgCu_4 was investigated between 10 to 300 K. The Yb 4d XPS spectra show both Yb species in all samples. The valence of the Cd- and In-containing compounds gradually decreases with decreasing temperature, while the valence in YbMgCu_4 does not change to lower temperatures.²⁸³ Upon replacing In with a precious metal like Ag, Au, and Pd, YbAgCu_4 , YbAuCu_4 and YbPdCu_4 can be obtained. The electronic structure of these three compounds was investigated by Kang et al. The XPS spectra were recorded with Al $K\alpha$ radiation and an excitation energy of 1486.6 eV at a temperature around 110 K. The spectra show the 4f line of Yb and the Cu 3d, Pd 4d, Pt 5d, and Ag 4d lines. Due to the overlap of the transition metal signals with the emission of divalent Yb between 0 and 4 eV, no valence can be reliably determined. However, based on the high intensity of the trivalent Yb multiplet, it can be assumed that the three compounds have a valence close to Yb^{3+} and also that the Pd containing compound is closer to the trivalent state than the Au- and Ag-containing ones.²⁸⁴

YbPd_2Al_3 and the solid solution $\text{Yb}_{1-x}\text{Ca}_x\text{Pd}_2\text{Al}_3$ crystallize in the hexagonal YNi_2Al_3 type structure ($P6/mmm$), containing two crystallographically different Yb positions. The solid solution has a mixing of Yb and Ca on both Yb positions. The compounds were analyzed by XPS with Al $K\alpha$ radiation

(1486 eV). The spectra depict the Yb 4d lines and possess five peaks for the Yb³⁺ and two rather small peaks forming a doublet for the Yb²⁺, in which a partial overlap of the trivalent multiplet with the divalent Yb peaks occurs. The calcium-substituted samples Yb_{0.33}Ca_{0.67}Pd₂Al₃ and Yb_{0.67}Ca_{0.33}Pd₂Al₃ became oxidized due to the handling in air or due the X-ray radiation, leading to an increased Yb³⁺ content, which cannot be used to determine the real amount of Yb²⁺ in the samples.⁶⁷

The Kondo lattice compounds Yb₂Al₁₅Pt₆ and Yb₂Ga₁₅Pt₆ were investigated via XPS at an excitation energy of 5.95 keV at 20 to 300 K. The Yb 3d levels indicate the presence of both di- and trivalent Yb. Also, in the Al-containing compound, with decreasing temperature, the intensity of the Yb³⁺ multiplet (1524–1536 eV) decreases and the Yb²⁺ single peak (1520 eV) intensity is observable, shifting the valence from +2.89 at 250 K to +2.83 at 20 K. In comparison, the Ga compound possesses a lower Yb valence of +2.34. However, this valence changes only minimally toward lower temperatures, meaning the Yb valence in Yb₂Ga₁₅Al₆ has nearly no temperature dependence. The peak of divalent Yb is at 1568 eV, and the multiplet of trivalent Yb at 1574–1582 eV.²⁸⁵

Zintl Phases

The Zintl compounds Yb₁₄MnSb₁₁ and Yb₁₄ZnSb₁₁ (both Ca₁₄AlSb₁₁ type, space group *I4₁/acd*) were measured by Holm et al. to analyze the Yb valence by XPS analysis with an excitation energy of 1250 eV. The spectrum for the Mn-containing sample shows the Yb 4s, 4p_{1/2}, 4p_{3/2}, 4d_{3/2}, and 4d_{5/2} core levels corresponding to the binding energies of 486, 395, 345, 197, and 188 eV. For the Zn sample, the Yb levels are slightly shifted and found at 484, 394, 345, 195, and 187 eV. Additional valence band scans with an excitation energy of 120 eV were taken, showing the Yb 4f multiplet for Yb³⁺ and the doublet of Yb²⁺, respectively. Also, it is stated that these compounds are prone to oxidation, leading to a higher amount of Yb³⁺ on the surface. The amount of trivalent Yb for Yb₁₄MnSb₁₁ is small compared to the divalent Yb and originates from the surface oxidation, in comparison to Yb₁₄ZnSb₁₁, which has a higher amount of Yb³⁺, leading to the assumption that trivalent Yb is intrinsically present in the sample, making Yb₁₄ZnSb₁₁ an intermediate Yb valence system.²⁸⁶

The Yb-filled skutterudites Yb_{0.075}CoSb₃, Yb_{0.5}CoSb₃, and YbFe₄Sb₁₂ have been studied by XPS measurements, showing the presence of both Yb²⁺ and Yb³⁺ in these compounds. The binding energies are in good agreement with Yb metal and Yb₂O₃, corresponding to divalent and trivalent Yb, respectively. The doublet for Yb²⁺ is located at 1–2.2 eV, while the multiplet corresponding to Yb³⁺ is between 6 and 14 eV.²⁸⁷

MAGNETIC RESONANCE SPECTROSCOPY

This chapter is supposed to give an overview about studies in which magnetic resonance spectroscopy was applied to intermetallic Yb compounds. Nuclear magnetic resonance (NMR) in these systems can on one hand be used directly on the ytterbium nucleus to investigate the electronic situation on the Yb atom itself, while on the other hand hetero nuclear NMR is important for the measurement of effects concerning the influence of Yb on its surrounding structure.^{288,289}

In addition, electron paramagnetic resonance (EPR) spectroscopy is a valuable option for paramagnetic species. Here most of the studies were conducted to investigate the interesting physical properties such as the Kondo effect or

heavy Fermion behavior.^{290–292} These methods are, so to say, complementary to many other methods like, e.g., structure determination, since NMR spectroscopy is mainly used to confirm the results of the obtained structural models since it is a site-specific technique. Temperature-dependent measurements of both methods can give information about the temperature of possible phase transitions as well as the electronic situations. Here, important information about the interactions of the 4f electrons and the conduction electrons in the intermetallic compounds are obtained.

Nuclear Magnetic Resonance (NMR) Spectroscopy

Starting with Yb NMR spectroscopy itself, it must be mentioned that in theory the application of NMR spectroscopy to two different Yb isotopes could be possible: ¹⁷¹Yb (*S* = 1/2, 14.3% natural abundance, 7.4 MHz T⁻¹) and ¹⁷³Yb (*S* = 5/2, 16.4% natural abundance, 1.3 MHz T⁻¹).²⁸⁸ In literature, to the best of our knowledge, except for the very first study on Yb metal, no ¹⁷³Yb study has been conducted, which is obviously due to the higher resonance frequency and the absence of a quadrupole moment in ¹⁷¹Yb.²⁸⁸

As for all compounds with ytterbium, the successful application of magnetic resonance is limited to the diamagnetic closed-shell systems. Besides Yb, only Sc, Y, La, and Lu can play a role here. Therefore, in principle one must exclude the trivalent Yb which has a paramagnetic ground state (4f¹³). The magnetic moment of Yb³⁺ leads to extremely short relaxation times and therefore to substantial line broadening and makes the detection of a NMR signal impossible.²⁸⁸ However, examples making use of these significant facts have been reported.

¹⁷¹Yb NMR

In one of the already mentioned early studies²⁸⁹ of ¹⁷¹Yb NMR spectroscopy, the resonance of metallic Yb and the resonance in the intermetallic aluminide YbAl₂ (MgCu₂ type, space group *Fd3m*) were compared to other divalent ionic species, namely YbCl₂ (SrI₂ type, space group *Pbca*) and YbS (NaCl type, space group *Fm3m*). Knight shifts were determined to be around 0 ppm in the metal and about 7.76% in the intermetallic compound YbAl₂. No temperature dependence of the measured Knight shift was found.²⁸⁹

In a following study, the two aluminides YbAl₂ (MgCu₂ type, space group *Fd3m*), and YbAl₃ (Cu₃Au type, space group *Pm3m*) as prototypes for temperature dependent valence fluctuating systems were investigated with NMR spectroscopy. Here it was possible to detect a signal for the magnetic Yb³⁺ ion at low temperatures (1.4 to 4.2 for YbAl₃ and 4.2–80 K in the case of YbAl₂), which is hardly the case in other studies. A determination of the hyperfine field and the relaxation rates has been carried out as well. An extremely large Knight shift of ~100% was identified in YbAl₃.²⁹³ In a recent ²⁷Al-NMR and Raman spectroscopic study, the partially divalent character of Yb in the cubic Laves phase YbAl₂ at room temperature was investigated by comparing the s electron densities with the observed isotropic resonance shifts $\delta(^{27}\text{Al})$. Here, Yb is not comparable to the results obtained for the formally trivalent diamagnetic members of the series.²⁹⁴

The Kondo semiconductor YbB₁₂ (UB₁₂ type, space group *Fm3m*) has been characterized at low temperatures using ¹¹B as well as ¹⁷¹Yb NMR spectroscopy.^{295,296} It was possible to observe a spin-echo signal at temperatures below 15 K for ¹⁷¹Yb. In this case, the results of the 1/T₁ relaxation of ¹⁷¹Yb is in contrast with the previous ¹¹B experiments. It is suggested

that the large susceptibility arises from magnetic moments of the Yb^{3+} ion, which stands in contrast to results obtained via ^{11}B NMR spectroscopy. The effect of such a behavior is still not fully understood.²⁹⁵ The studies discussed above show the rare case of the occurrence of a detectable NMR signal for trivalent or valence fluctuating, magnetic ytterbium. Here, the NMR signal is found at drastic shifts compared to divalent ionic Yb standards.

In agreement with the structural analysis of $\text{Yb}_3\text{Ag}_4\text{Mg}_{12}$ ($\text{Gd}_3\text{Ru}_4\text{Al}_{12}$ type, space group $P6_3/mmc$) via X-ray diffraction (one Yb site), one single resonance for the ^{171}Yb NMR spectra was observed. The temperature-dependent magnetic susceptibility measurements for this compound show the characteristics of a diamagnetic material, underlining the divalent character of Yb. The resonance of the strongly broadened spectrum recorded under static conditions applying the WURST-CPMG pulse sequence is found to be between 6800 and 7000 ppm, indicating a strong positive Knight shift. Between 200 and 300 K, the temperature dependence of the resonance shift was negligible, suggesting a strong orbital contribution to the Knight shift.⁹⁹

Recently, the influence on the ^{171}Yb NMR signal, when substituting ternary Yb compounds with Ca, was shown. The divalent, ternary compounds YbZnSn (NdPtSb type, space group $P6_3mc$), YbPdSn_2 , and YbAuIn_2 (both MgCuAl₂ type, space group $Cmcm$) as well as the solid solutions ($\text{Yb}_{0.5}\text{Ca}_{0.5}\text{ZnSn}$, ($\text{Yb}_{0.5}\text{Ca}_{0.5}\text{PdSn}_2$, and ($\text{Yb}_{0.5}\text{Ca}_{0.5}\text{AuIn}_2$) were investigated with ^{171}Yb NMR spectroscopy applying static WURST-CPMG pulse sequences.²⁹⁷ For all three ternary samples, the obtained results are in excellent agreement with the structural investigations and the magnetic susceptibility data for the compounds. In all cases, a single broadened ^{171}Yb spectrum could be recorded, indicating one crystallographic Yb site and underlining the diamagnetic character of Yb^{2+} in this compound. For YbAuIn_2 , the magnetic susceptibility data suggest paramagnetic impurities (resulting from intermediate-valent YbAuIn) in higher amounts than for the other compounds, which is given as the reason why here only a poor signal-to-noise-ratio was achieved in the NMR spectroscopic data. After Ca incorporation, a shift for the center of gravity as well as a line broadening is observed. This is due to the different local surrounding caused by the statistic mixing in a solid solution. As an example, the obtained NMR spectra are shown in Figure 13.

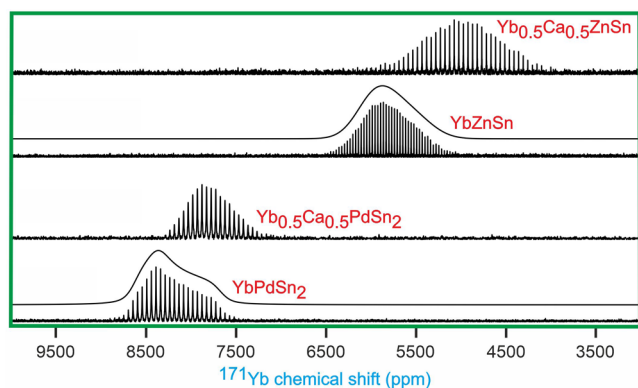


Figure 13. NMR spectra of YbZnSn and YbPdSn_2 and the respective Ca-substituted variants $\text{Yb}_{0.5}\text{Ca}_{0.5}\text{ZnSn}$ and $\text{Yb}_{0.5}\text{Ca}_{0.5}\text{PdSn}_2$.²⁹⁷

The germanide YbPtGe_2 crystallizes in the orthorhombic YrGe_2 type structure (space group $Immm$) with two distinct Yb sites. Via ^{171}Yb NMR spectroscopy, it was possible to prove that indeed two distinct Yb sites are present. Moreover, it becomes evident that one site is nearly divalent, while the Yb atoms on the other site are nearly trivalent. The authors explain this by the rather small shift of the observed signal. As mentioned above, in the case of paramagnetic ytterbium ions, larger Knight shifts are expected. Therefore, YbPtGe_2 is named a multivalent charge-ordered compound having two different Yb valences in one compound, with no dynamic behavior.²⁹⁸

Finally, in the compound YbGaGe (YPtAs type, $P6_3/mmc$) which has two Yb sites in an equivalent coordination, it is quite remarkable that, in a combined ^{171}Yb and $^{69,71}\text{Ga}$ NMR spectroscopic study, the two different Yb sites could be identified separately from each other in NMR spectra recorded at 4.2 K, confirming the proposed crystal structure. Here, no hints for trivalent or valence fluctuating Yb atoms could be found. The Knight shifts are reported with 0.41% (4100 ppm) and 1.1% (11000 ppm), respectively, being in the typical range of divalent nonmagnetic ytterbium compounds.²⁹⁹

EPR

In contrast to the already discussed NMR spectroscopic studies on intermetallic Yb compounds, in which Yb should preferably be in the divalent state, an EPR signal should be detectable, when paramagnetic species such as the open-shell Yb^{3+} are present. Furthermore, it is possible to obtain electron spin resonance spectra which occur due to conduction electrons. Therefore, EPR spectroscopy is a method that is able to probe the local moments of unpaired 4f electrons of a lanthanide atom as well as the interaction with the surrounding delocalized conduction electrons.²¹¹ By temperature-dependent measurements of the g tensor and the line width of the signal, information about the ground state of f electron systems responsible for some important phenomena can be obtained.³⁰⁰ For the determination of the valence state of the Yb atom, the results of EPR spectroscopy can be combined with magnetic measurements. In many recent studies, EPR spectroscopy has been applied to investigate Yb compounds with exceptional low temperature physical properties, such as the Kondo effect and heavy Fermion behavior.

In Kondo systems, the EPR signal should be affected by the Kondo effect in two ways: a temperature-dependent g shift due to the local susceptibility and an additional contribution to the EPR line width.³⁰¹ At this point, it is interesting to note that it seems to be necessary to have ferromagnetic fluctuations in samples to observe any EPR signal, which could be shown by a study of antiferromagnetic (CeOsPO) and ferromagnetic (CeRuPO) samples, since only the latter give rise to an EPR signal.³⁰²

In this chapter, only some selected EPR spectroscopic studies on the most prominent examples of intermetallic Yb compounds shall be summarized. As already mentioned, this quite often goes hand-in-hand with exceptional physical properties of these compounds.

In the first part, some examples will be discussed in which the rare earth atoms were introduced as a substituent/dopant/impurity. Later, it was shown that it is possible to receive experimental EPR spectroscopic data on phase-pure unsubstituted/undoped Yb samples, so to say in a dense lattice.

In many systems, it was not possible to obtain EPR spectra and thereby information about the electronic structure of rare

earth atoms by applying EPR spectroscopy on dense lattice systems. Due to ultrafast relaxation times, a doping or substitution of paramagnetic ions into diamagnetic compounds is necessary.²⁹⁰ One example for this is the EPR spectrum of ytterbium recorded in elemental gold (800 and 1600 ppm). Here, temperature-dependent measurements between 0.1 and 1 K resulted in the observation of a nonlinear behavior of the line width when lowering the temperature. This could be attributed to the Kondo effect.³⁰¹ In a study for the Yb-doped samples (100 up to 1000 ppm) with the composition MPd_3 ($M = Sc, Y, Lu, La,$ and Ce), crystallizing in the cubic Cu_3Au structure ($Pm\bar{3}m$), for all tested metals ($Er^{3+}, Gd^{3+},$ and Yb^{3+}), a Γ_7 ground state indicating trivalent character of the ytterbium was found. The EPR spectrum of YPd_3 (1000 ppm Yb) given in reference³⁰⁰ is affected by the hyperfine interaction of the localized moment with the two isotopes ^{171}Yb and ^{173}Yb resulting in additional satellites besides the central transition.

Some examples of EPR spectra of Yb in undoped nonmetallic phases such as hydride (YbH_x)³⁰³ or oxide phases ($Yb_xY_{1-x}Ba_2Cu_3O_y$)³⁰⁴ are reported. In these systems, a narrowing of the observed EPR line is described because of the spin-glass ordering and the absence of heavy Fermion behavior as well as exchange narrowing. In an early example, it is reported that the temperature-dependent EPR spectra of pure $YbBe_{13}$ and substituted diamagnetic $Y_{1-x}Yb_xBe_{13}$ ($x = 0.01$ and 0.09) are identical, which is linked to the rather large separation of ~ 500 pm of the rare earth atoms in the $NaZn_{13}$ type structure ($Fm\bar{3}c$), leading to a small crystal field splitting ($\Gamma_7 \rightarrow \Gamma_6 \rightarrow \Gamma_8$) and next to no interaction between the magnetic moments except for some RKKY exchange. For the exact CEF, the differences in the literature were already discussed above. In this EPR spectroscopic study, the valence state of Yb was determined to be trivalent with a Γ_7 ground state, equivalent to Eu and Sm, and in contrast to Ce which is in an intermediate valence state in this structure type.²³⁶

When looking in the literature, the application of EPR spectroscopy to intermetallic Yb compounds showing heavy Fermion behavior is the most prominent one. Especially, the compound $YbRh_2Si_2$ was the first compound in which the direct investigation of the EPR signal of the rare earth ion responsible for the Kondo effect, up to 25 K, so below and above the Kondo temperature, without any doping, substitution, or impurities, was possible. The detection of the signal was thought to be impossible until this proof. In previous studies of doped samples (e.g., with Gd^{3+}), one cannot exclude the influence of the dopant on the Kondo lattice. The exact origin of the EPR signal in this dense Kondo lattice below the relatively high Kondo temperature of $T_K = 20$ K in this compound is yet unclear.^{158,305,306} A similar EPR signal could be detected a little later in the isostructural silicide $YbIr_2Si_2$. The results are in good agreement with those of the Rh compound. Way below the Kondo temperature of 40 K, it was possible to detect a strong EPR signal down to 1 K. Therefore, it is the second example of strong, intense EPR lines in a dense Kondo heavy Fermion system.³⁰⁷ In the past years, more examples of direct EPR detection in heavy Fermion compounds were reported. For $YbNiAl_2$, the trivalent state of the Yb atom was confirmed by measuring an intense EPR spectrum below 20 K. However, here the authors mention that the intensity of the signal obtained at temperatures below 20 K was about an order of magnitude lower than for $YbRh_2Si_2$. By increasing the temperature, the EPR signal disappeared. The reason for the appearance of the EPR signal at low

temperatures in this dense heavy Fermion compound is not only the already mentioned ferromagnetic fluctuations but also magnetic anisotropy as well as cumulative effects of the surrounding crystal field and spin-orbit interactions.³⁰⁸

For the case of the above-mentioned heavy Fermion superconductor β - $YbAlB_4$, an interesting dual nature behavior of the EPR signal was observed. At high temperatures, an EPR signal was found for the Yb as well as for the Pauli-paramagnetic Lu compound. The Lu compound shows the characteristic temperature dependence of a conduction electron spin resonance over the whole temperature range (4.2 to 295 K), while in comparison, at 4.2 K, the Yb compound shows a hyperfine splitting caused by the ^{171}Yb isotope, confirming the characteristics of an Yb^{3+} -caused spin resonance. This is a unique behavior of the dual nature observed in EPR spectroscopy.²¹¹

For the compounds $YbBiPt$ and $YbRh_2Pb$, EPR measurements could be performed at temperatures of up to 110 K, although for discussion of the nature of the compounds, measurements at 4.4 K were used. The results give hints about the crystal electric field (CEF) for the Yb^{3+} atom in these ternary compounds. For the plumbide, an extremely small hybridization of the 4f electrons and the conduction electrons is suggested together with weak RKKY interactions. In contrast, the bismuthide shows a strongly broadened CEF due to large hybridization effects.²⁹⁰ In this context, one must mention one important class of isostructural compounds. All Yb compounds with the general formula YbT_2Zn_{20} ($T = Fe, Co, Ru, Rh, Os, Ir$)³⁰⁹ exhibit heavy Fermion behavior. Therefore, a comparison of the spectroscopic properties such as for the above-mentioned silicides $Yb(Ir,Rh)_2Si_2$ was possible.³⁰⁹ Here, the Co and Fe compounds have been investigated with EPR spectroscopy. In an analogous way to the already mentioned studies, it was possible to detect a spectrum without any dilution or paramagnetic impurity. A direct investigation of the dense Yb lattice was possible.^{290,305,309} A comparison of the EPR absorption of the Co and Fe compounds (Figure 14) gave hints about the

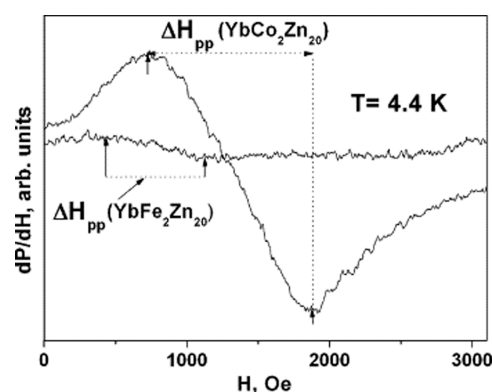


Figure 14. EPR spectra of $YbCo_2Zn_{20}$ and $YbFe_2Zn_{20}$. Reprinted from ref 290 with permission from Elsevier.

involvement of the d electrons of the magnetic atoms. With the Co compound EPR absorption being higher by a factor of 10, it was proposed that the increasing number of available d electrons also plays a crucial role in the intensity of the EPR signal and not only the localized magnetic moment of the f electrons on the rare earth atom.

¹⁷⁰Yb MÖSSBAUER SPECTROSCOPY

¹⁷⁰Yb is a Mössbauer-active isotope and thus allows studies of the ytterbium valence state, the coordination geometry, and magnetic hyperfine field splitting. The energy E_γ amounts to 84.25 keV. The decisive point for ¹⁷⁰Yb Mössbauer spectroscopic studies is the very low natural abundance of ¹⁷⁰Yb of only 3%, forcing long data collection times. The basic nuclear moment data for the different ytterbium isotopes (¹⁷⁰Yb, ¹⁷¹Yb, ¹⁷²Yb, ¹⁷⁴Yb, ¹⁷⁶Yb) have been summarized by Stevens and Dunlap;³¹⁰ however, ¹⁷⁰Yb is the usually studied isotope. Its basic Mössbauer spectroscopic characteristics are: $I_c = 2$ (nuclear spin operator in the excited state); $I_g = 0$ (nuclear spin quantum number in the ground state); transition energy of 84.25 keV; TmB_{12} as the usual source (typically 20 mCi) with a half-life of 130 d; and natural line width of 2.03 mm s⁻¹.^{288,311–313}

The ¹⁷⁰Yb isomer shift values for divalent and trivalent ytterbium vary only over a small range. For purely ionic compounds, representative values are $\delta = -0.49$ mm s⁻¹ for Yb^{II}SO₄ and +0.09 mm s⁻¹ for Yb^{III}Cl₃.³¹¹ It is clear that this marginal separation of the Yb^{II} and Yb^{III} isomer shifts hampers the studies of valence changes.³¹⁴ However, the ¹⁷⁰Yb data is very sensitive to the hyperfine splitting of the nuclear energy levels and thus allows detailed studies of the magnetic ordering phenomena. The basics for the ¹⁷⁰Yb Mössbauer spectroscopic data with respect to magnetic hyperfine splitting are summarized in a concise resource letter by Cadogan and Ryan.³¹² In the large field of ytterbium intermetallics, the magnetic ordering of the trivalent compounds often sets in only at very low temperatures. Consequently, ¹⁷⁰Yb Mössbauer spectra have frequently been measured down to the mK range. Determination of the quadrupole splitting parameter is the important feature for discriminating divalent and trivalent ytterbium. Yb^{II} has a filled 4f shell and thus no 4f contribution to the electric field gradient at the ¹⁷⁰Yb nucleus. The Yb^{III} compounds, in contrast, show paramagnetic quadrupole triplets.³¹⁵ Typical examples for divalent ytterbium intermetallics are the binary ytterbium–cadmium phases YbCd, YbCd₂, Yb₁₄Cd₅₁, YbCd_{5,7}, and YbCd₆³¹⁶ or the ternary stannide Yb₃Pd₂Sn₂.^{317,318}

The magnetically ordered Yb^{III} compounds show more or less well-resolved hyperfine field splitting. From the hyperfine field value H_{hf} , one can derive the ordered moment μ through the relation $H_{hf} = C\mu$ with a value of $C = 102$ T/ μ_B for Yb³⁺ (derived from accurate measurements of the paramagnetic hyperfine constant of ¹⁷⁰Yb³⁺ in the cubic Γ_7 state).^{319–321} Due to the meaninglessness of the isomer shift value, the ¹⁷⁰Yb Mössbauer spectroscopic studies on intermetallic compounds only report on the quadrupole splitting parameters and the magnetic hyperfine fields.

Temperature-dependent measurements in the magnetically ordered regimes allow for monitoring the evolution of the magnetic hyperfine field with decreasing temperature. These data can be fitted with an $S = 1/2$ law, and the magnetic ordering temperature can be derived as complementary experiment to the magnetic characterization. Data of binary Yb₃Pd₄³²² is presented in Figure 15. Further related examples are YbNiBC,³²³ or samples from the solid solution Yb₅Si_xGe_{4-x}.³²⁴ In several cases, the crystal field properties have also been derived from the ¹⁷⁰Yb Mössbauer spectroscopic data and compared to L_{III} -edge X-ray absorption spectra

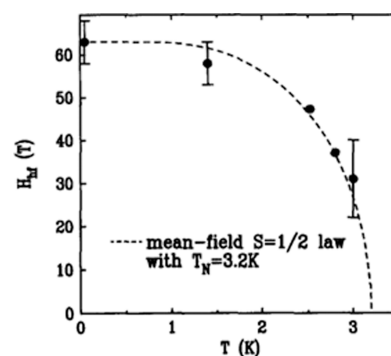


Figure 15. Temperature dependence of the hyperfine field at the ¹⁷⁰Yb nuclei in Yb₃Pd₄ ($T_N = 3.2$ K). The thermal variation follows an $S = 1/2$ mean field law (dashed line). Reprinted from ref 322 with permission from Elsevier.

and magnetic data. An exemplary investigation is the ¹⁷⁰Yb Mössbauer spectroscopic characterization of YbCu₃Al₂.³²⁵

Early work on ¹⁷⁰Yb Mössbauer spectroscopic data focused on the rocksalt type monopnictides YbP, YbAs, and YbSb (space group $Fm\bar{3}m$),^{326–328} which are Kondo-frustrated antiferromagnets with very low Néel temperatures <1 K (Table 3). Although the three phases have cubic symmetry, inhomogeneous hyperfine fields/hyperfine field distributions have been observed. Thus, ¹⁷⁰Yb Mössbauer spectroscopy is an excellent complementary tool for monitoring structural distortions. In the following, many other binary, ternary, and quaternary intermetallic phases have been characterized through their ¹⁷⁰Yb Mössbauer spectra. Some selected phases, which all have their own peculiarity, are shortly discussed in the following.

The incommensurate modulated structure of YbPtAl (TiNiSi type, space group $Pnma$, wave-vector $k = 0.30, 0, 0$) was studied by a combination of neutron powder diffraction and ¹⁷⁰Yb Mössbauer spectroscopic data.³²⁹ The low-temperature spectroscopic data (0.025 K) clearly shows that the modulated structure is not an antiphase one. The maximum moment of 2.5 μ_B was derived from the 1.6 K spectrum.

The ¹⁷⁰Yb Mössbauer spectroscopic data of YbNiAl₄ (YNiAl₄ type, space group $Cmcm$) is an important complementary result to specific heat data. While the latter points to the onset of magnetic ordering, no hyperfine field splitting is evident from the ¹⁷⁰Yb Mössbauer spectra down to 1.5 K.²³ This is consistent with an intermediate ytterbium valence, since the temperature dependence of the magnetic susceptibility also revealed a substantially reduced experimental magnetic moment.

The ytterbium valence change induced by substitution was studied for the solid solutions Yb₅Ge_{4-x}(Sb,Ga)_x with $x \leq 1$ (Sm₅Ge₄ type, space group $Pnma$).³³⁰ For influencing the ytterbium valence, the germanium atoms are partially substituted by gallium with lower and antimony with higher electron count. The Yb^{II}/Yb^{III} ratio could be derived from well-resolved ¹⁷⁰Yb Mössbauer spectra at 5 K through the subsignals with and without quadrupole splitting (vide infra). The Mössbauer spectroscopic data show an almost gradual increase of the Yb^{II}/Yb^{III} ratio from ~0.95 for Yb₅Ge₃Ga to ~1.55 for Yb₅Ge₃Sb.

The quadrupolar phase transition at 80 K in YbAl₃C₃ (ScAl₃C₃ type, space group $P6_3/mmc$) was monitored by ¹⁷⁰Yb Mössbauer spectroscopy.³³¹ Spectra were collected in the

Table 3. ^{170}Yb Mössbauer Spectroscopy Derived Parameters for Selected Intermetallic Ytterbium Compounds^a

| Compound | Structure Type | T_M/K | T_{MB}/K | B_{hf}/T | μ/μ_B | Reference |
|-------------------------------------|-------------------------------------|----------------|-------------------|--------------------------|-------------|-----------|
| YbBe_{13} | NaZn_{13} | $T_N = 1.28$ | 0.05 | 172 | 1.73 | 336 |
| YbB_{12} | UB_{12} | — | 0.04 | <10 | <0.1 | 337 |
| YbP | NaCl | $T_N = 0.41$ | 0.045 | 81 | 0.79 | 326 |
| YbAs | NaCl | $T_N = 0.58$ | 0.045 | 81 | 0.82 | 326 |
| YbSb | NaCl | $T_N = 0.32$ | 0.045 | 64 | 0.63 | 326 |
| YbNi_5 | CaCu_5 | $T_C = 0.55$ | 0.05 | 399(2) | 3.9 | 338 |
| Yb_3Pd_4 | Pu_3Pd_4 | $T_N = 3.2(1)$ | 0.05 | 63(5) | 0.62(5) | 322 |
| YbCu_3Al_2 | PrNi_2Al_3 | $T_N = 1.95$ | 0.12 | 290(10) | 2.84(10) | 325 |
| YbPtAl | TiNiSi | $T_N = 5.8$ | 4.2 | 159 | 1.56 | 329 |
| $\text{Yb}_3\text{Cu}_4\text{Ge}_4$ | $\text{Gd}_3\text{Cu}_4\text{Ge}_4$ | $T_N = 7.5$ | 1.45 | 370 | 3.6 | 332 |
| | | | | 148 | 1.45 | |
| $\text{Yb}_2\text{Co}_3\text{Al}_9$ | $\text{Y}_2\text{Co}_3\text{Al}_9$ | $T_N = 1.2$ | 0.06 | 95 | 0.93 | 333 |
| YbNiSb | MgAgAs | $T_N = 0.85$ | 0.13 | 108(10) | 1.06(10) | 334 |
| YbNiSn | TiNiSi | $T_N = 5.65$ | 1.48 | 870(20) | 0.85(2) | 125 |

^aParameters include: magnetic ordering temperature, T_M ; measurement temperature for the Mössbauer spectrum, T_{MB} ; magnetic hyperfine field, B_{hf} ; and magnetic moment at the ^{170}Yb nuclei, μ . Note that $\text{Yb}_3\text{Cu}_4\text{Ge}_4$ shows two sub-spectra with different hyperfine fields. Standard deviations are given in parentheses, when available.

entire range from 0.04 to 150 K. No magnetic ordering of the Yb^{3+} moments was evident down to the lowest measurement temperature. The symmetry reduction (loss of the mirror plane perpendicular to the 6_3 screw axis) is well expressed in the course of the quadrupole splitting in the ^{170}Yb spectra in the sequence 85 K \rightarrow 80 K \rightarrow 77 K \rightarrow 75 K with a nonaxial quadrupolar hyperfine interaction in the low-temperature phase. Also in this case, ^{170}Yb Mössbauer spectroscopy served as a valuable complementary probe for studying a structural phase transition.

$\text{Yb}_3\text{Cu}_4\text{Ge}_4$ with $\text{Gd}_3\text{Cu}_4\text{Ge}_4$ type structure (space group $Immm$) is one of the remarkable ytterbium intermetallics, since it exhibits two crystallographically independent ytterbium sites $4e$ and $2d$.³³² Although the magnetic data indicate a single transition temperature into the magnetically ordered state, these two ytterbium sites show distinctly different magnetic hyperfine spectra (Figure 16) with ordered moments of $3.6 \mu_B$ for the $4e$ and $1.45 \mu_B$ for the $2d$ site. Integration of the subspectra is consistent with the 2:1 multiplicity of the individual Wyckoff positions.

^{170}Yb Mössbauer spectroscopy was employed to differentiate the magnetic behavior of the Yb atoms in the isotopic compounds $\text{Yb}_2\text{Co}_3\text{Al}_9$ and $\text{Yb}_2\text{Co}_3\text{Ga}_9$ ($\text{Y}_2\text{Co}_3\text{Ga}_9$ type, space group $Cmcm$).³³³ The aluminum compound shows a stable $^2F_{7/2}$ ground state and well-resolved hyperfine field splitting (95 T) at 0.06 K, while $\text{Yb}_2\text{Co}_3\text{Ga}_9$ is a paramagnetic heavy-Fermion material showing no hyperfine field splitting over the whole temperature range.

The solid solution $\text{Yb}_{1-x}\text{In}_x\text{Cu}_2$ is structurally derived from the cubic Laves phase (space group $Fd\bar{3}m$, vide ultra). The sample with the composition $\text{Yb}_{0.4}\text{In}_{0.6}\text{Cu}_2$ shows a sharp valence transition around 50 K. ^{170}Yb Mössbauer spectra at 4.2 K indicate that the Yb^{3+} ions exhibit no magnetic hyperfine field splitting in the cubic environment; however, it shows a strong $4f$ – $5d$ hybridization.¹⁹¹

The final example shows the necessity of complementary techniques for the precise understanding of structure–property relations. The half-Heusler phase YbNiSb (MgAgAs type, space group $F\bar{4}3m$) has been characterized through ^{170}Yb Mössbauer spectra at 0.13 and 1.4 K.³³⁴ Spectra in the magnetically ordered regime revealed enlarged and inhomogeneous line widths. Based on these results, it was argued that the

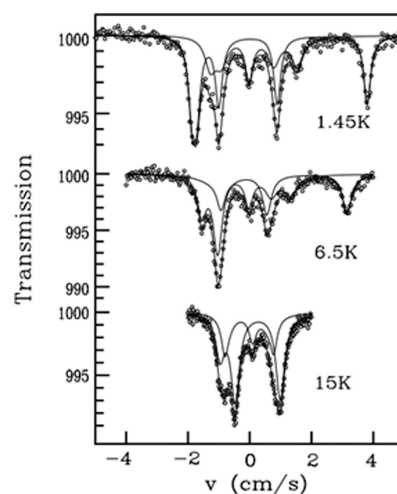


Figure 16. ^{170}Yb Mössbauer spectra of $\text{Yb}_3\text{Cu}_4\text{Ge}_4$. The spectrum at 15 K was taken in the paramagnetic range, while the 1.45 and 6.5 K spectra are derived from the magnetically ordered phase. The subspectra are marked by different solid lines. Reprinted from ref 332 with permission from Elsevier.

quadrupolar hyperfine interaction of the paramagnetic phase has no cubic site symmetry. Later, precise single crystal X-ray diffraction data showed that YbNiSb samples are a mixture of equiatomic YbNiSb as the main component along with a distribution of YbNi_xSb domains with different nickel content.³³⁵ Thus, the magnetically split spectrum is a superposition of the magnetically split subspectra of the distribution of YbNi_xSb domains.

Many other interesting examples for ^{170}Yb Mössbauer spectroscopic studies on ytterbium intermetallics have been published. In such a review, one can only present selected examples. Besides the data discussed above, we have added some further examples in Table 3 with respect to their basic Mössbauer spectroscopic data.

Besides the many ^{170}Yb Mössbauer spectroscopic studies under ambient conditions, some investigations were carried out under application of external magnetic fields or high pressure. The heavy Fermion silicide YbRh_2Si_2 was additionally studied by ^{170}Yb Mössbauer spectroscopy as a complementary

tool to ESR spectroscopy.³³⁹ The ESR data for this silicide gave hint for a slow relaxation rate. This issue could be clarified by ¹⁷⁰Yb Mössbauer spectroscopy. The ¹⁷⁰Yb spectrum only shows a single signal, which does not match with a simulated spectrum for slow relaxation at an applied field of 0.4 T. The ¹⁷⁰Yb data thus indicate that the Yb³⁺ ions relax more rapidly than expected from the ESR data. YbRh₂Si₂ was furthermore studied at 1.3 K and pressures ranging from 6.4 to 16.5 GPa.³⁴⁰ The experiments show a continuous line broadening with increasing pressure. The pressure-induced first-order magnetic phase transition sets in around 10 GPa. The line broadening indicates increasing magnetic hyperfine field splitting and thus an increase of the ordered moment at the ytterbium nuclei with a value of 1.9 μ_B (≡191 T) at 16.5 GPa, still reduced when compared with the free ion value of 4 μ_B.¹⁰⁵

The technical details for ¹⁷⁰Yb Mössbauer spectroscopy under high-pressure conditions are well documented in an article by Schöppner et al.,³⁴¹ which focuses on the pressure-induced ytterbium valence change in YbCuAl (ZrNiAl type, space group *P6̄2m*). The compound was studied at 4.2 K from 0 to 130 kbar pressure. The ¹⁷⁰Yb spectra show a continuous increase of the quadrupole splitting parameter with increasing pressure, manifesting the valence transition toward trivalent ytterbium with 4f³ configuration. This ground state is achieved already at around 50 kbar.

¹⁷⁰Yb Mössbauer spectroscopic data was collected for the TiNiSi type stannide YbNiSn (space group *Pnma*) up to 7 GPa.³⁴² A remarkable feature is the increase of the Curie temperature with increasing pressure with a maximum of *T*_C = 7.6 K at 1.7 GPa followed by a rapid decrease. In parallel, the quadrupole splitting parameter and the magnetic hyperfine field increase from ambient pressure to 7 GPa. The maximum field of 175 T corresponds to an ordered moment of 1.72 μ_B.

Also, the heavy Fermion compound Yb₂Ni₂Al (*W*₂CoB₂ type, space group *Immm*) shows a pressure-driven first-order magnetic phase transition.³⁴³ A crossover from a nonmagnetic heavy Fermion state to a magnetically ordered state occurs at pressures >8 GPa and below 2 K. The ¹⁷⁰Yb Mössbauer spectrum (1.8 K data) at the highest pressure of 9 GPa showed an ordered moment of ≈1 μ_B at the ytterbium nuclei.

Finally, we turn toward an interesting extension of ¹⁷⁴Yb Mössbauer spectroscopy which was realized recently using synchrotron radiation as the Mössbauer spectroscopy source. The classical experiments all used the ¹⁷⁰Yb isotope. The main disadvantage is its low natural abundance of only 3% as compared to 31.8% for ¹⁷⁴Yb. The synchrotron radiation-based technique is described in a resource article by Masuda et al.,³⁴⁴ and exemplified for an YbB₁₂ (*UB*₁₂ type, space group *Fm3̄m*) sample. Further advantages of this new technique are the higher brilliance of the synchrotron radiation as compared to X-rays deriving from a radioactive isotope, and there is no need for isotope enrichment. Along with the use of a windowless avalanche photodiode detector, fast data collections are possible, and this technique will also be helpful for future high-pressure studies. Two further examples for the application of ¹⁷⁴Yb Mössbauer spectroscopy are Yb₃Fe₁₄B (*Nd*₂Fe₁₄B type, space group *P4₂/mnm*)³⁴⁵ and α-YbAlB₄ (*YCrB*₄ type, space group *Pbam*).³⁴⁶

■ THERMOELECTRICS

Thermoelectric materials are usually heavily doped semiconductors which can produce a charge flow when exposed to a temperature gradient. Depending on the charge carrier type

in the respective material, these are denoted as p- or n-type semiconductors. The quality of a thermoelectric material is usually given by the dimensionless figure-of-merit *zT* which basically incorporates the Seebeck coefficient as well as the thermal and electrical conductivity. Details regarding these values and their interplay can be found in a number of reviews.^{347–352} However, the determination of the Seebeck coefficient can also be used for identifying magnetic transitions and other physical phenomena as it is very susceptible to changes in the electronic states. In the following chapter, examples of classical intermetallic Yb-compounds as well as examples of Zintl phases, being the more typical thermoelectric materials, will be addressed.

Binary Compounds

We will start this chapter with selected examples of classical intermetallic materials. For this, the binaries YbAl₃, YbSi₂, YbB₆, YbCd₆, and Yb₃Si₅ as well as the solid solutions Yb_{1-x}Sc_xAl₂, Yb_{1-x}In_xCu₂, and YbCu_{5-x}Ag_x have been chosen. From the ternary systems, equiatomic YbPtBi, YbNiSn, and YbPtGe, as well as YbAlB₄, YbNiAl₄, YbRh₂Al₂₀, and YbT₂Zn₂₀ (*T* = Fe, Co, Ru, Rh, Os, Ir), Yb₂Pt₃Sn₅, Yb₂T₃X₉ (*T* = Rh, Ir; *X* = Al, Ga), Yb₂Pt₆Al₁₅, and Yb₂Ni₁₂P₇ were selected.

YbAl₃ (*Cu*₃Au type, space group *Pm3̄m*) is, as mentioned before, a well studied compound due to the ambivalent nature of the Yb atoms leading to a change of the Yb valence with temperature.¹¹³ Due to this phenomenon, the Seebeck coefficient of intermediate valent/valence fluctuating Yb compounds is often significantly higher than expected. This is also the case for YbAl₃ where the Seebeck coefficient reaches values over -80 μV K⁻¹ near 120 K,³⁵³ and YbSi₂ (*AlB*₂ type, space group *P6/mmm*),³⁵⁴ also a mixed valent compound, shows values between -50 and -35 μV K⁻¹ between 300 and 525 K. The electrical resistivity, however, possesses abnormally large values due to spin-disorder scattering. YbSi₂ shows an almost temperature-independent electrical resistivity and a total thermal conductivity between 8 and 11 W m⁻¹ K⁻¹, leading to a *zT* between 0.08 at 300 K and 0.04 at 525 K. YbB₆ adopts the cubic CaB₆ type structure (space group *Pm3̄m*) and exhibits a certain phase width between *x* = 5.7 and 6.3.³⁵⁵ Therefore, this compound can be used to study and tune the thermoelectric properties. The compounds with *x* = 5.7, 5.9, and 6.0 exhibit a negative Seebeck coefficient of approximately -100 μV K⁻¹ between 300 and 1050 K. In contrast, the samples with *x* = 6.1 and 6.3 start with a positive Seebeck coefficient of +100 μV K⁻¹, which gradually changes to negative values at higher temperatures. YbCd₆, despite the same sum formula, crystallizes in a totally different crystal structure (*YCd*₆ type, space group *Im3̄*). Instead of octahedral B₆ clusters, here a quasi-crystal (QC) approximant with a shell-like structure is present. Both the QC YbCd_{5.7} and the approximant YbCd₆ were investigated with respect to their thermoelectric properties. Both show small positive Seebeck coefficients between +10 and +20 μV K⁻¹. The striking feature is a maximum in the electrical resistivity around 70 K for YbCd_{5.7}. A similar trend can be seen for the different compositions of the quasi-crystals, leading to *zT* values of 5 × 10⁻³ near RT.^{356,357} Finally, Yb₃Si₃ (*Mn*₃Si₃ type, space group *P6₃/mcm*) should be discussed as the last binary representative. Again, this compound is valence instable and shows fluctuations between di- and trivalent Yb, leading to two sign changes in the Seebeck coefficient. Below ~40 K, it is negative with a rather sharp minimum at 10 K, followed by a

broad maximum with positive values ($\sim 13 \mu\text{V K}^{-1}$) around 100 K, and again a change to a negative Seebeck coefficient close to 300 K. The resistivity is, compared to the close-shell system Lu_5Si_3 , enhanced by a factor of close to two, caused again by the valence fluctuation.³⁵⁸

The solid solution $\text{Yb}_{1-x}\text{Sc}_x\text{Al}_2$ (MgCu₂ type, space group $F\bar{d}3m$) was studied to probe the influence of “chemical pressure” on the properties of the valence fluctuating system YbAl_2 . Different compositions with $x = 0.6-1$ were synthesized and investigated. Magnetic susceptibility measurements clearly indicate that the intermediate valence (IV) state gets more pronounced with increasing Sc content and a shift toward more Yb^{3+} is visible. Samples with a pronounced IV state at the same time exhibit a drastically negative Seebeck coefficient up to $-50 \mu\text{V K}^{-1}$ below 50 K for $x = 0.9$. This leads to a maximum in the power factor (S^2/ρ) of $160 \mu\text{W cm}^{-1} \text{K}^{-2}$ for $x = 0.9$ around 50 K.³⁵⁹

Since $\text{Yb}_{1-x}\text{In}_x\text{Cu}_2$ (MgCu₂ type, space group $F\bar{d}3m$) shows a temperature-induced first-order valence phase transition, its Seebeck coefficient was investigated for $x = 0.6$ to probe the fine structure of the conduction electron band closely associated with the magnetic state. The temperature dependence of the Seebeck coefficient starts with a positive sign at high temperatures and exhibits a change of sign near 200 K. Around 40 K, a minimum with $S = -16 \mu\text{V K}^{-1}$ is visible, coinciding with the temperature of the valence phase transition.³⁶⁰

Equiatomic Ternary Compounds

For the ternary compounds, we will start with selected equiatomic representatives, i.e., YbNiSn , YbPdGe , YbPtGe , and YbPtBi . For YbNiSn (TiNiSi type, space group $Pnma$), the thermoelectric properties were studied to obtain further information about the crystal field splitting. Inelastic neutron scattering should yield three crystal field excitations based on the crystal structure. However, only two excitations were visible; therefore, the thermoelectric properties were determined to gain a deeper insight. The temperature dependence of the Seebeck coefficient shows a broad minimum around 100 K along with a peak at 7.5 K and a change of sign below 5 K. From these investigations, the degeneracy of two crystal field excitations was deduced.³⁶¹ YbPdGe (YbAuSn type, space group $Imm2$) and YbPtGe (TiNiSi type, space group $Pnma$) show a very similar behavior. The Seebeck coefficient shows a broad maximum around 120 K followed by a maximum at 30 K. Three contributions were deduced: a Mott's diffusion term as well as a Kondo and a resonance term. While the first one is small and temperature-independent, the Kondo term originates from Kondo scattering of conduction electrons by the 4f spins. The inelastic contribution to the resonance term originates from inelastic scattering of the conduction electrons by magnetic interactive spins, respectively.³⁶² Finally, YbPtBi (MgAgAs type, space group $F\bar{4}3m$) was investigated. This compound is of particular interest since it exhibits one of the largest Sommerfeld coefficients known ($\gamma = 7.4 \text{ J mol}^{-1} \text{K}^{-2}$).¹³⁷ Thin films of YbPtBi exhibit also a negative Seebeck coefficient with $-54 \mu\text{V K}^{-1}$.³⁶³

Further Ternary Compounds

While the silicides and germanides adopt the tetragonal body centered ThCr_2Si_2 type structure (space group $I4/mmm$), the pnictide-based Zintl phases of the same chemical composition crystallize in the trigonal space group $P\bar{3}m1$ and adopt the $\text{Ce}_2\text{O}_2\text{S}$ type structure.

YbRh_2Si_2 is an antiferromagnetic heavy Fermion compound;^{162,163,364,365} therefore, investigations of the thermoelectric properties (TEP) can give important information on the behavior of the conduction electrons. The TEP contain information about the relaxation time and the DOS of the quasiparticles at the Fermi level E_F . It is interesting to note that at very low temperatures, the TEP is commonly positive for Ce heavy Fermion compounds, in agreement with the Kondo picture, while it is negative for Yb heavy Fermion compounds.³⁶⁶ Field-dependent measurements of the Seebeck coefficient $S(H)$ have been conducted down to 120 mK and up to 16 T.³⁶⁷ Above 3.5 T, a cascade of sharp anomalies can be observed, pointing toward topological transitions of the Fermi surface. Upon substitution of rhodium by cobalt according to $\text{Yb}(\text{Rh}_{1-x}\text{Co}_x)_2\text{Si}_2$,^{368,369} the Kondo temperature decreases significantly, and the sole large minimum in the thermopower that is observed for YbRh_2Si_2 splits into two minima. In addition, the absolute thermopower is strongly reduced with increasing x , in line with a weaker exchange coupling of the 4f and the conduction electron states making pure YbCo_2Si_2 a stable trivalent system.^{241,242,369} However, still two minima are observed in the Seebeck coefficient, indicating weak residual Kondo scattering in line with a tiny residual hybridization between 4f and conduction electron states. A comparative study of the thermoelectric response under magnetic field of YbRh_2Si_2 and YbAlB_4 showed a significant difference in the Seebeck coefficient near the quantum critical points of both compounds. When approaching the critical field, S/T is drastically reduced in YbRh_2Si_2 ; however, an enhancement in $\beta\text{-YbAlB}_4$ is observed.³⁷⁰

YbPd_2Si_2 is another heavy Fermion material within the group of Yb intermetallics and has been studied broadly.³⁷¹⁻³⁷³ In the range between 1.5 and 300 K, the Seebeck coefficient is negative with a minimum around 50 K, which was attributed to the intermediate valence of this compound.³⁷⁴ Investigations of YbNi_2Si_2 and YbCu_2Si_2 revealed a similar behavior with minima between 50 and 100 K; however, the Seebeck coefficient gets positive for YbNi_2Si_2 below ~ 20 K, which was assigned to the antiferromagnetic ordering of this compound.^{375,376} High-pressure studies of YbCu_2Si_2 revealed that a magnetic phase transition emerges at $T_m = 1.9$ K around $T_C = 10.2$ GPa which shifts to higher temperatures with increasing pressure.³⁷⁷ This was later confirmed by high-pressure measurements of the Seebeck coefficient.³⁷⁵ $\text{YbPd}_2\text{Ge}_{1.7}$ also exhibits a nonmonotonous behavior and shows a negative Seebeck coefficient down to low temperatures, where again the sign changes.³⁷⁸ The solid solutions $\text{YbCu}_2\text{Si}_{2-x}\text{Ge}_x$ ³⁷⁹ and $\text{Yb}_{1-x}\text{La}_x\text{Cu}_2\text{Si}_2$ ³⁸⁰ finally were studied with respect to their thermoelectric properties. Materials with large Seebeck coefficients at low temperatures can be utilized for cryogenic Peltier elements for cooling infrared sensors on satellites. With this respect, the solid solutions were investigated to maximize the zT at cryogenic temperatures. In both cases, an enhancement of the power factor as well as a shift of the maximum to higher temperatures was observed. Alongside this, a reduction of the thermal conductivity was noted, leading to an overall higher zT . The observed changes were attributed to the changes in the unit cell dimensions that can be envisioned as “chemical pressure”.

YbAlB_4 and YbNiAl_4 , although having the same chemical composition, adopt two different structure types. YbAlB_4 is furthermore dimorphic and crystallizes either in the orthorhombic YCrB_4 ($\alpha\text{-YbAlB}_4$; space group $Pbam$) or ThMoB_4

(β -YbAlB₄; space group *Cmmm*) type structure (vide ultra). Due to the superconductivity observed in β -YbAlB₄²⁰⁴ and its heavy Fermion characteristics, the quantum-critical point (QCP) is of special interest. During these investigations, it became clear that the Seebeck coefficient for β -YbAlB₄ behaves significantly different compared to YbRh₂Si₂. $-S(T)/T$ becomes large for β -YbAlB₄ near the zero-field QCP, while for YbRh₂Si₂, $-S(T)/T$ is strongly suppressed.^{370,381}

Also, in the CeCr₂Al₂₀ type structure (space group *Fd $\bar{3}m$*), several Yb-containing compounds are known that exhibit Kondo or heavy Fermion properties. Similar to the examples discussed before, the members of the YbT₂Zn₂₀ (*T* = Fe, Ru, Os, Co, Rh, Ir) series also exhibit heavy Fermion Kondo lattices. In their thermoelectric properties, all members show large, negative minima (between -75 and -45 $\mu\text{V K}^{-1}$); however, variations with respect to the transition metal *T* can be observed. The local minimum in *S*(*T*) and the local maximum in ρ (*T*) can be correlated to the transition metals and the Kondo temperatures of the respective compounds as well as with the influence of the crystalline electric field splitting.³⁸² Wei and co-workers have shown, that the compounds of the YbT₂Zn₂₀ (*T* = Co, Rh, Ir) series exhibit increasing figures of merit with increasing mass of the transition metals at low temperatures, peaking at $zT = 0.07$ at 35 K for YbIr₂Zn₂₀.³⁸³

Finally, the thermoelectric investigations on Yb₂Pt₆Al₁₅ (Sc_{0.6}Fe₂Si_{4.9} type, space group *P6₃/mmc*),³⁸⁴ Yb₂T₃Al₉ (*T* = Rh, Ir; Y₂Co₃Ga₉ type, space group *Cmcm*),³⁸⁵ Yb₂Pt₃Sn₅ (own type, space group *Pnma*),³⁸⁶ and Yb₂Ni₁₂P₇ (Zr₂Fe₁₂P₇ type, space group *P6*)³⁸⁷ should be addressed. While the first two representatives have been characterized as heavy Fermion systems, Yb₂Pt₃Sn₅ is a rare example of a heterogeneous mixed-valence system. Yb₂Ni₁₂P₇ finally exhibits a crossover between Fermi-liquid and non-Fermi-liquid behavior and seems to be in close proximity to a quantum critical point. For both Yb₂Pt₆Al₁₅ and the Yb₂T₃Al₉ (*T* = Rh, Ir) series, the temperature dependence of the Seebeck coefficient shows a minimum at low temperatures, as expected for Yb-based Kondo lattice systems. While the platinum compound reaches -70 $\mu\text{V K}^{-1}$ around 35 K, Yb₂Rh₃Al₉ and Yb₂Ir₃Al₉ show a change of sign near 250 K and minima of -15 $\mu\text{V K}^{-1}$ and -25 $\mu\text{V K}^{-1}$ at 30 and 40 K, respectively. For the latter, an additional anomaly is observed near their Néel temperature.³⁸⁵ A single anomaly in *S*(*T*) is observed for Yb₂Pt₆Al₁₅ indicating that the Kondo energy scale is close to the CEF splitting. The temperature observed is compatible with a Kondo scale of the order of 60 K. The accordance of these temperatures supports the picture of a Kondo lattice with a large characteristic energy in which the whole multiplet is involved in the low-temperature physics.³⁸⁴ Yb₂Pt₃Sn₅ also shows a minimum in the Seebeck coefficient (-38 $\mu\text{V K}^{-1}$ at 60 K),³⁸⁶ which is typical for intermediate valent Yb compounds such as YbAgCu₄ and YbCu₂Si₂.³⁷⁴

Zintl Phases

Zintl phases are usually the class of materials that come to mind when speaking about thermoelectric properties. Due to their semiconducting properties, they can be utilized to produce energy based on a temperature gradient. In many cases, the materials have to be optimized with respect to their electronic properties like charge carrier concentration.

One compound with outstanding thermoelectric properties is probably Yb₁₄MnSb₁₁ (Ca₁₄AlSb₁₁ type, space group *I4₁/*

acd). In 2006, Brown et al. reported that Yb₁₄MnSb₁₁ “achieves quadrupled efficiency and virtually doubled figure of merit over the current state-of-the-art, SiGe”.³⁸⁸ The material reaches a figure of merit of ~ 1.0 at 1223 K (Figure 17). The Seebeck

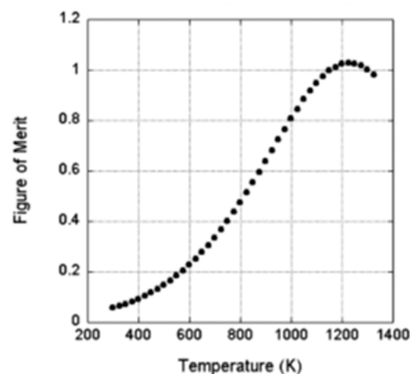


Figure 17. Figure of merit zT of Yb₁₄MnSb₁₁. Maximum zT value of ~ 1.0 at 1200 K. Reprinted with permission from ref 388. Copyright 2006 American Chemical Society.

coefficient is positive in the whole temperature range and increases linearly with increasing temperature, reaching $+185$ $\mu\text{V K}^{-1}$ at 1275 K. Since the resistivity also shows a linear behavior with temperature and Hall measurements indicate a constant carrier concentration over the investigated temperature range, the compound can be considered a heavily doped semiconductor. The high figure of merit finally arises from the low thermal conductivity of Yb₁₄MnSb₁₁, which is on the scale of a glass ($7\text{--}9$ $\text{mW cm}^{-1} \text{K}^{-1}$).

Since the initial report of Yb₁₄MnSb₁₁ being a high- zT material, numerous reports have been published that modified the original compound via the formation of solid solutions as well as investigations on isostructural compounds. In the following part, selected publications have been chosen to illustrate the overall ideas.

Yb₁₄MnSb₁₁ can be modified on the Yb, the Mn, and the Sb position, either by isovalent atoms, often leading to structural distortions and therefore changes in the electronic structure, or by elements which exhibit different formal oxidation states, leading to changes in the overall electron count. Isovalent substitutions on the Yb position can, for example, be realized by Ca. The solid solution Yb_{14-x}Ca_xMnSb₁₁ shows that the substitution of Yb by Ca reduces the carrier concentration leading to an increased Seebeck coefficient and at the same time to an increased electrical resistivity. In addition, the mass difference between Ca and Yb leads to a significantly reduced density and mass-disorder scattering is observed, resulting in a lowered lattice thermal conductivity. However, these changes do not lead to a significant improvement of zT . In addition, compositions with values of $x > 4$ get highly air-sensitive, making the characterization of the thermoelectric properties impossible.^{389,390}

As for a substitution of Yb via a trivalent rare earth element, Sc and Y,³⁹¹ La,³⁹² Lu,^{393,394} as well as the full RE³⁺ (La–Lu) series³⁹⁵ have been reported. While for the latter only the thermochemistry and thermal stability was analyzed, for the other substitutions the influence on the thermoelectric properties was also investigated since the trivalent rare earth cations change the carrier concentration. The Sc- and Y-substituted specimens show higher resistivities and thus higher

Seebeck coefficients; however, an overall reduction of the zT is observed.³⁹¹ Also for the Lu-substituted compounds, a reduced carrier concentration was reported as well as a reduced peak zT .³⁹⁴ Another study, however, reported an increased carrier concentration upon Lu substitution leading to a $\sim 30\%$ improvement in zT at 670 K.³⁹³ For La-substituted $\text{Yb}_{14-x}\text{La}_x\text{MnSb}_{11}$, finally an increased zT was reported for $x \sim 0.4$ with a peak zT of 1.15 at 1150 K.³⁹²

Also for the Mn position, an isovalent substitution is possible, e.g., in $\text{Yb}_{14}\text{Mn}_{1-x}\text{Zn}_x\text{Sb}_{11}$.³⁹⁶ The substitution shows a slight improvement up to $x \leq 0.4$ by reducing the lattice thermal conductivity at low temperatures; however, only a negligible impact at high temperatures is observed. This is based on the reduction of spin disorder scattering leading to an overall improvement of about 10% with a maximum thermoelectric figure of merit ~ 1.1 at 1275 K for $x = 0.4$. Substituting Mn^{2+} for Al^{3+} , however, again leads to a reduction of the carrier concentration,^{397,398} similar to the substitution of Yb^{2+} by RE^{3+} . For $x = 0.6$ and 0.8, an improvement of 30% was observed, equal to a $zT = 1.3$ at 1223 K.

Finally, modifications on the Sb positions should be mentioned. In the solid solution $\text{Yb}_{14}\text{MnSb}_{11-x}\text{Bi}_x$, overall lower zT values are observed,³⁹⁹ while $\text{Yb}_{14}\text{MnSb}_{11-x}\text{Te}_x$ shows an improved zT of 1.11 for $x = 0.07$ at 1240 K.⁴⁰⁰ This, again, can be attributed to a reduced carrier concentration.

Furthermore, the low-temperature behavior of the thermoelectric properties has been studied at ambient and increased pressure. Also in the range between 4.2 and 300 K, the Seebeck coefficient for $\text{Yb}_{14}\text{MnSb}_{11}$ is positive and increases upon heating.⁴⁰¹ Increasing the pressure up to 2.3 GPa leads to a further increase of the Seebeck coefficient in the same temperature range.⁴⁰²

Besides $\text{Yb}_{14}\text{MnSb}_{11}$, other Yb-containing compounds with the same composition and crystal structure were also investigated. As examples, $\text{Yb}_{14}\text{MgSb}_{11}$, $\text{Yb}_{14}\text{MnBi}_{11}$, and $\text{Yb}_{14}\text{MgBi}_{11}$ will be discussed. $\text{Yb}_{14}\text{MgSb}_{11}$ has, compared to its Mn-containing analogue, an increased Seebeck coefficient which leads to an increase of 45% in the figure of merit ($zT = 1.02$ at 1075 K) at the same temperature.⁴⁰³ The addition of iron leads to the formation of nanosized inclusions, which lead to an even further increase of zT .^{404,405} $\text{Yb}_{14}\text{MnBi}_{11}$ and $\text{Yb}_{14}\text{MgBi}_{11}$ are both metallic in nature, and $\text{Yb}_{14}\text{MgBi}_{11}$ has an increased carrier concentration in comparison to the isostructural antimonide which compensates potential improvements of the thermoelectric properties. Overall, the zT values of both compounds reach ~ 0.2 at 875 K.⁴⁰⁶

The MT_2X_2 compounds that adopt the trigonal $\text{Ce}_2\text{O}_2\text{S}$ type structure (space group $P\bar{3}m1$) with the general composition $\text{M}^{\text{II}}\text{T}^{\text{II}}_2\text{Pn}_2$ can also be considered as valence precise Zintl phases. M is a divalent alkaline earth or rare earth metal (Ca, Sr, Eu, Yb), while T is a divalent transition metal (Mn, Zn, Cd) or Mg, and Pn finally a pnictogen (As, Sb, Bi). These compounds are considered to be “electron precise” according to the Zintl formalism.

In the following paragraph, just a small number of studies will be mentioned as there is a plethora of studies related to the optimization of the thermoelectric properties by different strategies. One of the first reports is on the solid solution $\text{Ca}_x\text{Yb}_{1-x}\text{Zn}_2\text{Sb}_2$ from Gascoin and co-workers.⁴⁰⁷ They showed that YbZn_2Sb_2 has the smallest Seebeck coefficient but at the same time the smallest electrical resistivity. CaZn_2Sb_2 in contrast exhibits an over two times larger

Seebeck coefficient but also a 7-fold larger resistivity. The solid solution shows an intermediate behavior, depending on the composition. Subsequently, numerous solid solutions were investigated with respect to improving the TEP; for example, substitution of Yb by Eu according to $\text{Eu}_x\text{Yb}_{1-x}\text{Zn}_2\text{Sb}_2$ ^{408,409} or by La as in $\text{Yb}_{1-x}\text{La}_x\text{Zn}_2\text{Sb}_2$.⁴¹⁰ But also high-quality single crystals of YbZn_2Sb_2 were grown and investigated.⁴¹¹ Despite modifications by chemical substitution, nanoporous⁴¹² or Yb-deficient materials ($\text{Yb}_{1-\delta}\text{Zn}_2\text{Sb}_2$)⁴¹³ were also synthesized and investigated. But not only the substitution of the Yb is possible. Also, the formation of solid solutions with respect to the Zn or Sb position can influence the thermoelectric properties. For example, the solid solutions $\text{YbZn}_{2-x}\text{Mg}_x\text{Sb}_2$,⁴¹⁴ $\text{YbZn}_{2-x}\text{Mn}_x\text{Sb}_2$,^{415,416} $\text{YbZn}_{2-x}\text{Cd}_x\text{Sb}_2$,⁴¹⁷ and $\text{YbZn}_2\text{Sb}_{2-x}\text{Bi}_x$ ⁴¹⁸ should be named. Finally, it has been proven that Mg can substitute on both the Yb and Zn sites.⁴¹⁹ Besides YbZn_2Sb_2 , also YbMg_2Sb_2 ,⁴²⁰ YbMg_2Bi_2 ,^{421–423} YbMn_2Sb_2 ,⁴²⁴ YbCd_2Sb_2 , and the solid solutions $\text{YbCd}_{2-x}\text{Mn}_x\text{Sb}_2$ ⁴²⁵ have been investigated in great detail.

Finally, two other classes of important thermoelectric materials should be addressed: clathrates and skutterudites. Although clathrates are structurally very versatile materials, hardly any ytterbium-containing ones have been reported. Detailed information on the different clathrate structures and their applications can be found in a review.⁴²⁶ The key features that lead to their intriguing thermoelectric properties are the “rattling” atoms within the structure. These are located in the large polyhedra that form the framework and can effectively scatter the heat-carrying phonons, therefore reducing the thermal conductivity. The reports on Yb-substituted clathrates are mainly examples of type-I clathrates, which crystallize in space group $Pm\bar{3}n$ and exhibit the general formula $\text{G}_8[\text{F}_{46}]$, with F being the framework and G being the guest atoms. In the type-I clathrates, two different polyhedra can be found, a 20-vertex pentagonal dodecahedron and a 24-vertex tetrakaidcahedron. For the framework, different elements and elemental combinations are known as well as a large number of guest atoms occupying these polyhedra.⁴²⁶ The number of Yb-based type-I clathrates ($\text{Na}_4\text{Si}_{23}$ type, space group $Pm\bar{3}n$), however, is extremely low. To the best of our knowledge, no pure Yb clathrates have been reported, but the solid solutions $\text{Ba}_{8-x}\text{Yb}_x\text{Ga}_{16}\text{Si}_{30}$,⁴²⁷ $\text{Ba}_{8-x}\text{Yb}_x\text{Ga}_{16}\text{Ge}_{30}$,⁴²⁸ $\text{Ba}_{8-x}\text{Yb}_x\text{Ni}_{0.1}\text{Zn}_{0.54}\text{Ga}_{13.8}\text{Ge}_{31.56}$,⁴²⁹ $\text{Ba}_{8-x}\text{Yb}_x\text{Ni}_{3.8}\text{Si}_{42.2}$,⁴³⁰ and $\text{Ba}_{8-x}\text{Yb}_x\text{Cu}_{4.9}\text{Si}_{41.1}$ ⁴³⁰ have been investigated experimentally. In addition, first principle studies on $\text{Ba}_6\text{Yb}_2\text{Au}_6\text{Ge}_{40}$ ⁴³¹ have been conducted. For the silicide, it was shown that the substitution of Ba by Yb is possible, but only to a certain extent of $x = 0.25$ to 0.38.⁴²⁷ The substitution led to a slight decrease of the Seebeck coefficient, however, also to a significant decrease of the lattice thermal conductivity which resulted in a slight overall increase of zT for $\text{Ba}_{7.75}\text{Yb}_{0.25}\text{Si}_{31.9}\text{Ga}_{14.1}$.⁴²⁷ For the germanide series $\text{Ba}_{8-x}\text{Yb}_x\text{Ga}_{16}\text{Ge}_{30}$, in principle the same trend is observed. Here, samples with $x = 0$ to 1.3 could be synthesized and investigated, and again a decrease in the Seebeck coefficient is visible for $x \leq 0.7$ alongside a decrease of the lattice thermal conductivity leading to a zT of 1.1 (950 K) for $\text{Ba}_{7.5}\text{Yb}_{0.5}\text{Ga}_{16}\text{Ge}_{30}$. This is an increase of 90% compared to the Yb-free sample.⁴²⁸ Also in $\text{Ba}_{8-x}\text{Yb}_x\text{Ni}_{0.1}\text{Zn}_{0.54}\text{Ga}_{13.8}\text{Ge}_{31.56}$,⁴²⁹ a slightly increased zT (15%, $zT = 0.91$ at 900 K) was reported for $x = 0.3$. In this case, the electrical resistivity and lattice thermal conductivity decrease with increasing x , the Seebeck coefficient, however,

stays constant. Yb substitution in $\text{Ba}_{8-x}\text{Yb}_x\text{Ni}_{3.8}\text{Si}_{42.2}$ and $\text{Ba}_{8-x}\text{Yb}_x\text{Cu}_{4.9}\text{Si}_{41.1}$ revealed that the majority of the Yb precipitated as secondary phases. The solubility limit is only about 1% on the Ba site. The multiphase samples showed both a lower electrical resistivity and a lower Seebeck coefficient with respect to the unsubstituted compounds; however, the thermal conductivity increases. Overall, the thermoelectric figure of merit of the Ni-based system is not improved, while a slight enhancement above 800 K is observed for $\text{Ba}_{8-x}\text{Yb}_x\text{Cu}_{4.9}\text{Si}_{41.1}$.⁴³⁰ For $\text{Ba}_6\text{Yb}_2\text{Au}_6\text{Ge}_{40}$, finally, the thermoelectric properties were calculated using the full-potential linearized augmented plane wave method based on density functional theory. It was shown that the substitution enhances the density of states at the bottom of the conduction band, leading to an increased Seebeck coefficient due to an increased effective mass of the conduction band.⁴³¹

Finally, one report on a type-VIII clathrate ($G_8[F_{46}]$; own type, space group $I\bar{4}3m$) has been published, which investigated the substitution in $\text{Ba}_{8-x}\text{Yb}_x\text{Ga}_{16}\text{Sn}_{30}$.⁴³² Here, an improvement of the Seebeck coefficient up to $x = 1.0$ was observed. Overall, the situation is similar to the type-I clathrates: a substitution adjusts the Seebeck coefficient as well as the electrical and thermal conductivity, leading to an improvement of the figure of merit zT . In $\text{Ba}_{6.5}\text{Yb}_{1.5}\text{Ga}_{16}\text{Sn}_{30}$, this leads to a maximum zT of 1.35 at 489 K.

The last class of materials that should be discussed with respect to their thermoelectric properties are Yb-containing skutterudites. The name of this class of materials derives from the mineral skutterudite CoAs_3 with the general formula TX_3 (CoAs_3 type, space group $Im\bar{3}$). In the crystal structure of the skutterudites, two empty cavities can be found that can accompany a number of different atoms. In the late 1970s, Jeitschko and co-workers coined the term “filled skutterudites” for compounds with the general composition MT_4X_{12} ($\text{LaFe}_4\text{Sb}_{12}$ type, space group $Im\bar{3}$).^{433–436} In 1996, Sales⁴³⁷ and Fleurial⁴³⁸ showed that filled skutterudites exhibit excellent thermoelectric properties at elevated temperatures. The reviews by Uher from 2001 and Sales from 2003 summarize the important aspects of skutterudites.^{439,440} One of the first Yb-containing filled skutterudites investigated for its physical properties was $\text{YbFe}_4\text{Sb}_{12}$. Magnetic measurements indicate an intermediate valence state and a slightly enhanced Sommerfeld coefficient.^{441,442} In these reports, the potential for $\text{YbFe}_4\text{Sb}_{12}$ to exhibit good thermoelectric properties was outlined. Low-temperature thermoelectric property measurements showed that $\text{YbFe}_4\text{Sb}_{12}$ is a p-doped metal with a low carrier density. The high electrical resistivity leads to a $zT < 0.02$ below 300 K.⁴⁴³ The investigations of the high-temperature properties lead to a $zT = 0.4$ at 670 K.⁴⁴⁴ Within the solid solution $\text{Yb}_y\text{Fe}_{4-x}\text{Ni}_x\text{Sb}_{12}$, even zT values near 1 (750–850 K) could be obtained for $x = 0.6–0.8$.⁴⁴⁵

Due to the chemical versatility of the filled skutterudites, numerous compositions were investigated with respect to their thermoelectric properties. Within the field of Yb-based compounds, $\text{YbCo}_4\text{Sb}_{12}$ showed an excellent performance, leading to a large number of studies of tuned and improved materials. Therefore, only some examples will be summarized in the next paragraph. Studies on different compounds of the $\text{Yb}_x\text{T}_4\text{Sb}_{12}$ series ($x = 0.1–0.8$, $T = \text{Fe, Co, Rh, Ir}$) showed that the physical properties seem to correlate with the filling x and the electronic situation modified by changing T .⁴⁴⁶ At the same time, studies on $\text{Yb}_y\text{Co}_4\text{Sn}_x\text{Sb}_{12-x}$ indicated a maximum zT of 0.1 at 300 K for $\text{Yb}_{0.44}\text{Co}_4\text{Sb}_{12}$.⁴⁴⁷ More detailed studies

including Hall effect, electrical resistivity, Seebeck coefficient, and thermal conductivity measurements were conducted on the solid solution $\text{Yb}_y\text{Co}_4\text{Sb}_{12-x}\text{Sn}_x$ for $y = 0.19$ and 0.5. It was shown that substituting Sn on the Sb site does not alter the Fermi level with respect to the conduction band; instead, a p-type band for a sufficiently large Sn content x was observed. Therefore, this is not a valid method to optimize the thermoelectric properties of Yb-filled skutterudites.⁴⁴⁸ Double substitution according to $\text{Ba}_{0.08}\text{Yb}_{0.09}\text{Co}_4\text{Sb}_{12}$, however, led to a broad range of resonant phonon scattering and which resulted in a strong suppression in the lattice thermal conductivity. Therefore, high zT values of 1.36 at 800 K could be observed.⁴⁴⁹ A similar value in zT (1.36 at 850 K) could be observed for $\text{Al}_{0.3}\text{Yb}_{0.25}\text{Co}_4\text{Sb}_{12}$.⁴⁵⁰ By the help of ball-milling in combination with hot-pressing, the value of x in $\text{Yb}_x\text{Co}_4\text{Sb}_{12}$ could be improved to almost 0.5, leading to a zT of 1.2 at 823 K.⁴⁵¹ In recent years, studies addressing the band conversion in $\text{Yb}_x\text{Co}_4\text{Sb}_{12}$,⁴⁵² the achievement of ultralow thermal conductivities in $\text{Yb}_x\text{Co}_{4-y}\text{Fe}_y\text{Sb}_{12}$ with $x = 0.25–0.5$ and $y = 0.1–0.5$,⁴⁵³ the synthetic approach on $\text{Yb}_x\text{Co}_4\text{Sb}_{12}$,⁴⁵⁴ and introducing nano-inclusions⁴⁵⁵ have led to a deeper understanding of the possibilities to tailor the thermoelectric properties in skutterudite materials.

SUMMARY AND OUTLOOK

The present review impressively underlines that the family of ytterbium-based intermetallic compounds covers extremely broad facets of crystal structures along with interesting and, in some cases, even outstanding physical properties. This interplay is mostly driven by the ytterbium valence: divalent ($4f^{14}$), intermediate-valent, or trivalent ($4f^{13}$) ytterbium. Thus, one observes simple diamagnets, Pauli or Curie–Weiss paramagnets as well as valence fluctuating compounds, Kondo behavior, heavy Fermion ground states, or sometimes even superconductivity.

Some of the trivalent ytterbium intermetallics have gained deep interest due to these physical properties. The phases have been meticulously studied with respect to their properties using magnetic and transport measurements, specific heat data, NMR, ESR, and Mössbauer spectroscopy, elastic and inelastic neutron scattering, XAS and XPS data, as well as detailed thermoelectric measurements, then allowing the development of structure–property relations.

Among the binary Yb intermetallics, YbAl_2 and YbAl_3 have received the most attention due to their Kondo behavior. Overall, however, the number of binary compounds studied in detail is rather low compared to the ternary systems, given the significantly larger combinatory manifold in the ternary systems. Here, YbRh_2Si_2 is the most outstanding phase with >350 publications on this compound. It exhibits a non-Fermi-liquid behavior along with antiferromagnetic ordering at $T_N = 70$ mK. A quantum critical point at ambient pressure is suggested, at which the magnetic ordering can be suppressed by a magnetic field of only $B_c = 60$ mT. $\text{Yb}_2\text{Pt}_2\text{Pb}$ exhibits a Shastry–Sutherland lattice that causes a high anisotropy in the magnetic susceptibility with an about 30 times larger value for $\chi_{(100)}$ as compared to $\chi_{(001)}$. Finally, among the series of $\text{YbT}_2\text{Zn}_{20}$ compounds, the cobalt-containing representative $\text{YbCo}_7\text{Zn}_{20}$ exhibits Kondo interactions, and from specific heat measurements, a large Sommerfeld coefficient of $\gamma = 7.9 \text{ J}^{-1} \text{ mol}^{-1} \text{ K}^{-2}$ was deduced. Finally, $\text{Yb}_{14}\text{MnSb}_{11}$ is one of the most promising p-type thermoelectric materials with a high $zT > 1$, making this compound suitable for different applications.

Although most of these studies are located in basic research, they help with a deeper understanding of complex intermetallic compounds and motivate for future studies. Especially, the ytterbium-based thermoelectric materials might find application. Even though the family of ytterbium intermetallics is large, a weak point concerns the overall systemization of the property data, since only few larger isotypic series of compounds exist. Already, the equiatomic YbTX phases crystallize with more than 10 different structure types; many of them are superstructures of the aristotype AlB₂. The probably best investigated, and thus comparable, series of isotypic compounds concerns the CeCr₂Al₂₀ type zinc compounds YbT₂Zn₂₀ with T = Fe, Co, Ru, Rh, Os, and Ir.

The study of ytterbium intermetallics is still a vivid field in solid state chemistry and physics. Besides the discovery and characterization of new phases, the understanding and systemization of the structure–property relations is an important future task.


■ ASSOCIATED CONTENT

Data Availability Statement

The data underlying this study are available in the published article.


■ AUTHOR INFORMATION


Corresponding Authors

Oliver Janka – *Anorganische Festkörperchemie, Universität des Saarlandes, 66123 Saarbrücken, Germany*;  orcid.org/0000-0002-9480-3888; Email: oliver.janka@uni-saarland.de

Rainer Pöttgen – *Institut für Anorganische und Analytische Chemie, Universität Münster, 48149 Münster, Germany*; Email: pottgen@uni-muenster.de

Authors

Stefan Engel – *Anorganische Festkörperchemie, Universität des Saarlandes, 66123 Saarbrücken, Germany*;  orcid.org/0000-0002-6813-8490

Elias C. J. Giebelmann – *Anorganische Festkörperchemie, Universität des Saarlandes, 66123 Saarbrücken, Germany*;  orcid.org/0000-0001-6137-9729

Maximilian K. Reimann – *Institut für Anorganische und Analytische Chemie, Universität Münster, 48149 Münster, Germany*

Complete contact information is available at: <https://pubs.acs.org/10.1021/acsorginorgau.3c00054>

Author Contributions

[§]These authors contributed equally. CRediT: **Stefan Engel** conceptualization, formal analysis, writing-original draft, writing-review & editing; **Elias C. J. Giebelmann** conceptualization, formal analysis, writing-original draft, writing-review & editing; **Maximilian Kai Reimann** conceptualization, formal analysis, writing-original draft, writing-review & editing; **Rainer Pöttgen** conceptualization, formal analysis, project administration, supervision, validation, visualization, writing-original draft, writing-review & editing; **Oliver Janka** conceptualization, formal analysis, funding acquisition, investigation, supervision, validation, visualization, writing-original draft, writing-review & editing.

Funding

Funding is provided by the Deutsche Forschungsgemeinschaft DFG (JA 1891-10-1).

Notes

The authors declare no competing financial interest.

■ REFERENCES

- (1) Szytuła, A.; Leciejewicz, J. *Handbook of Crystal Structures and Magnetic Properties of Rare Earth Intermetallics*. CRC Press: Boca Raton, 1994.
- (2) Matar, S. F. Review on cerium intermetallic compounds: A bird's eye outlook through DFT. *Prog. Solid State Chem.* **2013**, *41*, 55–85.
- (3) Pöttgen, R.; Chevalier, B. Cerium intermetallics with ZrNiAl-type structure – a review. *Z. Naturforsch.* **2015**, *70b*, 289–304.
- (4) Pöttgen, R.; Chevalier, B. Equiatomic cerium intermetallics CeXX' with two p elements. *Z. Naturforsch.* **2015**, *70b*, 695–704.
- (5) Pöttgen, R.; Janka, O.; Chevalier, B. Cerium intermetallics CeTX – review III. *Z. Naturforsch.* **2016**, *71b*, 165–191.
- (6) Janka, O.; Niehaus, O.; Pöttgen, R.; Chevalier, B. Cerium intermetallics with TiNiSi-type structure. *Z. Naturforsch.* **2016**, *71b*, 737–764.
- (7) Ramirez, D.; Gallagher, A.; Baumbach, R.; Siegrist, T. Synthesis and characterization of the divalent samarium Zintl-phases SmMg₂Bi₂ and SmMg₂Sb₂. *J. Solid State Chem.* **2015**, *231*, 217–222.
- (8) Pöttgen, R.; Johrendt, D. Equiatomic intermetallic europium compounds: syntheses, crystal chemistry, chemical bonding, and physical properties. *Chem. Mater.* **2000**, *12*, 875–897.
- (9) Ramarao, S. D.; Singh, A. K.; Subbarao, U.; Peter, S. C. An overview on the structural diversity of europium based ternary intermetallics. *J. Solid State Chem.* **2020**, *281*, 121048.
- (10) Engel, S.; Giebelmann, E. C. J.; Pöttgen, R.; Janka, O. Trivalent europium – a scarce case in intermetallics. *Rev. Inorg. Chem.* **2023**, *43* (4), 571.
- (11) Klaasse, J. C. P.; Mattens, W. C. M.; van Ommen, A. H.; de Boer, F. R.; de Châtel, P. F. Valency and magnetic behaviour of ytterbium in intermetallic compounds. *AIP Conf. Proc.* **1976**, *34*, 184–186.
- (12) Klaasse, J. C. P.; de Boer, F. R.; de Châtel, P. F. Systematics in intermetallic compounds containing intermediate-valent ytterbium. *Physica B* **1981**, *106*, 178–194.
- (13) Pöttgen, R.; Johrendt, D.; Kußmann, D., Structure property relations of ternary equiatomic YbTX intermetallics. In *Handbook on the Physics and Chemistry of Rare Earths*, Gschneidner, Jr, K. A.; Bünzli, J.-C., Eds.; North-Holland/Elsevier: Amsterdam, 2001; Vol. 32, pp 453–513.
- (14) Lai, Y.; Chan, J. Y.; Baumbach, R. E. Electronic landscape of the f-electron intermetallics with the ThCr₂Si₃ structure. *Sci. Adv.* **2022**, *8*, No. eabp8264.
- (15) Doniach, S. The Kondo lattice and weak antiferromagnetism. *Physica B* **1977**, *91*, 231–234.
- (16) Stewart, G. R. Heavy-fermion systems. *Rev. Mod. Phys.* **1984**, *56*, 755–787.
- (17) Boursier, R.; Villaume, A.; Lapertot, G.; Aoki, D.; Knebel, G.; Flouquet, J. Comparison between Ce and Yb heavy fermion compounds: CeRh₂Si₂ versus YbRh₂Si₂. *Physica B* **2008**, *403*, 726–730.
- (18) Villars, P.; Cenzual, K. *Pearson's Crystal Data: Crystal Structure Database for Inorganic Compounds*; ASM International: Materials Park, Ohio, USA, release 2022/2023.
- (19) CAS. SciFinder[®]. <https://scifinder-n.cas.org/>. Last accessed 6th October 2023.
- (20) Emsley, J. *The Elements*. Clarendon Press, Oxford University Press: Oxford, NY, 1998.
- (21) Pöttgen, R.; Johrendt, D. *Intermetallics*. 2nd ed.; De Gruyter: Berlin, 2019.

- (22) Rossi, D.; Marazza, R.; Ferro, R. Ternary RMe_2X_2 alloys of the rare earths with the precious metals and silicon (or germanium). *J. Less-Common Met.* **1979**, *66*, P17–P25.
- (23) Saensunon, B.; Nishimura, K.; Voyer, C. J.; Ryan, D. H.; Hutchison, W. D.; Stewart, G. A. Magnetic ground state at the ytterbium site in $YbNiAl_4$. *J. Appl. Phys.* **2009**, *105*, 07E123.
- (24) Voßwinkel, D.; Niehaus, O.; Gerke, B.; Benndorf, C.; Eckert, H.; Pöttgen, R. Silicon-tin-ordering in $RE_3Rh_3Si_2Sn_3$ ($RE = Y, Sm, Gd - Lu$). *Z. Anorg. Allg. Chem.* **2015**, *641*, 238–246.
- (25) West, A. R. *Solid State Chemistry and its Applications*. 2nd ed.; John Wiley & Sons Inc.: Hoboken, USA, 2022.
- (26) Kuz'ma, Y.; Chykhrij, S. *Phosphides*. In *Handbook on the Physics and Chemistry of Rare Earths*, Gschneidner, Jr, K. A.; Eyring, L., Eds.; Elsevier Science: Amsterdam, 1996; Vol. 23, pp 285–433.
- (27) Pöttgen, R.; Gulden, T.; Simon, A. Miniaturisierte Lichtbogenapparat für den Laborbedarf. *GIT Labor-Fachz.* **1999**, *43*, 133–136.
- (28) Kußmann, D.; Hoffmann, R.-D.; Pöttgen, R. Syntheses and crystal structures of $CaCuGe$, $CaAuIn$, and $CaAuSn$ – three different superstructures of the KHg_2 type. *Z. Anorg. Allg. Chem.* **1998**, *624*, 1727–1735.
- (29) Pöttgen, R.; Lang, A.; Hoffmann, R.-D.; Künnen, B.; Kotzyba, G.; Müllmann, R.; Mosel, B. D.; Rosenhahn, C. The stannides $YbPtSn$ and $Yb_2Pt_3Sn_5$. *Z. Kristallogr.* **1999**, *214*, 143–150.
- (30) Canfield, P. C.; Fisk, Z. Growth of single crystals from metallic fluxes. *Philos. Mag.* **1992**, *65*, 1117–1123.
- (31) Kanatzidis, M. G.; Pöttgen, R.; Jeitschko, W. The metal flux: A preparative tool for the exploration of intermetallic compounds. *Angew. Chem., Int. Ed.* **2005**, *44*, 6996–7023.
- (32) Canfield, P. C. Design, discovery and growth of novel materials. *Philos. Mag.* **2012**, *92*, 2398–2400 (and review articles within this special issue).
- (33) Gille, P.; Grin, Y. *Crystal Growth of Intermetallics*. De Gruyter: Berlin, Boston, 2019.
- (34) Krellner, C.; Taube, S.; Westerkamp, T.; Hossain, Z.; Geibel, C. Single-crystal growth of $YbRh_2Si_2$ and $YbIr_2Si_2$. *Philos. Mag.* **2012**, *92*, 2508–2523.
- (35) Peter, S. C.; Subbarao, U.; Sarkar, S.; Vaitheeswaran, G.; Svane, A.; Kanatzidis, M. G. Crystal structure of Yb_2CuGe_6 and $Yb_3Cu_4Ge_4$ and the valency of ytterbium. *J. Alloys Compd.* **2014**, *589*, 405–411.
- (36) Sarkar, S.; Peter, S. C. Single crystal growth of europium and ytterbium based intermetallic compounds using metal flux technique. *J. Chem. Sci.* **2012**, *124*, 1385–1390.
- (37) Phelan, W. A.; Menard, M. C.; Kangas, M. J.; McCandless, G. T.; Drake, B. L.; Chan, J. Y. Adventures in crystal growth: synthesis and characterization of single crystals of complex intermetallic compounds. *Chem. Mater.* **2012**, *24*, 409–420.
- (38) Pfannenschmidt, U.; Rodewald, U. Ch.; Pöttgen, R. Bismuth flux crystal growth of $RE_3Rh_3P_4$ ($RE = Sc, Yb, Lu$): new phosphides with a superstructure of the $LiCo_6P_4$ type. *Monatsh. Chem.* **2011**, *142*, 219–224.
- (39) Canfield, P. C.; Kong, T.; Kaluarachchi, U. S.; Jo, N. H. Use of frit-disc crucibles for routine and exploratory solution growth of single crystalline samples. *Philos. Mag.* **2016**, *96*, 84–92.
- (40) Gottlieb-Schönmeyer, S.; Brühne, S.; Ritter, F.; Assmus, W.; Balanetsky, S.; Feuerbacher, M.; Weber, T.; Steurer, W. Crystal growth of copper-rich ytterbium compounds: The predicted giant unit cell structures $YbCu_{4.4}$ and $YbCu_{4.25}$. *Intermetallics* **2009**, *17*, 6–10.
- (41) Schappacher, F. M.; Katoh, K.; Pöttgen, R. Bridgman crystal growth of $Yb_2Ru_3Ge_4$ – A ternary germanide with a three-dimensional network of condensed distorted $RuGe_5$ and $RuGe_6$ units. *J. Solid State Chem.* **2007**, *180*, 186–190.
- (42) Katoh, K.; Heying, B.; Hoffmann, R.-D.; Rodewald, U. Ch.; Pöttgen, R. Bridgman crystal growth and structure refinement of $YbPdGe$ and $YbPtGe$ – Two different superstructures of the KHg_2 type. *Z. Anorg. Allg. Chem.* **2008**, *634*, 1296–1300.
- (43) Shannon, R. D. Revised effective ionic radii and systematic studies of interatomic distances in halides and chalcogenides. *Acta Crystallogr.* **1976**, *A32*, 751–767.
- (44) Eckerlin, P.; Wölfel, E. Die Kristallstruktur von Ca_2Si und Ca_2Ge . *Z. Anorg. Allg. Chem.* **1955**, *280*, 321–331.
- (45) Merlo, F.; Palenzona, A.; Pani, M. Yb_2Ge , Eu_2Ge and Eu_2Si : new $PbCl_2$ -type compounds. *J. Alloys Compd.* **2003**, *348*, 173–175.
- (46) Ganguli, A. K.; Corbett, J. D. Structure, bonding, and properties of $CaZn_{1-x}Cd_xSn$ and $CaSn_{0.5}Ge_{1.5}$. *J. Solid State Chem.* **1993**, *107*, 480–488.
- (47) Pöttgen, R.; Arpe, P. E.; Felser, C.; Kußmann, D.; Müllmann, R.; Mosel, B. D.; Künnen, B.; Kotzyba, G. Structure and properties of $YbZnSn$, $YbAgSn$, and Yb_2Pt_2Pb . *J. Solid State Chem.* **1999**, *145*, 668–677.
- (48) Wiethölter, J.; Koldemir, A.; Reimann, M. K.; Block, T.; Kösters, J.; Janka, O.; Pöttgen, R. Mössbauer-spectroscopic characterization of the stannides Sr_2Pd_2Sn and Eu_2Pd_2Sn . *Z. Naturforsch.* **2023**, *78b*, 301–306.
- (49) Stegemann, F.; Block, T.; Klenner, S.; Zhang, Y.; Fokwa, B. P. T.; Timmer, A.; Mönig, H.; Doerenkamp, C.; Eckert, H.; Janka, O. From 3D to 2D: structural, spectroscopical and theoretical investigations of the dimensionality reduction in the $[PtAl_2]^{δ-}$ polyanions of the isotopic $MPtAl_2$ series ($M = Ca-Ba, Eu$). *Chem.—Eur. J.* **2019**, *25*, 10735–10747.
- (50) Koizumi, T.; Honda, F.; Sato, Y. J.; Li, D.; Aoki, D.; Haga, Y.; Gouchi, J.; Nagasaki, S.; Uwatoko, Y.; Kaneko, Y.; Ōnuki, Y. Abrupt change in electronic states under pressure in new compound $EuPt_3Al_5$. *J. Phys. Soc. Jpn.* **2022**, *91*, 043704.
- (51) Engel, S.; Bönnighausen, J.; Stegemann, F.; Touzani, R. S.; Janka, O. $SrAl_3Pt_3$ and $Sr_2Al_4Pt_9$ – two new strontium aluminum platinides. *Z. Naturforsch.* **2022**, *77*, 367–379.
- (52) Gerke, B.; Pöttgen, R. Alkaline earth-gold-aluminides: synthesis and structure of $SrAu_3Al_2$, $SrAu_{2.83}Al_{2.17}$, $BaAu_{2.89}Al_{2.11}$ and $BaAu_{7.09}Al_{5.91}$. *Z. Naturforsch.* **2015**, *70b*, 903–909.
- (53) Schmiegel, J.-P.; Block, T.; Gerke, B.; Fickenscher, T.; Touzani, R. S.; Fokwa, B. P. T.; Janka, O. $EuAu_3Al_2$: Crystal and electronic structures and spectroscopic, magnetic, and magnetocaloric properties. *Inorg. Chem.* **2016**, *55*, 9057–9064.
- (54) Hulliger, F.; Nissen, H. U.; Wessicken, R. On new $CaBe_2Ge_2$ -type representatives MAu_2Al_2 . *J. Alloys Compd.* **1994**, *206*, 263–266.
- (55) Stegemann, F.; Benndorf, C.; Zhang, Y.; Bartsch, M.; Zacharias, H.; Fokwa, B. P. T.; Eckert, H.; Janka, O. On ternary intermetallic aurides: $CaAu_2Al_2$, $SrAu_{2-x}Al_{2+x}$ and $Ba_3Au_{5+x}Al_{6-x}$. *Z. Anorg. Allg. Chem.* **2017**, *643*, 1379–1390.
- (56) Muts, I.; Zaremba, V. I.; Pöttgen, R. Ternary indides Eu_2Pd_2In and Eu_2Pt_2In . *Z. Anorg. Allg. Chem.* **2012**, *638*, 64–67.
- (57) Muts, I.; Nilges, T.; Rodewald, U. C.; Zaremba, V. I.; Pöttgen, R. Synthesis and structure of Sr_2Pd_2In and Sr_2Pt_2In . *Z. Naturforsch.* **2007**, *62b*, 1563–1566.
- (58) Pöttgen, R.; Kußmann, D. New indium-rich compounds $EuRhIn_2$ and $EuRh_2In_8$. *Z. Anorg. Allg. Chem.* **2001**, *627*, 55–60.
- (59) Muts, I. R.; Zaremba, V. I.; Pöttgen, R. Centered indium cubes as structural motifs in $SrRh_2In_8$ and $SrIrIn_4$. *Z. Anorg. Allg. Chem.* **2007**, *633*, 2234–2237.
- (60) Evers, J.; Oehlinger, G. Ternary phases $MPtSi$ ($M = Ca, Eu, Sr, Ba$) with the $LalSi$ -type structure. *J. Solid State Chem.* **1986**, *62*, 133–137.
- (61) Mayer, I.; Yetor, P. D. MPt_2Si_2 compounds of the $ThCr_2Si_2$ type. *J. Less-Common Met.* **1977**, *55*, 171–176.
- (62) Iandelli, A. Equiatomic ternary compounds of rare earths with the Fe_2P or $ZrNiAl$ structure type. *J. Alloys Compd.* **1992**, *182*, 87–90.
- (63) Dhar, S. K.; Kulkarni, R.; Manfrinetti, P.; Pani, M.; Yonezawa, Y.; Aoki, Y. Synthesis, crystal structure, and physical properties of $YbTZn$ ($T = Pd, Pt, Au$) and $LuPtZn$. *Phys. Rev. B* **2007**, *76*, 054411.
- (64) Mishra, T.; Heymann, G.; Huppertz, H.; Pöttgen, R. Dimorphism in the $REPdZn$ series. *Intermetallics* **2012**, *20*, 110–114.

- (65) Melnyk, G.; Gulay, L. D.; Tremel, W. Crystal structures of new ternary compounds in RE–Pt–Pb and RE–Au–Pb systems (RE = rare earth metal). *J. Alloys Compd.* **2012**, *528*, 70–73.
- (66) Gesing, T.-M.; Pöttgen, R.; Jeitschko, W.; Wortmann, U. Crystal structure and physical properties of the carbides UAl_3C_3 and YbAl_3C_3 . *J. Alloys Compd.* **1992**, *186*, 321–331.
- (67) Stegemann, F.; Stahl, J.; Bartsch, M.; Zacharias, H.; Johrendt, D.; Janka, O. Temperature induced valence phase transition in intermediate-valent YbPd_2Al_3 . *Chem. Sci.* **2019**, *10*, 11086–11094.
- (68) Kösters, J.; Pöttgen, R. Ytterbium valence ordering in the low-temperature superstructure of $\text{Yb}_2\text{Pd}_2\text{Cd}$. *Z. Kristallogr.* **2024**, *239*, DOI: 10.1515/ZKRI-2023-0043. In Press.
- (69) Parthé, E.; Gelato, L. M.; Chabot, B.; Penzo, M.; Cenzual, K.; Gladyshevskii, E. I. TYPIX–Standardized data and crystal chemical characterization of inorganic structure types. In *Gmelin Handbook of Inorganic and Organometallic Chemistry*; Springer, Germany: Berlin, 1993.
- (70) Zumdick, M. F.; Pöttgen, R. Determination of the superstructures for the stannides ZrIrSn , HfCoSn , and HfRhSn . *Z. Kristallogr.* **1999**, *214*, 90–97.
- (71) Bojin, M. D.; Hoffmann, R. The REME Phases I. An overview of their structural variety. *Helv. Chim. Acta* **2003**, *86*, 1653–1682.
- (72) Bojin, M. D.; Hoffmann, R. The REME phases II. What's possible? *Helv. Chim. Acta* **2003**, *86*, 1683–1708.
- (73) Haszko, S. E. Intermediate phases with the MgCu_2 structure. *Trans. Metall. Soc. AIME* **1960**, *218*, 958.
- (74) Van Vucht, J. H. N.; Buschow, K. H. J. On the binary aluminium-rich compounds of the rare-earth elements. *Philips Res. Rep.* **1964**, *19*, 319–322.
- (75) Moriarty, J. L., Jr.; Humphreys, J. E.; Gordon, R. O.; Baenziger, N. C. X-ray examination of some rare-earth-containing binary alloy systems. *Acta Crystallogr.* **1966**, *21*, 840–841.
- (76) Sysa, L. V.; Zaremba, V. I.; Kalychak, Y. M.; Baranyak, V. M. New ternary compounds with indium, rare-earth and 3d metals with MgCu_4Sn and ZrNiAl type structure. *Visn. Lviv. Derzh. Univ., Ser. Khim.* **1988**, *29*, 32–34.
- (77) Giebelmann, E. C. J.; Pöttgen, R.; Janka, O. Laves phases: superstructures induced by coloring and distortions. *Z. Anorg. Allg. Chem.* **2023**, *649*, No. e202300109.
- (78) Seidel, S.; Pöttgen, R. $\text{Yb}_6\text{Ir}_5\text{Ga}_7$ – A MgZn_2 superstructure. *Z. Anorg. Allg. Chem.* **2017**, *643*, 261–265.
- (79) Eustermann, F.; Pominov, A.; Pöttgen, R. Rare earth (RE) gallides with closely related compositions: REIrGa and $\text{RE}_6\text{Ir}_5\text{Ga}_7$. *Z. Anorg. Allg. Chem.* **2018**, *644*, 1297–1303.
- (80) Eustermann, F.; Stegemann, F.; Radzieowski, M.; Janka, O. Intermetallic $\text{RE}_6\text{T}_5\text{Al}_7$ phases (RE = Sc, Y, Ce–Nd, Sm, Gd–Lu, T = Ru, Ir): Diversity in their magnetic, magnetocaloric and critical properties. *Inorg. Chem.* **2019**, *58*, 16211–16226.
- (81) Just, G.; Paufler, P. On the coordination of ThCr_2Si_2 (BaAl_4 -type compounds within the field of free parameters). *J. Alloys Compd.* **1996**, *232*, 1–25.
- (82) Shatruck, M. ThCr_2Si_2 structure type: The “perovskite” of intermetallics. *J. Solid State Chem.* **2019**, *272*, 198–209.
- (83) Zaremba, V. I.; Rodewald, U. Ch.; Hoffmann, R.-D.; Kalychak, Y. M.; Pöttgen, R. The indium-rich intermetallics YbCoIn_5 , YbRhIn_5 , and YbPtIn_4 . *Z. Anorg. Allg. Chem.* **2003**, *629*, 1157–1161.
- (84) Gladyshevskii, E. I.; Yarmolyuk, Y. P.; Grin, Y. Structures of ternary gallides of rare-earth metals-members of the homologous series $\text{R}_m\text{R}'_{3m+2n}\text{X}_n$ and $\text{R}_{m+n}\text{R}'_n\text{X}_{m+n}$. *Acta Crystallogr.* **1978**, *A34*, S148b.
- (85) Zaremba, V. I.; Rodewald, U. Ch.; Pöttgen, R. Synthesis and structure of YbIrIn_5 . *Z. Naturforsch.* **2003**, *58b*, 805–808.
- (86) Lukachuk, M.; Pöttgen, R. Intermetallic compounds with ordered U_3Si_2 or Zr_3Al_2 type structure – crystal chemistry, chemical bonding and physical properties. *Z. Kristallogr.* **2003**, *218*, 767–787.
- (87) Klenner, S.; Pöttgen, R. Rare earth transition metal plumbides – An update. In *Handbook on the Physics and Chemistry of Rare Earths*, Bünzli, J.-C. G.; Pecharsky, V. K., Eds.; Elsevier: 2020; Vol. 57, pp 1–44.
- (88) Pöttgen, R.; Janka, O. $\text{CeCr}_2\text{Al}_{20}$ -type intermetallics – structure-property relationships. *Rev. Inorg. Chem.* **2023**, *43*, 357–383.
- (89) Jia, S.; Ni, N.; Bud'ko, S. L.; Canfield, P. C. Magnetic properties of $\text{RFe}_2\text{Zn}_{20}$ and $\text{RCo}_2\text{Zn}_{20}$ (R = Y, Nd, Sm, Gd–Lu). *Phys. Rev. B* **2009**, *80*, 104403.
- (90) Niepmann, D.; Prots, Y. M.; Pöttgen, R.; Jeitschko, W. The order of the palladium and germanium atoms in the germanides LnPdGe (Ln = La–Nd, Sm, Gd, Tb) and the new compound $\text{Yb}_3\text{Pd}_4\text{Ge}_4$. *J. Solid State Chem.* **2000**, *154*, 329–337.
- (91) Sebastian, C. P.; Salvador, J.; Martin, J. B.; Kanatzidis, M. G. New intermetallics YbAu_2In_4 and $\text{Yb}_2\text{Au}_3\text{In}_3$. *Inorg. Chem.* **2010**, *49*, 10468–10474.
- (92) Kußmann, D.; Pöttgen, R.; Kotzyba, G. New $\text{Yb}_2\text{Pt}_3\text{Sn}_3$ type stannides. *J. Solid State Chem.* **2000**, *150*, 112–120.
- (93) Macaluso, R. T.; Nakatsuji, S.; Kuga, K.; Thomas, E. L.; Machida, Y.; Maeno, Y.; Fisk, Z.; Chan, J. Y. Crystal structure and physical properties of polymorphs of LnAlB_4 (Ln = Yb, Lu). *Chem. Mater.* **2007**, *19*, 1918–1922.
- (94) Mikhalenko, S. I.; Kuz'ma, Y. B.; Korsukova, M. M.; Gurin, V. N. Ternary borides containing a rare earth and aluminum, with YCrB_4 and Y_2ReB_6 structures. *Inorg. Mater.* **1980**, *16*, 1325–1328.
- (95) Bonrath, H.; Hellwege, K. H.; Nicolay, K.; Weber, G. Antiferromagnetische Umwandlung von Dy_2O_3 , Er_2O_3 und Yb_2O_3 im Temperaturbereich von 1,1 bis 4,2 K. *Phys. Kondens. Mater.* **1966**, *4*, 382–390.
- (96) Zell, W.; Pott, R.; Roden, B.; Wohlleben, D. Pressure and temperature dependence of the magnetic susceptibility of some ytterbium compounds with intermediate valence. *Solid State Commun.* **1981**, *40*, 751–754.
- (97) Klaasse, J. C. P.; Sterkenburg, J. W. E.; Bleyendaal, A. H. M.; de Boer, F. R. Ambiguous magnetic behaviour of some Yb-compounds. *Solid State Commun.* **1973**, *12*, 561–564.
- (98) Tappe, F.; Schwickert, C.; Eul, M.; Pöttgen, R. Intermetallic cadmium compounds $\text{M}_5\text{T}_2\text{Cd}$ (M = Ca, Yb, Eu; T = Cu, Ag, Au) with $\text{Mo}_3\text{B}_2\text{Si}$ -type structure. *Z. Naturforsch.* **2011**, *66b*, 1219–1224.
- (99) Reimann, M. K.; Klenner, S.; Gerdes, J. M.; Hansen, M. R.; Pöttgen, R. Magnesium-rich intermetallic compounds $\text{RE}_3\text{Ag}_4\text{Mg}_{12}$ (RE = Y, La–Nd, Sm–Dy, Yb) and $\text{AE}_3\text{Ag}_4\text{Mg}_{12}$ (AE = Ca, Sr). *Z. Kristallogr.* **2022**, *237*, 417–427.
- (100) Johrendt, D.; Kotzyba, G.; Trill, H.; Mosel, B. D.; Eckert, H.; Fickenscher, T.; Pöttgen, R. Magnetic and electrical properties, ^{151}Eu Mössbauer spectroscopy, and chemical bonding of REAgMg (RE = La, Ce, Eu, Yb) and EuAuMg . *J. Solid State Chem.* **2002**, *164*, 201–209.
- (101) Mishra, R.; Pöttgen, R.; Hoffmann, R.-D.; Kaczorowski, D.; Piotrowski, H.; Mayer, P.; Rosenhahn, C.; Mosel, B. D. Ternary rare earth (RE) gold compounds REAuCd and $\text{RE}_2\text{Au}_2\text{Cd}$. *Z. Anorg. Allg. Chem.* **2001**, *627*, 1283–1291.
- (102) Fickenscher, T.; Kotzyba, G.; Hoffmann, R.-D.; Pöttgen, R. Synthesis, structure, and magnetic properties of EuAgCd and YbAgCd . *Z. Naturforsch.* **2001**, *56b*, 598–603.
- (103) Galadzhun, Y. V.; Hoffmann, R.-D.; Kotzyba, G.; Künnen, B.; Pöttgen, R. EuPdIn_2 , YbPdIn_2 , and YbAuIn_2 : Syntheses, structures, and properties of new intermetallic compounds with ordered Re_3B -type structure. *Eur. J. Inorg. Chem.* **1999**, *1999*, 975–979.
- (104) Katoh, K.; Takabatake, T.; Minami, A.; Oguro, I.; Sawa, H. Crystal growth of YbTX (T = Cu, Ag, Pt, Au; X = Sn, Sb) and the magnetic and transport properties. *J. Alloys Compd.* **1997**, *261*, 32–36.
- (105) Lueken, H. *Magnetochemie*. B. G. Teubner: Stuttgart, Leipzig, 1999.
- (106) Szytuła, A.; Jezierski, A.; Penc, B.; Winiarski, A.; Leithe-Jasper, A.; Kaczorowski, D. Electronic structure of YbTX compounds. *J. Alloys Compd.* **2003**, *360*, 41–46.
- (107) Fritsch, G. “Heavy Fermionen”-Systeme. *Phys. Unserer Zeit* **1987**, *18*, 17–20.
- (108) Fisk, Z.; Maple, M. B. On the existence of heavy fermion ytterbium compounds. *J. Alloys Compd.* **1992**, *183*, 303–311.
- (109) Jeong, T. Electronic structure and magnetism of YbRhSn . *Eur. Phys. J. B* **2006**, *53*, 213–217.

- (110) Pietri, R.; Andracka, B.; Kaczorowski, D.; Leithe-Jasper, A.; Rogl, P. Magnetoresistance and low-temperature specific heat of the Yb compounds YbRhSn, YbPdBi, and YbPtSn. *Phys. Rev. B* **2000**, *61*, 12169–12173.
- (111) Sales, B. C.; Wohlleben, D. K. Susceptibility of interconfiguration-fluctuation compounds. *Phys. Rev. Lett.* **1975**, *35*, 1240–1244.
- (112) Grytsiv, A.; Kaczorowski, D.; Leithe-Jasper, A.; Rogl, P.; Potel, M.; Noël, H.; Pikul, A. P.; Velikanova, T. Structure and properties of Yb₃Ge₅. *J. Solid State Chem.* **2002**, *165*, 178–181.
- (113) Havinga, E. E.; Buschow, K. H. J.; van Daal, H. J. The ambivalence of Yb in YbAl₂ and YbAl₃. *Solid State Commun.* **1973**, *13*, 621–627.
- (114) Klaasse, J. C. P.; Mattens, W. C. M.; de Boer, F. R.; de Châtel, P. F. Magnetic properties of ytterbium intermetallic compounds with intermediate valency. *Physica B* **1977**, *86–88*, 234–236.
- (115) Kaindl, G.; Reihl, B.; Eastman, D. E.; Pollak, R. A.; Mårtensson, N.; Barbara, B.; Penney, T.; Plaskett, T. S. Surface core-level shifts and surface valence change in mixed-valent YbAl₂. *Solid State Commun.* **1982**, *41*, 157–160.
- (116) Matsunami, M.; Chainani, A.; Taguchi, M.; Eguchi, R.; Takata, Y.; Oura, M.; Yabashi, M.; Tamazaki, K.; Nishino, Y.; Ishikawa, T.; Kosaka, M.; Shin, S. Photoemission evidence for valence fluctuations and Kondo resonance in YbAl₂. *J. Phys. Soc. Jpn.* **2012**, *81*, 073702.
- (117) Matsunami, M.; Hajiri, T.; Miyazaki, H.; Kosaka, M.; Kimura, S. Strongly hybridized electronic structure of YbAl₂: An angle-resolved photoemission study. *Phys. Rev. B* **2013**, *87*, 165141.
- (118) Cornelius, A. L.; Lawrence, J. M.; Ebihara, T.; Riseborough, P. S.; Booth, C. H.; Hundley, M. F.; Pagliuso, P. G.; Sarrao, J. L.; Thompson, J. D.; Jung, M. H.; Lacerda, A. H.; Kwei, G. H. Two energy scales and slow crossover in YbAl₃. *Phys. Rev. Lett.* **2002**, *88*, 117201.
- (119) Okamura, H.; Michizawa, T.; Nanba, T.; Ebihara, T. Pseudogap formation and heavy-carrier dynamics in intermediate-valence YbAl₃. *J. Phys. Soc. Jpn.* **2004**, *73*, 2045–2048.
- (120) Christianson, A. D.; Fanelli, V. R.; Lindsay, L.; Mu, S.; Rahn, M. C.; Mazzone, D. G.; Qaid, A. H.; Ronning, F.; Bauer, E. D.; Lawrence, J. M. Phonons, Q-dependent Kondo spin fluctuations, and 4f phonon resonance in YbAl₃. *Phys. Rev. B* **2020**, *102*, 205135.
- (121) Kasaya, M.; Tani, T.; Iga, F.; Kasuya, T. Electrical resistivity, hall constant and magnetic susceptibility in the Kondo states Ce(Ni_{1-x}Pd_x)Sn and YbNiSn. *J. Magn. Magn. Mater.* **1988**, *76–77*, 278–280.
- (122) Kasaya, M.; Tani, T.; Kawate, K.; Mizushima, T.; Isikawa, Y.; Sato, K. Magnetic properties of the dense Kondo compound YbNiSn. *J. Phys. Soc. Jpn.* **1991**, *60*, 3145–3149.
- (123) Kasaya, M.; Tani, T.; Ohoyama, K.; Kohgi, M.; Isikawa, Y. Magnetic properties of the dense Kondo compounds CePdSn and YbNiSn. *J. Magn. Magn. Mater.* **1992**, *104–107*, 665–666.
- (124) Bellot, P.; Bonville, P.; Hammann, J.; Hodges, J. A.; Imbert, P.; Jéhanho, G.; Leylekian, L.; D'Onofrio, L. Ferromagnetic ordering in the Kondo lattice YbNiSn. *J. Magn. Magn. Mater.* **1992**, *108*, 141–142.
- (125) Bonville, P.; Bellot, P.; Hodges, J. A.; Imbert, P.; Jéhanho, G.; Le Bras, G.; Hammann, J.; Leylekian, L.; Chevrier, G.; Thuéry, P.; D'Onofrio, L.; Hamzic, A.; Barthélémy, A. YbNiSn, a ferromagnetic Kondo lattice. *Physica B* **1992**, *182*, 105–117.
- (126) Trovarelli, O.; Geibel, C.; Cardoso, R.; Mederle, S.; Borth, R.; Buschinger, B.; Grosche, F. M.; Grin, Y.; Sparn, G.; Steglich, F. Low-temperature properties of the Yb-based heavy-fermion antiferromagnets YbPtIn, YbRhSn, and YbNiGa. *Phys. Rev. B* **2000**, *61*, 9467–9474.
- (127) Kaczorowski, D.; Leithe-Jasper, A.; Rogl, P.; Flandorfer, H.; Cichorek, T.; Pietri, R.; Andracka, B. Magnetic, thermodynamic, and electrical transport properties of ternary equiatomic ytterbium compounds YbTM (T = transition metal, M = Sn and Bi). *Phys. Rev. B* **1999**, *60*, 422–433.
- (128) Kato, K.; Terui, G.; Niide, Y.; Aoki, H.; Ochiai, A. Magnetic properties and electrical resistivity of YbRhSn and YbIrSn. *Physica B* **1999**, *259–261*, 161–162.
- (129) Muro, Y.; Haizaki, Y.; Kim, M. S.; Umeo, K.; Tou, H.; Sera, M.; Takabatake, T. Heavy-fermion weak-ferromagnet YbRhSb. *Phys. Rev. B* **2004**, *69*, 020401.
- (130) Muro, Y.; Haizaki, Y.; Umeo, K.; Tou, H.; Sera, M.; Sakakibara, T.; Takabatake, T. Effects of magnetic field and pressure on the weak ferromagnetism of YbRhSb. *Physica B* **2005**, *359–361*, 124–126.
- (131) Umeo, K.; Kubo, H.; Muro, Y.; Nakamura, F.; Suzuki, T.; Takabatake, T. Pressure-induced ferromagnetic order in the weak ferromagnet YbRhSb. *J. Phys.: Conf. Series* **2009**, *150*, 042223.
- (132) Umeo, K.; Yamane, H.; Kubo, H.; Muro, Y.; Takabatake, T. Pressure-induced transition from a canted antiferromagnetic state to a ferromagnetic state in YbRhSb. *J. Phys.: Conf. Series* **2010**, *200*, 012215.
- (133) Umeo, K.; Yamane, H.; Kubo, H.; Muro, Y.; Nakamura, F.; Suzuki, T.; Takabatake, T.; Sengupta, K.; Forthaus, M. K.; Abd-Elmeguid, M. M. Interplay between crystal electric field and magnetic exchange anisotropies in the heavy-fermion antiferromagnet YbRhSb under pressure. *Phys. Rev. B* **2012**, *85*, 024412.
- (134) Marazza, R.; Rossi, D.; Ferro, R. Magnesium silver arsenide-type phases in the ternary systems of rare earths with palladium and bismuth. *Gazz. Chim. Ital.* **1980**, *11* (44), 357–359.
- (135) Canfield, P. C.; Thompson, J. D.; Beyermann, W. P.; Lacerda, A.; Hundley, M. F.; Peterson, E.; Fisk, Z.; Ott, H. R. Magnetism and heavy fermion-like behavior in the RbPt series. *J. Appl. Phys.* **1991**, *70*, 5800–5802.
- (136) Fisk, Z.; Canfield, P. C.; Beyermann, W. P.; Thompson, J. D.; Hundley, M. F.; Ott, H. R.; Felder, E.; Maple, M. B.; Lopez de la Torre, M. A.; Visani, P.; Seaman, C. L. Massive electron state in YbBiPt. *Phys. Rev. Lett.* **1991**, *67*, 3310–3313.
- (137) Mun, E.; Bud'ko, S. L.; Lee, Y.; Martin, C.; Tanatar, M. A.; Prozorov, R.; Canfield, P. C. Quantum oscillations in the heavy-fermion compound YbPtBi. *Phys. Rev. B* **2015**, *92*, 085135.
- (138) Movshovich, R.; Lacerda, A.; Canfield, P. C.; Thompson, J. D.; Fisk, Z. Fermi surface instability and symmetry breaking in heavy-fermion compound YbBiPt. *Phys. Rev. Lett.* **1994**, *73*, 492–495.
- (139) Lacerda, A.; Movshovich, R.; Hundley, M. F.; Canfield, P. C.; Arms, D.; Sparn, G.; Thompson, J. D.; Fisk, Z.; Fisher, R. A.; Phillips, N. E.; Ott, H. R. Doping and pressure studies on YbBiPt. *J. Appl. Phys.* **1993**, *73*, 5415–5417.
- (140) Movshovich, R.; Lacerda, A.; Canfield, P. C.; Thompson, J. D.; Fisk, Z. Low-temperature phase diagram of YbBiPt. *J. Appl. Phys.* **1994**, *76*, 6121–6123.
- (141) Ueland, B. G.; Kreyssig, A.; Prokeš, K.; Lynn, J. W.; Harriger, L. W.; Pratt, D. K.; Singh, D. K.; Heitmann, T. W.; Sauerbrei, S.; Saunders, S. M.; Mun, E. D.; Bud'ko, S. L.; McQueeney, R. J.; Canfield, P. C.; Goldman, A. I. Fragile antiferromagnetism in the heavy-fermion compound YbBiPt. *Phys. Rev. B* **2014**, *89*, 180403.
- (142) Ueland, B. G.; Kreyssig, A.; Mun, E. D.; Lynn, J. W.; Harriger, L. W.; Pratt, D. K.; Prokeš, K.; Hüsages, Z.; Toft-Petersen, R.; Sauerbrei, S.; Saunders, S. M.; Furukawa, Y.; Bud'ko, S. L.; McQueeney, R. J.; Canfield, P. C.; Goldman, A. I. Magnetic-field effects on the fragile antiferromagnetism in YbBiPt. *Phys. Rev. B* **2019**, *99*, 184431.
- (143) Krypyakevych, P. I.; Markiv, V. Y.; Mel'nyk, E. V. Crystal structures of the compounds ZrNiAl, ZrCuGa and their analogues. *Dopov. Akad. Nauk Ukr. RSR* **1967**, *Ser. A*, 750–753.
- (144) Dwight, A. E.; Mueller, M. H.; Conner, R. A., Jr.; Downey, J. W.; Knott, H. W. Ternary compounds with the Fe₂P-type structure. *Trans. Metall. Soc. AIME* **1968**, *242*, 2075–2080.
- (145) Zumdick, M. F.; Hoffmann, R.-D.; Pöttgen, R. The intermetallic zirconium compounds ZrNiAl, ZrRhSn, and ZrPtGa - structural distortions and metal-metal bonding in Fe₂P related compounds. *Z. Naturforsch.* **1999**, *54b*, 45–53.

- (146) Mattens, W. C. M.; Elenbaas, R. A.; de Boer, F. R. Mixed-valence behavior in the intermetallic compound ytterbium-copper-aluminum (YbCuAl). *Commun. Phys.* **1977**, *2*, 147–150.
- (147) Mattens, W. C. M.; de Châtel, P. F.; Moleman, A. C.; de Boer, F. R. Intermediate-valence state of Yb in Y- and Gd-substituted YbCuAl. *Physica B* **1979**, *96*, 138–143.
- (148) Pott, R.; Schefzyk, R.; Wohlleben, D.; Junod, A. Thermal expansion and specific heat of intermediate valent YbCuAl. *Z. Phys. B: Condens. Matter* **1981**, *44*, 17–24.
- (149) Bonville, P. Kondo effect and heavy fermions in Yb compounds. *Hyperfine Interact.* **1988**, *40*, 15–29.
- (150) Friedemann, S.; Wirth, S.; Oeschler, N.; Krellner, C.; Geibel, C.; Steglich, F.; MaQuillon, S.; Fisk, Z.; Paschen, S.; Zwicky, G. Hall effect measurements and electronic structure calculations on YbRh₂Si₂ and its reference compounds LuRh₂Si₂ and YbIr₂Si₂. *Phys. Rev. B* **2010**, *82*, 035103.
- (151) Kummer, K.; Patil, S.; Chikina, A.; Güttler, M.; Höppner, M.; Generalov, A.; Danzenbächer, S.; Seiro, S.; Hannaske, A.; Krellner, C.; Kucherenko, Y.; Shi, M.; Radovic, M.; Rienks, E.; Zwicky, G.; Matho, K.; Allen, J. W.; Laubschat, C.; Geibel, C.; Vyalikh, D. V. Temperature-independent Fermi surface in the Kondo lattice YbRh₂Si₂. *Phys. Rev. X* **2015**, *5*, 011028.
- (152) Zwicky, G. The utility of band theory in strongly correlated electron systems. *Rep. Prog. Phys.* **2016**, *79*, 124501.
- (153) Li, Y.; Wang, Q.; Xu, Y.; Xie, W.; Yang, Y.-F. Nearly degenerate $p_x + ip_y$ and $d_{x^2-y^2}$ pairing symmetry in the heavy fermion superconductor YbRh₂Si₂. *Phys. Rev. B* **2019**, *100*, 085132.
- (154) Güttler, M.; Kummer, K.; Kliemt, K.; Krellner, C.; Seiro, S.; Geibel, C.; Laubschat, C.; Kubo, Y.; Sakurai, Y.; Vyalikh, D. V.; Koizumi, A. Visualizing the Kondo lattice crossover in YbRh₂Si₂ with Compton scattering. *Phys. Rev. B* **2021**, *103*, 115126.
- (155) Stock, C.; Broholm, C.; Demmel, F.; Van Duijn, J.; Taylor, J. W.; Kang, H. J.; Hu, R.; Petrovic, C. From incommensurate correlations to mesoscopic spin resonance in YbRh₂Si₂. *Phys. Rev. Lett.* **2012**, *109*, 127201.
- (156) Gegenwart, P.; Custers, J.; Tokiwa, Y.; Geibel, C.; Steglich, F. Ferromagnetic quantum critical fluctuations in YbRh₂(Si_{0.95}Ge_{0.05})₂. *Phys. Rev. Lett.* **2005**, *94*, 076402.
- (157) Ishida, K.; Okamoto, K.; Kawasaki, Y.; Kitaoka, Y.; Trovarelli, O.; Geibel, C.; Steglich, F. YbRh₂Si₂: Spin fluctuations in the vicinity of a quantum critical point at low magnetic field. *Phys. Rev. Lett.* **2002**, *89*, 107202.
- (158) Sichelschmidt, J.; Ivanshin, V. A.; Ferstl, J.; Geibel, C.; Steglich, F. Low temperature electron spin resonance of the Kondo ion in a heavy fermion metal: YbRh₂Si₂. *Phys. Rev. Lett.* **2003**, *91*, 156401.
- (159) Abrahams, E.; Wölfle, P. Electron spin resonance in Kondo systems. *Phys. Rev. B* **2008**, *78*, 104423.
- (160) Wölfle, P.; Abrahams, E. Phenomenology of ESR in heavy-fermion systems: Fermi-liquid and non-Fermi-liquid regimes. *Phys. Rev. B* **2009**, *80*, 235112.
- (161) Ishida, K.; MacLaughlin, D. E.; Young, B.-L.; Okamoto, K.; Kawasaki, Y.; Kitaoka, Y.; Nieuwenhuys, G. J.; Heffner, R. H.; Bernal, O. O.; Higemoto, W.; Koda, A.; Kadono, R.; Trovarelli, O.; Geibel, C.; Steglich, F. Low-temperature magnetic order and spin dynamics in YbRh₂Si₂. *Phys. Rev. B* **2003**, *68*, 184401.
- (162) Gegenwart, P.; Custers, J.; Geibel, C.; Neumaier, K.; Tayama, T.; Tenya, K.; Trovarelli, O.; Steglich, F. Magnetic-field induced quantum critical point in YbRh₂Si₂. *Phys. Rev. Lett.* **2002**, *89*, 056402.
- (163) Custers, J.; Gegenwart, P.; Wilhelm, H.; Neumaier, K.; Tokiwa, Y.; Trovarelli, O.; Geibel, C.; Steglich, F.; Pépin, C.; Coleman, P. The break-up of heavy electrons at a quantum critical point. *Nature* **2003**, *424*, 524–527.
- (164) Hamann, S.; Zhang, J.; Jang, D.; Hannaske, A.; Steinke, L.; Lausberg, S.; Pedrero, L.; Klingner, C.; Baenitz, M.; Steglich, F.; Krellner, C.; Geibel, C.; Brando, M. Evolution from ferromagnetism to antiferromagnetism in Yb(Rh_{1-x}Co_x)₂Si₂. *Phys. Rev. Lett.* **2019**, *122*, 077202.
- (165) Lausberg, S.; Hannaske, A.; Steppke, A.; Steinke, L.; Gruner, T.; Pedrero, L.; Krellner, C.; Klingner, C.; Brando, M.; Geibel, C.; Steglich, F. Doped YbRh₂Si₂: Not only ferromagnetic correlations but ferromagnetic order. *Phys. Rev. Lett.* **2013**, *110*, 256402.
- (166) Schuberth, E.; Tippmann, M.; Steinke, L.; Lausberg, S.; Steppke, A.; Brando, M.; Krellner, C.; Geibel, C.; Yu, R.; Si, Q.; Steglich, F. Emergence of superconductivity in the canonical heavy-electron metal YbRh₂Si₂. *Science* **2016**, *351*, 485–488.
- (167) Nguyen, D. H.; Sidorenko, A.; Taupin, M.; Knebel, G.; Lapertot, G.; Schuberth, E.; Paschen, S. Superconductivity in an extreme strange metal. *Nature Commun.* **2021**, *12*, 4341.
- (168) Knapp, J.; Levitin, L. V.; Nyéki, J.; Ho, A. F.; Cowan, B.; Saunders, J.; Brando, M.; Geibel, C.; Kliemt, K.; Krellner, C. Electronuclear transition into a spatially modulated magnetic state in YbRh₂Si₂. *Phys. Rev. Lett.* **2023**, *130*, 126802.
- (169) Trovarelli, O.; Geibel, C.; Steglich, F. Low-temperature properties of YbRh₂Si₂. *Physica B* **2000**, *284–288*, 1507–1508.
- (170) Sriram Shastry, B.; Sutherland, B. Exact ground state of a quantum mechanical antiferromagnet. *Physica B+C* **1981**, *108*, 1069–1070.
- (171) Miyahara, S.; Ueda, K. Exact dimer ground state of the two dimensional Heisenberg spin system SrCu₂(BO₃)₂. *Phys. Rev. Lett.* **1999**, *82*, 3701–3704.
- (172) Lee, J. Y.; You, Y.-Z.; Sachdev, S.; Vishwanath, A. Signatures of a deconfined phase transition on the Shastry-Sutherland lattice: Applications to quantum critical SrCu₂(BO₃)₂. *Phys. Rev. X* **2019**, *9*, 041037.
- (173) Kim, M. S.; Bennett, M. C.; Aronson, M. C. Yb₂Pt₂Pb: Magnetic frustration in the Shastry-Sutherland lattice. *Phys. Rev. B* **2008**, *77*, 144425.
- (174) Kim, M. S.; Bennett, M. C.; Aronson, M. C. Yb₂Pt₂Pb: A new quasi-two-dimensional antiferromagnet. *Physica B* **2008**, *403*, 1411–1413.
- (175) Shimura, Y.; Sakakibara, T.; Iwakawa, K.; Ōnuki, Y.; Sugiyama, K. Magnetization steps in Yb₂Pt₂Pb with the Shastry-Sutherland lattice. *J. Korean Phys. Soc.* **2013**, *63*, 551–554.
- (176) Miiller, W.; Wu, L. S.; Kim, M. S.; Orvis, T.; Simonson, J. W.; Gamza, M.; McNally, D. M.; Nelson, C. S.; Ehlers, G.; Podlesnyak, A.; Helton, J. S.; Zhao, Y.; Qiu, Y.; Copley, J. R. D.; Lynn, J. W.; Zalitznyak, I.; Aronson, M. C. Magnetic structure of Yb₂Pt₂Pb: Ising moments on the Shastry-Sutherland lattice. *Phys. Rev. B* **2016**, *93*, 104419.
- (177) Ochiai, A.; Inukai, T.; Matsumura, T.; Oyama, A.; Katoh, K. Spin gap state of $I = 1/2$ Heisenberg antiferromagnet YbAl₃C₃. *J. Phys. Soc. Jpn.* **2007**, *76*, 123703.
- (178) Matsumura, T.; Inami, T.; Kosaka, M.; Kato, Y.; Inukai, T.; Ochiai, A.; Nakao, H.; Murakami, Y.; Katano, S.; Suzuki, H. Structural phase transition in the spin gap system YbAl₃C₃. *J. Phys. Soc. Jpn.* **2008**, *77*, 103601.
- (179) Mito, T.; Tomisawa, S.; Wada, S.; Harima, H.; Hashi, K.; Shimizu, T.; Goto, A.; Ohki, S.; Kato, Y.; Kosaka, M. ²⁷Al NMR/NQR Studies of YbAl₃C₃. *J. Phys. Soc. Jpn.* **2009**, *78*, 014709.
- (180) Hara, K.; Matsuda, S.; Matsuoka, E.; Tanigaki, K.; Ochiai, A.; Nakamura, S.; Nojima, T.; Katoh, K. Quantum spin state in the rare-earth compound YbAl₃C₃. *Phys. Rev. B* **2012**, *85*, 144416.
- (181) Kittaka, S.; Sugiyama, T.; Shimura, Y.; Sakakibara, T.; Matsuda, S.; Ochiai, A. Singlet-triplet crossover in the two-dimensional dimer spin system YbAl₃C₃. *J. Korean Phys. Soc.* **2013**, *62*, 2088–2092.
- (182) Kato, Y.; Kosaka, M.; Nowatari, H.; Saiga, Y.; Yamada, A.; Kobiyama, T.; Katano, S.; Ohoyama, K.; Suzuki, H.; Aso, N.; Iwasa, K. Spin-singlet ground state in the two-dimensional frustrated triangular lattice: YbAl₃C₃. *J. Phys. Soc. Jpn.* **2008**, *77*, 053701.
- (183) Torikachvili, M. S.; Jia, S.; Mun, E. D.; Hannaske, S. T.; Black, R. C.; Neils, W. K.; Martien, D.; Bud'ko, S. L.; Canfield, P. C. YbT₂Zn₂₀ (T = Fe, Co, Ru, Rh, Os, Ir): six closely related heavy fermion compounds. *Proc. Natl. Acad. Sci. U. S. A.* **2007**, *104*, 9960.
- (184) Saiga, Y.; Matsubayashi, K.; Fujiwara, T.; Kosaka, M.; Katano, S.; Hedo, M.; Matsumoto, T.; Uwatoko, Y. Pressure-induced

magnetic transition in a single crystal of $\text{YbCo}_2\text{Zn}_{20}$. *J. Phys. Soc. Jpn.* **2008**, *77*, 053710.

(185) Matsubayashi, K.; Saiga, Y.; Matsumoto, T.; Uwatoko, Y. Fermi-liquid properties of the heavy fermion systems $\text{YbT}_2\text{Zn}_{20}$ ($T = \text{Ir, Rh and Co}$) under pressure. *J. Phys.: Conf. Series* **2009**, *150*, 042117.

(186) Yamanaka, R.; Matsubayashi, K.; Saiga, Y.; Kawae, T.; Uwatoko, Y. Heat capacity measurement of heavy Fermion $\text{YbCo}_2\text{Zn}_{20}$ under magnetic field. *J. Phys.: Conf. Series* **2012**, *391*, 012078.

(187) Gladyshevskii, E. I.; Krypyakevych, P. I.; Teslyuk, M. Y. Crystal structure of the ternary phase Cu_4MgSn . *Dokl. Akad. Nauk. SSSR* **1952**, *85*, 81–84.

(188) Osamura, K.; Murakami, Y. Crystal structures of CuSnMg and Cu_4SnMg ternary compounds. *J. Less-Common Met.* **1978**, *60*, 311–313.

(189) Kojima, K.; Hayashi, H.; Minami, A.; Kasamatsu, Y.; Hihara, T. Crystal phases and Yb valence transition in $\text{Yb}_x\text{In}_{1-x}\text{Cu}_2$. *J. Magn. Mater.* **1989**, *81*, 267–272.

(190) Felner, I.; Nowik, I. First-order valence phase transition in cubic $\text{Yb}_x\text{In}_{1-x}\text{Cu}_2$. *Phys. Rev. B* **1986**, *33*, 617–619.

(191) Felner, I.; Nowik, I.; Vaknin, D.; Potzel, U.; Moser, J.; Kalvius, G. M.; Wortmann, G.; Schmiester, G.; Hilscher, G.; Gratz, E.; Schmitzer, C.; Pillmayr, N.; Prasad, K. G.; de Waard, H.; Pinto, H. Ytterbium valence phase transition in $\text{Yb}_x\text{In}_{1-x}\text{Cu}_2$. *Phys. Rev. B* **1987**, *35*, 6956–6963.

(192) Sato, H.; Shimada, K.; Arita, M.; Hiraoka, K.; Kojima, K.; Takeda, Y.; Yoshikawa, K.; Sawada, M.; Nakatake, M.; Namatame, H.; Taniguchi, M.; Takata, Y.; Ikenaga, E.; Shin, S.; Kobayashi, K.; Tamasaku, K.; Nishino, Y.; Miwa, D.; Yabashi, M.; Ishikawa, T. Valence transition of YbInCu_4 observed in hard X-ray photoemission spectra. *Phys. Rev. Lett.* **2004**, *93*, 246404.

(193) Sarrao, J. L. Physics of YbInCu_4 and related compounds. *Physica B* **1999**, *259–261*, 128–133.

(194) Lawrence, J. M.; Kwei, G. H.; Sarrao, J. L.; Fisk, Z.; Mandrus, D.; Thompson, J. D. Structure and disorder in YbInCu_4 . *Phys. Rev. B* **1996**, *54*, 6011–6014.

(195) Sato, H.; Taniguchi, M.; Hiraoka, K.; Kojima, K. Valence transition of YbInCu_4 observed by photoemission spectroscopy. *e-J. Surf. Sci. Nanotechnol.* **2011**, *9*, 90–94.

(196) H. Matsuda, Y.; Inami, T.; Ohwada, K.; Murata, Y.; Nojiri, H.; Murakami, Y.; Ohta, H.; Zhang, W.; Yoshimura, K. High-magnetic-field X-ray absorption spectroscopy of field-induced valence transition in YbInCu_4 . *J. Phys. Soc. Jpn.* **2007**, *76*, 034702.

(197) Dallera, C.; Grioni, M.; Shukla, A.; Vankó, G.; Sarrao, J. L.; Rueff, J. P.; Cox, D. L. New spectroscopy solves an old puzzle: The Kondo scale in heavy fermions. *Phys. Rev. Lett.* **2002**, *88*, 196403.

(198) Hancock, J. N.; McKnew, T.; Schlesinger, Z.; Sarrao, J. L.; Fisk, Z. Kondo scaling in the optical response of $\text{YbIn}_{1-x}\text{Ag}_x\text{Cu}_4$. *Phys. Rev. Lett.* **2004**, *92*, 186405.

(199) Lawrence, J. M.; Shapiro, S. M.; Sarrao, J. L.; Fisk, Z. Inelastic neutron scattering in single-crystal YbInCu_4 . *Phys. Rev. B* **1997**, *55*, 14467–14472.

(200) Zhang, M. Y.; Chen, R. Y.; Dong, T.; Wang, N. L. Dramatic change of photoexcited quasiparticle relaxation dynamics across Yb valence state transition in YbInCu_4 . *Phys. Rev. B* **2017**, *95*, 165104.

(201) Cornelius, A. L.; Lawrence, J. M.; Sarrao, J. L.; Fisk, Z.; Hundley, M. F.; Kwei, G. H.; Thompson, J. D.; Booth, C. H.; Bridges, F. Experimental studies of the phase transition in $\text{YbIn}_{1-x}\text{Ag}_x\text{Cu}_4$. *Phys. Rev. B* **1997**, *56*, 7993–8000.

(202) Kishimoto, Y.; Kawasaki, Y.; Ohno, T. Mixed valence state in Ce and Yb compounds studied by magnetic susceptibility. *Phys. Lett. A* **2003**, *317*, 308–314.

(203) Sarrao, J. L.; Immer, C. D.; Benton, C. L.; Fisk, Z.; Lawrence, J. M.; Mandrus, D.; Thompson, J. D. Evolution from first-order valence transition to heavy-fermion behavior in $\text{YbIn}_{1-x}\text{Ag}_x\text{Cu}_4$. *Phys. Rev. B* **1996**, *54*, 12207–12211.

(204) Nakatsuji, S.; Kuga, K.; Machida, Y.; Tayama, T.; Sakakibara, T.; Karaki, Y.; Ishimoto, H.; Yonezawa, S.; Maeno, Y.; Pearson, E.;

Lonzarich, G. G.; Balicas, L.; Lee, H.; Fisk, Z. Superconductivity and quantum criticality in the heavy-fermion system $\beta\text{-YbAlB}_4$. *Nat. Phys.* **2008**, *4*, 603–607.

(205) Kuga, K.; Karaki, Y.; Matsumoto, Y.; Machida, Y.; Nakatsuji, S. Superconducting properties of the non-Fermi-liquid system $\beta\text{-YbAlB}_4$. *Phys. Rev. Lett.* **2008**, *101*, 137004.

(206) Nakatsuji, S.; Kuga, K.; Tomita, T.; Matsumoto, Y. Pronounced non-Fermi-liquid behavior of the quantum critical heavy fermion superconductor $\beta\text{-YbAlB}_4$. *Phys. Status Solidi B* **2010**, *247*, 485–489.

(207) Okawa, M.; Matsunami, M.; Ishizaka, K.; Eguchi, R.; Taguchi, M.; Chainani, A.; Takata, Y.; Yabashi, M.; Tamasaku, K.; Nishino, Y.; Ishikawa, T.; Kuga, K.; Horie, N.; Nakatsuji, S.; Shin, S. Strong valence fluctuation in the quantum critical heavy fermion superconductor $\beta\text{-YbAlB}_4$: A hard X-ray photoemission study. *Phys. Rev. Lett.* **2010**, *104*, 247201.

(208) Sakaguchi, Y.; Ikeda, S.; Kuga, K.; Suzuki, S.; Nakatsuji, S.; Hirao, N.; Ohishi, Y.; Kobayashi, H. Pressure-induced local structural changes in heavy fermion $\beta\text{-YbAlB}_4$. *J. Phys. Soc. Jpn.* **2016**, *85*, 023602.

(209) Matsumoto, Y.; Nakatsuji, S.; Kuga, K.; Karaki, Y.; Horie, N.; Shimura, Y.; Sakakibara, T.; Nevidomskyy, A. H.; Coleman, P. Quantum criticality without tuning in the mixed valence compound $\beta\text{-YbAlB}_4$. *Science* **2011**, *331*, 316–319.

(210) Ramires, A.; Coleman, P.; Nevidomskyy, A. H.; Tselik, A. M. $\beta\text{-YbAlB}_4$: A critical nodal metal. *Phys. Rev. Lett.* **2012**, *109*, 176404.

(211) Holanda, L. M.; Vargas, J. M.; Iwamoto, W.; Rettori, C.; Nakatsuji, S.; Kuga, K.; Fisk, Z.; Oseroff, S. B.; Pagliuso, P. G. Quantum critical Kondo quasiparticles probed by ESR in $\beta\text{-YbAlB}_4$. *Phys. Rev. Lett.* **2011**, *107*, 026402.

(212) Watanabe, S.; Miyake, K. Charge transfer effect under odd-parity crystalline electric field: Divergence of magnetic toroidal fluctuation in $\beta\text{-YbAlB}_4$. *J. Phys. Soc. Jpn.* **2019**, *88*, 033701.

(213) Ramires, A.; Coleman, P. Theory of the electron spin resonance in the heavy fermion metal $\beta\text{-YbAlB}_4$. *Phys. Rev. Lett.* **2014**, *112*, 116405.

(214) Komijani, Y.; Coleman, P. Model for a ferromagnetic quantum critical point in a 1D Kondo lattice. *Phys. Rev. Lett.* **2018**, *120*, 157206.

(215) Kowalczyk, A.; Falkowski, M.; Toliński, T. Valence fluctuations in YbNiAl_4 compound. *J. Appl. Phys.* **2010**, *107*, 123917.

(216) Falkowski, M.; Kowalczyk, A. Thermal and electron transport studies on the valence fluctuating compound YbNiAl_4 . *J. Appl. Phys.* **2018**, *123*, 175106.

(217) Brubaker, Z. E.; Stillwell, R. L.; Chow, P.; Xiao, Y.; Kenney-Benson, C.; Ferry, R.; Popov, D.; Donald, S. B.; Söderlind, P.; Campbell, D. J.; Paglione, J.; Huang, K.; Baumbach, R. E.; Zieve, R. J.; Jeffries, J. R. Pressure-dependent intermediate valence behavior in YbNiGa_4 and YbNiIn_4 . *Phys. Rev. B* **2018**, *98*, 214115.

(218) Sichevych, O.; Prots, Y.; Utsumi, Y.; Akselrud, L.; Schmidt, M.; Burkhardt, U.; Coduri, M.; Schnelle, W.; Bobnar, M.; Wang, Y.-T.; Wu, Y.-H.; Tsuei, K.-D.; Tjeng, L. H.; Grin, Y. Intermediate-valence ytterbium compound $\text{Yb}_4\text{Ga}_{24}\text{Pt}_9$: Synthesis, crystal structure, and physical properties. *Inorg. Chem.* **2017**, *56*, 9343–9352.

(219) Schumacher, L.; Engelbert, S.; Reimann, M. K.; Kösters, J.; Pöttgen, R. Intermediate ytterbium valence in YbRhSn_2 . *Z. Naturforsch.* **2022**, *77b*, 687–692.

(220) Grin, Y.; Pöttgen, R.; Ormeci, A.; Kremer, R. K.; Wagner, F. E. Intermediate-valence intermetallic phase $\text{YbIn}_{1-x}\text{Au}_{1+x}$ ($x = 0\text{--}0.3$). *Crust. Res. Technol.* **2017**, *52*, 1700101.

(221) Jiang, W. B.; Yang, L.; Guo, C. Y.; Hu, Z.; Lee, J. M.; Smidman, M.; Wang, Y. F.; Shang, T.; Cheng, Z. W.; Gao, F.; Ishii, H.; Tsuei, K. D.; Liao, Y. F.; Lu, X.; Tjeng, L. H.; Chen, J. M.; Yuan, H. Q. Crossover from a heavy fermion to intermediate valence state in noncentrosymmetric $\text{Yb}_2\text{Ni}_{12}(\text{P,As})_7$. *Sci. Rep.* **2015**, *5*, 17608.

(222) Fisk, Z.; Yang, N. N.; Maple, M. B.; Ott, H. R. In *Valence fluctuations in solids*, Falicov, L. M.; Hanke, W.; Maple, M. B., Eds.; North-Holland: Amsterdam, 1981.

- (223) Utsumi, Y.; Sato, H.; Ohara, S.; Yamashita, T.; Mimura, K.; Motonami, S.; Shimada, K.; Ueda, S.; Kobayashi, K.; Yamaoka, H.; Tsujii, N.; Hiraoka, N.; Namatame, H.; Taniguchi, M. Electronic structure of Kondo lattice compounds YbNi_3X_9 ($X = \text{Al, Ga}$) studied by hard X-ray spectroscopy. *Phys. Rev. B* **2012**, *86*, 115114.
- (224) Falkowski, M.; Kowalczyk, A.; Toliński, T. Specific heat of YbNi_4Si compound. *Acta Phys. Polon., A* **2008**, *113*, 641–644.
- (225) Yamaoka, H.; Tsujii, N.; Utsumi, Y.; Sato, H.; Jarrige, I.; Yamamoto, Y.; Lin, J.-F.; Hiraoka, N.; Ishii, H.; Tsuei, K.-D.; Mizuki, J. I. Valence transitions in the heavy-fermion compound YbCuAl as a function of temperature and pressure. *Phys. Rev. B* **2013**, *87*, 205120.
- (226) Sales, B. C.; Viswanathan, R. Demagnetization due to interconfiguration fluctuations in the $\text{RE-Cu}_2\text{Si}_2$ compounds. *J. Low Temp. Phys.* **1976**, *23*, 449–467.
- (227) Rossel, C.; Yang, K. N.; Maple, M. B.; Fisk, Z.; Zirngiebl, E.; Thompson, J. D. Strong electronic correlations in a new class of Yb-based compounds: YbXCu_4 ($X = \text{Ag, Au, Pd}$). *Phys. Rev. B* **1987**, *35*, 1914–1918.
- (228) Jaime, M.; Movshovich, R.; Harrison, N.; L. Sarrao, J. Two energy scales in YbInCu_4 from specific heat in high magnetic fields. *Physica B* **2002**, *312–313*, 344–345.
- (229) Sarrao, J. L.; Ramirez, A. P.; Darling, T. W.; Freibert, F.; Migliori, A.; Immer, C. D.; Fisk, Z.; Uwatoko, Y. Thermodynamics of the first-order valence transition in YbCuIn_4 . *Phys. Rev. B* **1998**, *58*, 409–413.
- (230) Katoh, K.; Abe, H.; Negishi, D.; Terui, G.; Niide, Y.; Ochiai, A. Magnetic and transport properties of $\text{Yb}_4\text{Rh}_7\text{Ge}_6$ and $\text{Yb}_4\text{Ir}_7\text{Ge}_6$. *J. Magn. Magn. Mater.* **2004**, *279*, 118–124.
- (231) Katoh, K.; Nakagawa, S.; Terui, G.; Ochiai, A. Magnetic and transport properties of single-crystal YbPtGe . *J. Phys. Soc. Jpn.* **2009**, *78*, 104721.
- (232) Kaczorowski, D.; Andraka, B.; Zaremba, V.; Marucha, C. YbPtIn – a new ytterbium-based magnetic Kondo lattice. *Physica B* **2000**, *281–282*, 44–46.
- (233) Kim, M. S.; Aronson, M. C. Spin liquids and antiferromagnetic order in the Shastry-Sutherland-lattice compound $\text{Yb}_2\text{Pt}_2\text{Pb}$. *Phys. Rev. Lett.* **2013**, *110*, 017201.
- (234) Rhyne, J. J. Neutron scattering in intermetallics. *J. Magn. Magn. Mater.* **1987**, *70*, 88–96.
- (235) Walter, U.; Fisk, Z.; Holland-Moritz, E. Magnetic excitations and quasielastic linewidths in YbBe_{13} from neutron scattering. *J. Magn. Magn. Mater.* **1985**, *47–48*, 159–162.
- (236) Heinrich, G.; Kappler, J. P.; Meyer, A. Magnetic-properties and EPR of YbBe_{13} . *Phys. Lett. A* **1979**, *74*, 121–124.
- (237) Besnus, M. J.; Panissod, P.; Kappler, J. P.; Heinrich, G.; Meyer, A. Crystal field parameters in the REBe_{13} intermetallics. *J. Magn. Magn. Mater.* **1983**, *31–34*, 227–228.
- (238) Walter, U.; Wohleben, D. Unusual magnetic response of intermediate-valent YbPd and Yb_3Pd_4 as studied by inelastic neutron scattering. *Phys. Rev. B* **1987**, *35*, 3576–3584.
- (239) Murani, A. P.; Pierre, J. Low temperature paramagnetic scattering from YbInAu_2 and YbAl_3 . *Physica B* **1995**, *206–207*, 329–331.
- (240) Lawrence, J. M.; Osborn, R.; Sarrao, J. L.; Fisk, Z. Time-of-flight neutron-scattering study of YbInCu_4 and $\text{YbIn}_{0.3}\text{Ag}_{0.7}\text{Cu}_4$. *Phys. Rev. B* **1999**, *59*, 1134–1140.
- (241) Goremychkin, E. A.; Osborn, R. Crystal field excitations in YbT_2Si_2 ($T = \text{Fe, Co, Ni}$). *J. Appl. Phys.* **2000**, *87*, 6818–6820.
- (242) Klingner, C.; Krellner, C.; Brando, M.; Geibel, C.; Steglich, F. Magnetic behaviour of the intermetallic compound YbCo_2Si_2 . *New J. Phys.* **2011**, *13*, 083024.
- (243) Szytuła, A.; Szott, I. Magnetic properties of ternary RMn_2Si_2 and RMn_2Ge_2 compounds. *Solid State Commun.* **1981**, *40*, 199–202.
- (244) Hofmann, M.; Campbell, S. J.; Edge, A. V. J.; Studer, A. J. The magnetic structures of YbMn_2Si_2 . *J. Phys.: Condens. Matter* **2001**, *13*, 9773.
- (245) Mole, R. A.; Hofmann, M.; Adroja, D. T.; Moze, O.; Campbell, S. J. Crystal field excitations of YbMn_2Si_2 . *J. Magn. Magn. Mater.* **2013**, *347*, 86–94.
- (246) Campbell, S. J.; Hofmann, M.; Mole, R. A.; Prokes, K.; Wallacher, D.; Wang, J. L. Magnetic order in YbMn_2Si_2 – Neutron scattering investigation. *J. Korean Phys. Soc.* **2013**, *63*, 314–319.
- (247) Stockert, O.; Koza, M. M.; Ferstl, J.; Murani, A. P.; Geibel, C.; Steglich, F. Crystalline electric field excitations of the non-Fermi-liquid YbRh_2Si_2 . *Physica B* **2006**, *378–380*, 157–158.
- (248) Leushin, A. M.; Ivanshin, V. A.; Kurkin, I. N. Crystal field of Yb^{3+} tetragonal centers in the YbRh_2Si_2 intermetallic compound. *Phys. Solid State* **2007**, *49*, 1417–1421.
- (249) Hiess, A.; Stockert, O.; Koza, M. M.; Hossain, Z.; Geibel, C. Magnetisation dynamics of YbIr_2Si_2 . *Physica B* **2006**, *378–380*, 748–749.
- (250) Leushin, A. M.; Ivanshin, V. A. Crystalline electric fields and the ground state of YbRh_2Si_2 and YbIr_2Si_2 . *Physica B* **2008**, *403*, 1265–1267.
- (251) Beaupaire, E.; Kappler, J. P.; Krill, G. Xanes study of trivalent and homogeneous mixed valent rare earth systems. *Solid State Commun.* **1986**, *57*, 145–149.
- (252) Dallera, C.; Annese, E.; Rueff, J. P.; Palenzona, A.; Vankó, G.; Braicovich, L.; Shukla, A.; Grioni, M. Determination of pressure-induced valence changes in YbAl_3 by resonant inelastic x-ray emission. *Phys. Rev. B* **2003**, *68*, 245114.
- (253) Tjeng, L. H.; Oh, S.; Cho, E.; Lin, H.; Chen, C. T.; Gweon, G.; Park, J.; Allen, J. W.; Suzuki, T.; Makivic, M. S.; Cox, D. L. Temperature dependence of the Kondo resonance in YbAl_3 . *Phys. Rev. Lett.* **1993**, *71*, 1419–1422.
- (254) Kumar, R. S.; Svane, A.; Vaitheeswaran, G.; Kanchana, V.; Bauer, E. D.; Hu, M.; Nicol, M. F.; Cornelius, A. L. Pressure-induced valence change in YbAl_3 : A combined high-pressure inelastic X-ray scattering and theoretical investigation. *Phys. Rev. B* **2008**, *78*, 075117.
- (255) Rojas, D. P.; Fernández Barquín, L.; Espeso, J. I.; Rodríguez Fernández, J.; Chaboy, J. Reduction of the Yb valence in YbAl_3 nanoparticles. *Phys. Rev. B* **2008**, *78*, 094412.
- (256) Schwarz, U.; Giedigkeit, R.; Niewa, R.; Schmidt, M.; Schnelle, W.; Cardoso, R.; Hanfland, M.; Hu, Z.; Klementiev, K.; Grin, Y. Pressure-induced oxidation state change of ytterbium in YbGa_2 . *Z. Anorg. Allg. Chem.* **2001**, *627*, 2249–2256.
- (257) Rams, M.; Królas, K.; Bonville, P.; Alleno, E.; Godart, C.; Kaczorowski, D.; Canepa, F. Valence states of Yb in Yb_3Si_3 . *Phys. Rev. B* **1997**, *56*, 3690–3696.
- (258) Subbarao, U.; Sarkar, S.; Joseph, B.; Peter, S. C. Magnetic and X-ray absorption studies on the $\text{RE}_5\text{X}_2\text{Sb}_6$ ($\text{RE} = \text{Eu, Yb}; X = \text{Al, Ga, In}$) compounds. *J. Alloys Compd.* **2016**, *658*, 395–401.
- (259) Kanatzidis, M. G. *Chemistry and Properties of Complex Intermetallics from Metallic Fluxes*; Northwestern University: Evanston, IL, USA, 2015.
- (260) Booth, C. H.; Christianson, A. D.; Lawrence, J. M.; Pham, L. D.; Lashley, J. C.; Drymiotis, F. R. Ytterbium divalency and lattice disorder in near-zero thermal expansion YbGaGe . *Phys. Rev. B* **2007**, *75*, 012301.
- (261) Nakai, H.; Ebihara, T.; Tsutsui, S.; Mizumaki, M.; Kawamura, N.; Michimura, S.; Inami, T.; Nakamura, T.; Kondo, A.; Kindo, K.; Matsuda, Y. H. Temperature and magnetic field dependent Yb valence in YbRh_2Si_2 observed by X-ray absorption spectroscopy. *J. Phys. Soc. Jpn.* **2013**, *82*, 124712.
- (262) Hatwar, T. K.; Nayak, R. M.; Padalia, B. D.; Ghatikar, M. N.; Sampathkumaran, E. V.; Gupta, L. C.; Vijayaraghavan, R. X-ray absorption spectroscopic study of mixed valence systems EuCu_2Si_2 , YbCu_2Si_2 and Sm_4Bi_3 . *Solid State Commun.* **1980**, *34*, 617–620.
- (263) Ghatikar, M. N.; Hatwar, T. K.; Padalia, B. D.; Sampathkumaran, E. V.; Gupta, L. C.; Vijayaraghavan, R. Study of X-ray absorption edges of rare earths and gallium in RAl_2Ga_2 intermetallics. *Phys. Status Solidi B* **1981**, *106*, K89–K93.
- (264) Qiao, Y.; Song, Y.; Sanson, A.; Fan, L.; Sun, Q.; Hu, S.; He, L.; Zhang, H.; Xing, X.; Chen, J. Negative thermal expansion in YbMn_2Ge_2 induced by the dual effect of magnetism and valence transition. *npj Quantum Mater.* **2021**, *6*, 49.
- (265) Honda, F.; Hirose, Y.; Miyake, A.; Mizumaki, M.; Kawamura, N.; Tsutsui, S.; Watanuki, T.; Watanabe, S.; Takeuchi, T.; Settai, R.

- Aoki, D.; Ōnuki, Y. X-ray absorption spectroscopy and novel electronic properties in heavy fermion compounds $\text{YbT}_2\text{Zn}_{20}$ (T: Rh and Ir). *J. Phys.: Conf. Series* **2015**, *592*, 012021.
- (266) Mito, T.; Koyama, T.; Nakagawara, K.; Ishida, T.; Ueda, K.; Kohara, T.; Matsubayashi, K.; Saiga, Y.; Munakata, K.; Uwatoko, Y.; Mizumaki, M.; Kawamura, N.; Idzikowski, B.; Reiffers, M. Mechanism of field induced Fermi liquid state in Yb-based heavy-fermion compound: X-ray absorption spectroscopy and nuclear magnetic resonance studies of $\text{YbCo}_2\text{Zn}_{20}$. *J. Phys. Soc. Jpn.* **2012**, *81*, 033706.
- (267) Fahl, A.; Grossi, R.; Rigitano, D.; Cabrera-Baez, M.; Avila, M. A.; Adriano, C.; Granado, E. Crystal, local atomic, and local electronic structures of $\text{YbFe}_2\text{Zn}_{20-x}\text{Cd}_x$ ($0 \leq x \leq 1.4$): A multiband system with possible coexistence of light and heavy fermions. *Phys. Rev. B* **2021**, *103*, 155116.
- (268) Hosokawa, S.; Happo, N.; Hayashi, K.; Kimura, K.; Matsushita, T.; Stellhorn, J. R.; Mizumaki, M.; Suzuki, M.; Sato, H.; Hiraoka, K. Valence-selective local atomic structures on an YbInCu_4 valence transition material by X-ray fluorescence holography. *J. Phys. Soc. Jpn.* **2020**, *89*, 034603.
- (269) Yamaoka, H.; Ohmura, A.; Furue, Y.; Tsujii, N.; Ishii, H.; Hiraoka, N. Direct observation of pressure-induced Yb valence transition in YbInCu_4 . *J. Phys. Soc. Jpn.* **2021**, *90*, 124801.
- (270) Lawrence, J. M.; Kwei, G. H.; Canfield, P. C.; DeWitt, J. G.; Lawson, A. C. L_{III} X-ray absorption in Yb compounds: Temperature dependence of the valence. *Phys. Rev. B* **1994**, *49*, 1627–1631.
- (271) Subbarao, U.; Sarkar, S.; Joseph, B.; Peter, S. C. Magnetic and X-ray absorption studies on the $\text{RE}_2\text{X}_2\text{Sb}_6$ ($\text{RE} = \text{Eu}, \text{Yb}$; $\text{X} = \text{Al}, \text{Ga}, \text{In}$) compounds. *J. Alloys Compd.* **2016**, *658*, 395–401.
- (272) He, A.; Wille, E. L. K.; Moreau, L. M.; Thomas, S. M.; Lawrence, J. M.; Bauer, E. D.; Booth, C. H.; Kauzlarich, S. M. Intermediate Yb valence in the Zintl phases $\text{Yb}_{14}\text{MSb}_{11}$ ($\text{M} = \text{Zn}, \text{Mn}, \text{Mg}$): XANES, magnetism, and heat capacity. *Phys. Rev. Mater.* **2020**, *4*, 114407.
- (273) Oh, S. J.; Allen, J. W.; Torikachvili, M. S.; Maple, M. B. Temperature-induced valence change of YbAl_2 studied by XPS and BIS. *J. Magn. Magn. Mater.* **1985**, *52*, 183–186.
- (274) Buschow, K. H. J.; Campagna, M.; Wertheim, G. K. Intermediate valence in YbAl_3 and EuCu_2Si_2 by X-ray photoemission (XPS). *Solid State Commun.* **1977**, *24*, 253–256.
- (275) Joyce, J. J.; Andrews, A. B.; Arko, A. J.; Bartlett, R. J.; Blyth, R. I. R.; Olson, C. G.; Benning, P. J.; Canfield, P. C.; Poirier, D. M. Photoelectron spectroscopy of strongly correlated Yb compounds. *Phys. Rev. B* **1996**, *54*, 17515–17535.
- (276) Joyce, J. J.; Arko, A. J.; Morales, L. A.; Sarrao, J. L.; Höchst, H. Comment on "Photoemission experiments on YbInCu_4 : Surface effects and temperature dependence. *Phys. Rev. B* **2001**, *63*, 197101.
- (277) Wertheim, G. K.; Wernick, J. H.; Crecelius, G. Surface effects on valence in rare-earth intermetallic compounds. *Phys. Rev. B* **1978**, *18*, 875–879.
- (278) Iga, F.; Takakuwa, Y.; Takahashi, T.; Kasaya, M.; Kasuya, T.; Sagawa, T. XPS study of rare earth dodecaborides: TmB_{12} , YbB_{12} and LuB_{12} . *Solid State Commun.* **1984**, *50*, 903–905.
- (279) Suga, S.; Ogawa, S.; Namatame, H.; Taniguchi, M.; Kakizaki, A.; Ishii, T.; Fujimori, A.; Oh, S.-J.; Kato, H.; Miyahara, T.; Ochiai, A.; Suzuki, T.; Kasuya, T. XPS and UPS studies of valence fluctuation and surface states of Yb_4As_3 , Yb_4Sb_3 and Yb_4Bi_3 . *J. Phys. Soc. Jpn.* **1989**, *58*, 4534–4543.
- (280) Gegner, J.; Koethe, T. C.; Wu, H.; Hu, Z.; Hartmann, H.; Lorenz, T.; Fickenscher, T.; Pöttgen, R.; Tjeng, L. H. Electronic structure of RAuMg and RAgMg ($\text{R} = \text{Eu}, \text{Gd}, \text{Yb}$). *Phys. Rev. B* **2006**, *74*, 073102.
- (281) Rao, C. N. R.; Sarma, D. D.; Sarode, P. R.; Sampathkumaran, E. V.; Gupta, L. C.; Vijayaraghavan, R. Valence fluctuation in some Yb intermetallics by X-ray photoemission and X-ray absorption. *Chem. Phys. Lett.* **1980**, *76*, 413–415.
- (282) Maeda, K.; Sato, H.; Akedo, Y.; Kawabata, T.; Abe, K.; Shimokasa, R.; Yasui, A.; Mizumaki, M.; Kawamura, N.; Ikenaga, E.; Tsutsui, S.; Matsumoto, K.; Hiraoka, K.; Mimura, K. Yb L_3 resonant hard X-ray photoemission spectroscopy of valence transition compound YbInCu_4 . In *Proceedings of the International Conference on Strongly Correlated Electron Systems (SCES2019)*, Okayama, 2020; Vol. 30, p. 011137.
- (283) Sato, H.; Hiraoka, K.; Taniguchi, M.; Nishikawa, Y.; Nagasaki, F.; Fujino, H.; Takeda, Y.; Arita, M.; Shimada, K.; Namatame, H.; Kimura, A.; Kojima, K. X-dependent electronic structure of YbXCu_4 ($\text{X} = \text{In}, \text{Cd}, \text{Mg}$) investigated by high-resolution photoemission spectroscopy. *J. Phys.: Condens. Matter* **2002**, *14*, 4445–4459.
- (284) Kang, J.; Allen, J. W.; Rossel, C.; Seaman, C. L.; Maple, M. B. Electron-spectroscopy study of YbXCu_4 ($\text{X} = \text{Ag}, \text{Au}, \text{Pd}$). *Phys. Rev. B* **1990**, *41*, 4078–4082.
- (285) Rousuli, A.; Nakamura, S.; Sato, H.; Ueda, T.; Matsumoto, Y.; Ohara, S.; Schvier, E. F.; Nagasaki, T.; Mimura, K.; Anzai, H.; Ichiki, K.; Ueda, S.; Shimada, K.; Namatame, H.; Taniguchi, M. Photoemission study of the electronic structure of the Kondo lattices $\text{Yb}_2\text{Pt}_6\text{X}_{15}$ ($\text{X} = \text{Al}, \text{Ga}$). *Phys. Rev. B* **2017**, *96*, 045117.
- (286) Holm, A. P.; Ozawa, T. C.; Kauzlarich, S. M.; Morton, S. A.; Dan Waddill, G.; Tobin, J. G. X-ray photoelectron spectroscopy studies of $\text{Yb}_{14}\text{MnSb}_{11}$ and $\text{Yb}_{14}\text{ZnSb}_{11}$. *J. Solid State Chem.* **2005**, *178*, 262–269.
- (287) Anno, H.; Ashida, K.; Matsubara, K.; Nolas, G. S.; Akai, K.; Matsuura, M.; Nagao, J. Electronic structure and thermoelectric properties of ytterbium-filled skutterudites. *MRS Proc.* **2001**, *691*, G2.4.1–G2.4.6.
- (288) Eckert, H.; Pöttgen, R. Solid-state NMR and Mößbauer spectroscopy. In *Rare Earth Chemistry*, Pöttgen, R.; Jüstel, T.; Strasser, C. A., Eds.; De Gruyter: Berlin, 2020; pp 299–322.
- (289) Gossard, A. C.; Jaccarino, V.; Wernick, J. H. Ytterbium NMR: ^{171}Yb nuclear moment and Yb metal Knight shift. *Phys. Rev.* **1964**, *133*, A881–A884.
- (290) Ivanshin, V. A.; Sukhanov, A. A.; Sokolov, D. A.; Aronson, M. C.; Jia, S.; Bud'ko, S. L.; Canfield, P. C. Electron spin resonance of dense Yb-based heavy-fermion compounds: New experimental data. *J. Alloys Compd.* **2009**, *480*, 126–127.
- (291) Kochelaev, B. I.; Belov, S. I.; Skvortsova, A. M.; Kutuzov, A. S.; Sichelschmidt, J.; Wykhoff, J.; Geibel, C.; Steglich, F. Why could electron spin resonance be observed in a heavy fermion Kondo lattice? *Eur. Phys. J. B* **2009**, *72*, 485–489.
- (292) Schlottmann, P. Electron spin resonance in heavy-fermion systems. *Phys. Rev. B* **2009**, *79*, 045104.
- (293) Shimizu, T.; Takigawa, M.; Yasuoka, H.; Wernick, J. H. ^{171}Yb nuclear magnetic resonance in YbAl_2 and YbAl_3 . *J. Magn. Magn. Mater.* **1985**, *52*, 187–189.
- (294) Giesselmann, E. C. J.; Engel, S.; Kostusiak, W.; Zhang, Y.; Herbeck-Engel, P.; Kickelbick, G.; Janka, O. Raman and NMR spectroscopic and theoretical investigations of the cubic laves-phases REAl_2 ($\text{RE} = \text{Sc}, \text{Y}, \text{La}, \text{Yb}, \text{Lu}$). *Dalton Trans.* **2023**, *52*, 3391–3402.
- (295) Ikushima, K.; Kato, Y.; Takigawa, M.; Iga, F.; Hiura, S.; Takabatake, T. ^{171}Yb NMR in the Kondo semiconductor YbB_{12} . *Physica B* **2000**, *281–282*, 274–275.
- (296) Kasaya, M.; Iga, F.; Takigawa, M.; Kasuya, T. Mixed valence properties of YbB_{12} . *J. Magn. Magn. Mater.* **1985**, *47–48*, 429–435.
- (297) Gerdes, J. M.; Schumacher, L.; Hansen, M. R.; Pöttgen, R. A solid-state ^{171}Yb NMR spectroscopic characterization of selected divalent ytterbium intermetallics. *Z. Naturforsch.* **2024**, *79b*, DOI: 10.1515/ZNB-2023-0070. In Press.
- (298) Sarkar, R.; Gumeniuk, R.; Leithe-Jasper, A.; Schnelle, W.; Grin, Y.; Geibel, C.; Baenitz, M. Unconventional magnetism in multivalent charge-ordered YbPtGe_2 probed by ^{195}Pt - and ^{171}Yb -NMR. *Phys. Rev. B* **2013**, *88*, No. 201101(R).
- (299) Iwamoto, Y.; Akazawa, T.; Ueda, K., NMR study of YbGaGe . In *Proceedings of the International Conference on Strongly Correlated Electron Systems (SCES2013)*, Tokyo, 2014.
- (300) Gambke, T.; Elschner, B.; Kremer, R.; Schanz, M. Electron-spin-resonance of some rare-earths ions in cubic intermetallic compounds (AuCu_3 -structure). *J. Magn. Magn. Mater.* **1983**, *36*, 115–124.

- (301) Nagel, J.; Baberschke, K.; Tsang, E. ESR of Er^{3+} and Yb^{3+} in gold between 100 mK and 1 K. *J. Magn. Magn. Mater.* **1980**, *15*, 18–730.
- (302) Krellner, C.; Forster, T.; Jeevan, H.; Geibel, C.; Sichelschmidt, J. Relevance of ferromagnetic correlations for the electron spin resonance in Kondo lattice systems. *Phys. Rev. Lett.* **2008**, *100*, 066401.
- (303) Kotel'nikova, E. E.; Suleimanov, N. M.; Khaliollin, G. G.; Drulis, H.; Iwasieczko, W. Spin-glass transition as the cause of a false heavy-fermion behavior of the YbH_x system. *Zh. Eksp. Teor. Fiz.* **1993**, *58*, 276–279.
- (304) Likodimos, V.; Guskos, N.; Wabia, M.; Typek, J. Exchange interactions of Yb^{3+} ions in $\text{Yb}_x\text{Y}_{1-x}\text{Ba}_2\text{Cu}_3\text{O}_y$. *Phys. Rev. B* **1998**, *58*, 8244–8247.
- (305) Ivanshin, V. A.; Litvinova, T. O.; Sukhanov, A. A.; Ivanshin, N. A.; Jia, S.; Bud'ko, S. L.; Canfield, P. C. Dual nature of electron spin resonance in $\text{YbCo}_2\text{Zn}_{20}$ intermetallic compound. *JETP Lett.* **2014**, *99*, 153–157.
- (306) Ivan'shin, V. A.; Aminov, L. K.; Kurkin, I. N.; Sichelschmidt, J.; Stockert, O.; Ferstl, J.; Geibel, C. Electron Paramagnetic Resonance of Yb^{3+} Ions in a concentrated YbRh_2Si_2 compound with heavy fermions. *JETP Lett.* **2003**, *77*, 526–529.
- (307) Sichelschmidt, J.; Wykchhoff, J.; Krug von Nidda, H.-A.; Fazlishanov, I. I.; Hossain, Z.; Krellner, C.; Geibel, C.; Steglich, F. Electron spin resonance of YbIr_2Si_2 below the Kondo temperature. *J. Phys.: Condens. Matter* **2007**, *19*, 016211.
- (308) Gataullin, E. M.; Ivanshin, V. A.; Izotov, V. V.; Yavkin, B. V.; Ivanshin, N. A.; Sokolov, D. A. Electron paramagnetic resonance in YbNiAl_2 single crystals with strong magnetic anisotropy. *Phys. Solid State* **2017**, *59*, 434–437.
- (309) Torikachvili, M. S.; Jia, S.; Mun, E. D.; Hannahs, S. T.; Black, R. C.; Neils, W. K.; Martien, D.; Bud'ko, S. L.; Canfield, P. C. Six closely related $\text{YbT}_2\text{Zn}_{20}$ ($T = \text{Fe, Co, Ru, Rh, Os, Ir}$) heavy fermion compounds with large local moment degeneracy. *Proc. Natl. Acad. Sci. U.S.A.* **2007**, *104*, 9960–9963.
- (310) Stevens, J. G.; Dunlap, B. D. Nuclear moments and moment ratios as determined by Mössbauer spectroscopy. *J. Phys. Chem. Ref. Data* **1976**, *5*, 1093–1122.
- (311) Shenoy, G. K.; Wagner, F. E. *Mössbauer Isomer Shifts*. North-Holland Publishing: Amsterdam, 1978.
- (312) Cadogan, J. M.; Ryan, D. H. An Overview of ^{166}Er , ^{169}Tm and ^{170}Yb Mössbauer Spectroscopy. *Hyperfine Interact.* **2004**, *153*, 25–41.
- (313) Gubbens, P. C. M., Rare earth Mössbauer spectroscopy measurements on lanthanide intermetallics: A survey. In *Handbook of Magnetic Materials*, Buschow, K. H. J., Ed.; Elsevier: Amsterdam, 2012; Vol. 20, pp 227–335.
- (314) Eckert, H. Mössbauer spectroscopy of mixed-valent compounds. In *Mössbauer Spectroscopy Applied to Inorganic Chemistry*, Long, G. J., Ed.; Plenum Press: New York, 1987; Vol. 2.
- (315) Cadogan, J. M.; Ryan, D. H. A study on the magnetic behaviour of polymorphic YbFe_6Ge_6 . *J. Phys.: Condens. Matter* **2010**, *22*, 016009.
- (316) Ryan, D. H.; Saleema, N. M.; Gagnon, R.; van Lierop, J. ^{170}Yb Mössbauer study of the $\text{YbCd}_{3.7}$ binary quasi-crystal and related phases. *J. Phys.: Condens. Matter* **2001**, *13*, 10159.
- (317) Solokha, P.; Čurlík, I.; Giovannini, M.; Lee-Hone, N. R.; Reiffers, M.; Ryan, D. H.; Saccone, A. Structural and physical properties of the new intermetallic compound $\text{Yb}_3\text{Pd}_2\text{Sn}_2$. *J. Solid State Chem.* **2011**, *184*, 2498–2505.
- (318) Čurlík, I.; Reiffers, M.; Giovannini, M.; Solokha, P.; Saccone, A.; Il'kovič, S.; Ryan, D. H. Crystal structure and physical properties of the novel stannide $\text{Yb}_3\text{Pd}_2\text{Sn}_2$. *J. Phys.: Conf. Series* **2012**, *391*, 012008.
- (319) Bonville, P.; Imbert, P.; Jéhanno, G.; Gonzalez-Jimenez, F.; Hartmann-Boutron, F. Emission Mössbauer spectroscopy and relaxation measurements in hyperfine levels out of thermal equilibrium: Very-low-temperature experiments on the Kondo alloy Au^{170}Yb . *Phys. Rev. B* **1984**, *30*, 3672–3690.
- (320) Bonville, P.; Conte, R. Evidence for random strain at the cubic site of Yb^{3+} in palladium by Mössbauer spectroscopy on ^{170}Yb . *J. Phys. (Paris)* **1985**, *46*, 1553–1563.
- (321) Bonville, P.; Hodges, J. A.; Imbert, P.; Jéhanno, G.; Jaccard, D.; Sierro, J. Magnetic ordering and paramagnetic relaxation of Yb^{3+} in YbNi_2Si_2 . *J. Magn. Magn. Mater.* **1991**, *97*, 178–186.
- (322) Bonville, P.; Hodges, J. A.; Imbert, P.; Jéhanno, G.; Thuéry, P. A neutron diffraction and ^{170}Yb Mössbauer study of Yb_3Pd_4 . *J. Magn. Magn. Mater.* **1994**, *136*, 238–244.
- (323) Bonville, P.; Hodges, J. A.; Hossain, Z.; Nagarajan, R.; Dhar, S. K.; Gupta, L. C.; Alleno, E.; Godart, C. Heavy electron $\text{YbNi}_2\text{B}_2\text{C}$ and giant exchange YbNiBC : ^{170}Yb Mössbauer spectroscopy and magnetization studies. *Eur. Phys. J. B* **1999**, *11*, 377–383.
- (324) Voyer, C. J.; Ryan, D. H.; Ahn, K.; Gschneidner, K. A.; Pecharsky, V. K. Valence and magnetic ordering in the $\text{Yb}_5\text{Si}_x\text{Ge}_{4-x}$ pseudobinary system. *Phys. Rev. B* **2006**, *73*, 174422.
- (325) Bonville, P.; Bauer, E. A ^{170}Yb Mössbauer spectroscopy and L_{III} -edge study of the Kondo lattice YbCu_3Al_2 . *J. Phys.: Condens. Matter* **1996**, *8*, 7797–7812.
- (326) Bonville, P.; Hodges, J. A.; Hulliger, F.; Imbert, P.; Jéhanno, G.; Marimon da Cunha, J. B.; Ott, H. R. ^{170}Yb Mössbauer study of the heavy-electron pnictides YbP , YbAs and YbSb . *J. Magn. Magn. Mater.* **1988**, *76–77*, 473–474.
- (327) Le Bras, G.; Bonville, P.; Hodges, J. A.; Imbert, P.; Polatsek, G.; Fischer, P.; Keller, L.; Dönni, A.; Kohgi, M.; Suzuki, T. ^{170}Yb Mössbauer and neutron diffraction investigation of the antiferromagnetic phase in the Kondo lattices YbP and YbN . *Physica B* **1993**, *190*, 333–346.
- (328) Bonville, P.; Polatsek, G.; Hodges, J. A.; Imbert, P.; LeBras, G. Giant exchange fields and reduced moments in Yb Kondo lattices. *Physica B* **1993**, *186–188*, 254–257.
- (329) Bonville, P.; Abd-Elmeguid, M.; Malaman, B.; Ressouche, E.; Sanchez, J. P.; Geibel, C.; Trovarelli, O. Incommensurate modulated magnetic structure in the heavy electron compound YbPtAl . *Physica B* **2000**, *281–282*, 144–146.
- (330) Ryan, D. H.; Lee-Hone, N. R.; Cadogan, J. M.; Ahn, K.; Pecharsky, V. K.; Gschneidner, K. A. Doping-induced valence change in $\text{Yb}_5\text{Ge}_{4-x}(\text{Sb, Ga})_x$ ($x \leq 1$). *Hyperfine Interact.* **2012**, *208*, 59–63.
- (331) Dhar, S. K.; Manfrinetti, P.; Fornasini, M. L.; Bonville, P. Phase transition in YbAl_3C_3 . *Eur. Phys. J. B* **2008**, *63*, 187–192.
- (332) Dhar, S. K.; Singh, S.; Bonville, P.; Mazumdar, C.; Manfrinetti, P.; Palenzona, A. Magnetic behavior of $\text{Yb}_3\text{Cu}_4\text{Ge}_4$ and $\text{Gd}_3\text{Cu}_4\text{Ge}_4$. *Physica B* **2002**, *312–313*, 846–847.
- (333) Dhar, S. K.; Mitra, C.; Bonville, P.; Rams, M.; Królas, K.; Godart, C.; Alleno, E.; Suzuki, N.; Miyake, K.; Watanabe, N.; Onuki, Y.; Manfrinetti, P.; Palenzona, A. Magnetic and 4f quadrupolar behavior of $\text{Yb}_2\text{Co}_3\text{Al}_9$ and the Kondo lattice compound $\text{Yb}_2\text{Co}_3\text{Ga}_9$. *Phys. Rev. B* **2001**, *64*, 094423.
- (334) LeBras, G.; Bonville, P.; Hodges, J. A.; Hammann, J.; Besnus, M. J.; Schmerber, G.; Dhar, S. K.; Aliev, F. G.; Andre, G. Local symmetry lowering in the cubic intermetallics YbPdBi and YbNiSb . *J. Phys.: Condens. Matter* **1995**, *7*, 5665.
- (335) Mishra, R.; Pöttgen, R.; Hoffmann, R.-D.; Fickenscher, T.; Eschen, M.; Trill, H.; Mosel, B. D. Ternary antimonides YbTSb ($T = \text{Ni, Pd, Pt, Cu, Ag, Au}$) – synthesis, structure, homogeneity ranges, and ^{121}Sb Mössbauer spectroscopy. *Z. Naturforsch.* **2002**, *57b*, 1215–1223.
- (336) Bonville, P.; Imbert, P.; Jéhanno, G. Low-temperature Mössbauer study of ^{170}Yb in YbBe_{13} . *J. Phys. F: Metal Phys.* **1986**, *16*, 1873–1883.
- (337) Yaouanc, A.; Dalmas de Réotier, P.; Bonville, P.; LeBras, G.; Gubbens, P. C. M.; Mulders, A. M.; Kunii, S. Dynamical magnetic correlations in the Kondo insulator YbB_{12} . *Europhys. Lett.* **1999**, *47*, 247–253.
- (338) Hodges, J. A.; Bonville, P.; Ocio, M. Magnetic properties of YbNi_5 from ^{170}Yb Mössbauer and magnetisation measurements. *Eur. Phys. J. B* **2007**, *57*, 365–370.
- (339) Knebel, G.; Boursier, R.; Hassinger, E.; Lapertot, G.; G. Niklowitz, P.; Pourret, A.; Salce, B.; P. Sanchez, J.; Sheikin, I.

- Bonville, P.; Harima, H.; Flouquet, J. Localization of 4f state in YbRh_2Si_2 under magnetic field and high pressure: Comparison with CeRh_2Si_2 . *J. Phys. Soc. Jpn.* **2006**, *75*, 114709.
- (340) Plessel, J.; Abd-Elmeguid, M. M.; Sanchez, J. P.; Knebel, G.; Geibel, C.; Trovarelli, O.; Steglich, F. Unusual behavior of the low-moment magnetic ground state of YbRh_2Si_2 under high pressure. *Phys. Rev. B* **2003**, *67*, 180403.
- (341) Schöppner, M.; Moser, J.; Kratzer, A.; Potzel, U.; Mignot, J. M.; Kalvius, G. M. Changes of valence state of Yb in YbCuAl at high pressure: A Mössbauer study. *Z. Phys. B: Condens. Matter* **1986**, *63*, 25–32.
- (342) Drescher, K.; Abd-Elmeguid, M. M.; Micklitz, H.; Sanchez, J. P. Competing anisotropies in the ferromagnetic Kondo-lattice compound YbNiSn : Observation of a complex magnetic ground state under high pressure. *Phys. Rev. Lett.* **1996**, *77*, 3228–3231.
- (343) Winkelmann, H.; Abd-Elmeguid, M. M.; Micklitz, H.; Sanchez, J. P.; Geibel, C.; Steglich, F. Pressure-induced local moment magnetism in the nonmagnetic heavy fermion compound $\text{Yb}_2\text{Ni}_2\text{Al}$. *Phys. Rev. Lett.* **1998**, *81*, 4947–4950.
- (344) Masuda, R.; Kobayashi, Y.; Kitao, S.; Kurokuzu, M.; Saito, M.; Yoda, Y.; Mitsui, T.; Iga, F.; Seto, M. Synchrotron radiation-based Mössbauer spectra of ^{174}Yb measured with internal conversion electrons. *Appl. Phys. Lett.* **2014**, *104*, 082411.
- (345) Meyer, C.; Gavigan, J. P.; Czjzek, G.; Bornemann, H. J. A study of crystal fields in $\text{Yb}_2\text{Fe}_{14}\text{B}$ by ^{174}Yb Mössbauer spectroscopy. *Solid State Commun.* **1989**, *69*, 83–86.
- (346) Oura, M.; Ikeda, S.; Masuda, R.; Kobayashi, Y.; Seto, M.; Yoda, Y.; Hira, N.; Kawaguchi, S. I.; Ohishi, Y.; Suzuki, S.; Kuga, K.; Nakatsuji, S.; Kobayashi, H. Valence fluctuating compound $\alpha\text{-YbAlB}_4$ studied by ^{174}Yb Mössbauer spectroscopy and X-ray diffraction using synchrotron radiation. *Physica B* **2018**, *536*, 162–164.
- (347) Snyder, G. J.; Toberer, E. S. Complex thermoelectric materials. *Nat. Mater.* **2008**, *7*, 105–114.
- (348) Gayner, C.; Kar, K. K. Recent advances in thermoelectric materials. *Prog. Mater. Sci.* **2016**, *83*, 330–382.
- (349) Orr, B.; Akbarzadeh, A.; Mochizuki, M.; Singh, R. A review of car waste heat recovery systems utilising thermoelectric generators and heat pipes. *Appl. Therm. Eng.* **2016**, *101*, 490–495.
- (350) Liu, W.; Hu, J.; Zhang, S.; Deng, M.; Han, C.-G.; Liu, Y. New trends, strategies and opportunities in thermoelectric materials: A perspective. *Mater. Today Phys.* **2017**, *1*, 50–60.
- (351) Kauzlarich, S. M.; Zevallink, A.; Toberer, E.; Snyder, G. J. Zintl phases: recent developments in thermoelectrics and future outlook. In *Thermoelectric Materials and Devices*; The Royal Society of Chemistry: Cambridge, England, 2017; pp 1–26.
- (352) Shuai, J.; Mao, J.; Song, S.; Zhang, Q.; Chen, G.; Ren, Z. Recent progress and future challenges on thermoelectric Zintl materials. *Mater. Today Phys.* **2017**, *1*, 74–95.
- (353) van Daal, H. J.; van Aken, P. B.; Buschow, K. H. J. The Seebeck coefficient of YbAl_2 and YbAl_3 . *Phys. Lett. A* **1974**, *49*, 246–248.
- (354) Tanusilp, S.-A.; Ohishi, Y.; Muta, H.; Yamanaka, S.; Nishide, A.; Hayakawa, J.; Kurosaki, K. Ytterbium silicide (YbSi_2): A promising thermoelectric material with a high power factor at room temperature. *Phys. Status Solidi RRL* **2018**, *12*, 1700372.
- (355) Massalski, T. B.; Okamoto, H.; Subramanian, P. R.; Kacprzak, L. *Binary alloy phase diagrams*, 2nd Ed. ASM International: Ohio, U.S.A., 1990.
- (356) Pope, A. L.; Tritt, T. M.; Gagnon, R.; Strom-Olsen, J. Electronic transport in Cd-Yb and Y-Mg-Zn quasicrystals. *Appl. Phys. Lett.* **2001**, *79*, 2345–2347.
- (357) Kuo, Y. K.; Lai, J. R.; Huang, C. H.; Ku, W. C.; Lue, C. S.; Lin, S. T. Thermoelectric properties of binary Cd-Yb quasicrystals and Cd_6Yb . *J. Appl. Phys.* **2004**, *95*, 1900–1905.
- (358) Iizuka, T.; Hori, T.; Matsunami, M.; Takeuchi, T. Thermoelectric properties of Yb_3Si_3 . *Jpn. J. Appl. Phys.* **2020**, *59*, 010902.
- (359) Lehr, G. J.; Morelli, D. T.; Jin, H.; Heremans, J. P. Enhanced thermoelectric power factor in $\text{Yb}_{1-x}\text{Sc}_x\text{Al}_2$ alloys using chemical pressure tuning of the Yb valence. *J. Appl. Phys.* **2013**, *114*, 223712.
- (360) Itoh, Y.; Kadomatsu, H.; Sakurai, J.; Fujiwara, H. Transport properties of $\text{Yb}_x\text{In}_{1-x}\text{Cu}_2$. *Phys. Status Solidi A* **1990**, *118*, 513–517.
- (361) Adroja, D. T.; Rainford, B. D.; Takabatake, T. Crystal field excitations in the ferromagnetic Kondo lattice: YbNiSn . *Physica B* **1998**, *253*, 269–277.
- (362) Itoh, Y.; Kadomatsu, H. Electrical and magnetic properties of YbPdGe and YbPtGe . *J. Alloys Compd.* **1998**, *280*, 39–43.
- (363) Guner, S.; Budak, S.; Muntele, C. I.; Ila, D. Thermoelectric properties of YbBiPt and YBiPt thin films. *Mater. Res. Soc. Online Proc. Lib.* **2008**, *1100*, 6.
- (364) Gegenwart, P.; Tokiwa, Y.; Westerkamp, T.; Weickert, F.; Custers, J.; Ferstl, J.; Krellner, C.; Geibel, C.; Kersch, P.; Müller, K. H.; Steglich, F. High-field phase diagram of the heavy-fermion metal YbRh_2Si_2 . *New J. Phys.* **2006**, *8*, 171.
- (365) Trovarelli, O.; Geibel, C.; Mederle, S.; Langhammer, C.; Grosche, F. M.; Gegenwart, P.; Lang, M.; Sparn, G.; Steglich, F. YbRh_2Si_2 : pronounced non-Fermi-liquid effects above a low-lying magnetic phase transition. *Phys. Rev. Lett.* **2000**, *85*, 626–629.
- (366) Behnia, K.; Jaccard, D.; Flouquet, J. On the thermoelectricity of correlated electrons in the zero-temperature limit. *J. Phys.: Condens. Matter* **2004**, *16*, S187.
- (367) Pourret, A.; Knebel, G.; D. Matsuda, T.; Lapertot, G.; Flouquet, J. Magnetic polarization and Fermi surface instability: case of YbRh_2Si_2 . *J. Phys. Soc. Jpn.* **2013**, *82*, 053704.
- (368) Stockert, U.; Klingner, C.; Krellner, C.; Zlatić, V.; Geibel, C.; Steglich, F. Thermopower evolution in $\text{Yb}(\text{Rh}_{1-x}\text{Co}_x)_2\text{Si}_2$ upon 4f localization. *J. Low Temp. Phys.* **2019**, *196*, 364–374.
- (369) Klingner, C.; Krellner, C.; Brando, M.; Geibel, C.; Steglich, F.; Vyalikh, D. V.; Kummer, K.; Danzenbächer, S.; Molodtsov, S. L.; Laubschat, C.; Kinoshita, T.; Kato, Y.; Muro, T. Evolution of magnetism in $\text{Yb}(\text{Rh}_{1-x}\text{Co}_x)_2\text{Si}_2$. *Phys. Rev. B* **2011**, *83*, 144405.
- (370) Machida, Y.; Tomokuni, K.; Ogura, C.; Izawa, K.; Kuga, K.; Nakatsuji, S.; Lapertot, G.; Knebel, G.; Brison, J. P.; Flouquet, J. Thermoelectric response near a quantum critical point of $\beta\text{-YbAlB}_4$ and YbRh_2Si_2 : a comparative study. *Phys. Rev. Lett.* **2012**, *109*, 156405.
- (371) Polatsek, G.; Bonville, P. Interpretation of neutron magnetic scattering in the Kondo lattices YbPd_2Si_2 and YbAgCu_4 . *Z. Phys. B: Condens. Matter* **1992**, *88*, 189–193.
- (372) Bonville, P.; Hamann, J.; Hodges, J.; Imbert, P.; Jéhanno, G.; Besnus, M.; Meyer, A. Hybridization and crystal field in YbPd_2Si_2 . *Physica B* **1991**, *171*, 171–174.
- (373) Dhar, S. K.; Sampathkumaran, E. V.; Vijayaraghavan, R.; Kuentzler, R. YbPd_2Si_2 , A moderate heavy fermion system. *Solid State Commun.* **1987**, *61*, 479–481.
- (374) Casanova, R.; Jaccard, D.; Marcenat, C.; Hamdaoui, N.; Besnus, M. J. Thermoelectric power of YbMCu_4 ($M = \text{Ag, Au}$ and Pd) and YbPd_2Si_2 . *J. Magn. Magn. Mater.* **1990**, *90–91*, 587–588.
- (375) Alami-Yadri, K.; Jaccard, D.; Andreica, D. Thermopower of Yb heavy fermion compounds at high pressure. *J. Low Temp. Phys.* **1999**, *114*, 135–149.
- (376) Duc Dung, N.; D. Matsuda, T.; Haga, Y.; Ikeda, S.; Yamamoto, E.; Ishikura, T.; Endo, T.; Tatsuoka, S.; Aoki, Y.; Sato, H.; Takeuchi, T.; Settai, R.; Harima, H.; Onuki, Y. de Haas–van Alphen effect and Fermi surface properties in high-quality single crystals YbCu_2Si_2 and YbCu_2Ge_2 . *J. Phys. Soc. Jpn.* **2009**, *78*, 084711.
- (377) Alami-Yadri, K.; Wilhelm, H.; Jaccard, D. Pressure-induced magnetically ordered Kondo lattice state in YbCu_2Si_2 . *Eur. Phys. J. B* **1998**, *6*, 5–11.
- (378) Nikiforov, V. N.; Pryadun, V. V.; Gribov, A. V.; Irkhin, V. Y. Electronic properties of the ternary system $\text{YbPd}_2\text{Ge}_{2-x}$. *Physica B* **2018**, *545*, 312–314.
- (379) Lehr, G. J.; Morelli, D. T. Interplay of chemical expansion, Yb valence, and low temperature thermoelectricity in the $\text{YbCu}_2\text{Si}_{2-x}\text{Ge}_x$ solid solution. *J. Appl. Phys.* **2015**, *117*, 135101.
- (380) Lehr, G. J.; Morelli, D. T.; Jin, H.; Heremans, J. P. YbCu_2Si_2 – LaCu_2Si_2 solid solutions with enhanced thermoelectric power factors. *J. Electron. Mater.* **2015**, *44*, 1663–1667.

- (381) Machida, Y.; Ogura, C.; Izawa, K.; Kuga, K.; Nakatsuji, S. Low-temperature thermal transport coefficients of heavy fermion β -YbAl₄. *J. Phys.: Conf. Series* **2011**, 273, 012005.
- (382) Mun, E. D.; Jia, S.; Bud'ko, S. L.; Canfield, P. C. Thermoelectric power of the YbT₂Zn₂₀ ($T = \text{Fe, Ru, Os, Ir, Rh, and Co}$) heavy fermions. *Phys. Rev. B* **2012**, 86, 115110.
- (383) Wei, K.; Neu, J. N.; Lai, Y.; Chen, K.-W.; Hobbis, D.; Nolas, G. S.; Graf, D. E.; Siegrist, T.; Baumbach, R. E. Enhanced thermoelectric performance of heavy-fermion compounds YbTM₂Zn₂₀ ($TM = \text{Co, Rh, Ir}$) at low temperatures. *Sci. Adv.* **2019**, 5, No. eaaw6183.
- (384) Deppe, M.; Hartmann, S.; Macovei, M. E.; Oeschler, N.; Nicklas, M.; Geibel, C. Investigation of Yb₂Pt₃Al₁₅ single crystals: heavy fermion system with a large local moment degeneracy. *New J. Phys.* **2008**, 10, 093017.
- (385) Trovarelli, O.; Geibel, C.; Buschinger, B.; Borth, R.; Mederle, S.; Grosche, M.; Sparn, G.; Steglich, F.; Brosch, O.; Donnevert, L. Magnetic, transport, and thermal properties of Yb₂T₃X₉ compounds ($T = \text{Rh, Ir; X = Al, Ga}$). *Phys. Rev. B* **1999**, 60, 1136–1143.
- (386) Muro, Y.; Yamane, K.; Kim, M.-S.; Takabatake, T.; Godart, C.; Rogl, P. Magnetic and thermoelectric properties of a heterogeneous mixed-valence system, Yb₂Pt₃Sn₅. *J. Phys. Soc. Jpn.* **2003**, 72, 1745–1750.
- (387) Jang, S.; White, B. D.; Ho, P. C.; Kanchanavatee, N.; Janoschek, M.; Hamlin, J. J.; Maple, M. B. Crossover between Fermi liquid and non-Fermi liquid behavior in the non-centrosymmetric compound Yb₂Ni₁₂P₇. *J. Phys.: Condens. Matter* **2014**, 26, 425601.
- (388) Brown, S. R.; Kauzlarich, S. M.; Gascoin, F.; Snyder, G. J. Yb₁₄MnSb₁₁: New high efficiency thermoelectric material for power generation. *Chem. Mater.* **2006**, 18, 1873–1877.
- (389) Cox, C. A.; Brown, S. R.; Snyder, G. J.; Kauzlarich, S. M. Effect of Ca doping on the thermoelectric performance of Yb₁₄MnSb₁₁. *J. Electron. Mater.* **2010**, 39, 1373–1375.
- (390) Uvarov, C. A.; Ortega-Alvarez, F.; Kauzlarich, S. M. Enhanced High-Temperature Thermoelectric Performance of Yb_{14-x}Ca_xMnSb₁₁. *Inorg. Chem.* **2012**, 51, 7617–7624.
- (391) Grebenkemper, J. H.; Klemenz, S.; Albert, B.; Bux, S. K.; Kauzlarich, S. M. Effects of Sc and Y substitution on the structure and thermoelectric properties of Yb₁₄MnSb₁₁. *J. Solid State Chem.* **2016**, 242, 55–61.
- (392) Toberer, E. S.; Brown, S. R.; Ikeda, T.; Kauzlarich, S. M.; Snyder, J. G. High thermoelectric efficiency in lanthanum doped Yb₁₄MnSb₁₁. *Appl. Phys. Lett.* **2008**, 93, 123–128.
- (393) Yu, C.; Chen, Y.; Xie, H. H.; Snyder, G. J.; Fu, C. G.; Xu, J. S.; Zhao, X. B.; Zhu, T. J. Improved Thermoelectric Properties in Lu-doped Yb₁₄MnSb₁₁ Zintl Compounds. *Appl. Phys. Express* **2012**, 5, 031801.
- (394) Justl, A. P.; Bux, S. K.; Kauzlarich, S. M. Evolution of the Thermoelectric and Oxidation Properties in Lu-Substituted Yb₁₄MnSb₁₁. *ACS Appl. Energy Mater.* **2023**, 6, 471–483.
- (395) Vasilyeva, I. G.; Nikolaev, R. E.; Abdusaljamova, M. N.; Kauzlarich, S. M. Thermochemistry study and improved thermal stability of Yb₁₄MnSb₁₁ alloyed by Ln³⁺ (La–Lu). *J. Mater. Chem. C* **2016**, 4, 3342–3348.
- (396) Brown, S. R.; Toberer, E. S.; Ikeda, T.; Cox, C. A.; Gascoin, F.; Kauzlarich, S. M.; Snyder, G. J. Improved thermoelectric performance in Yb₁₄Mn_{1-x}Zn_xSb₁₁ by the reduction of spin-disorder scattering. *Chem. Mater.* **2008**, 20, 3412–3419.
- (397) Toberer, E. S.; Cox, C. A.; Brown, S. R.; Ikeda, T.; May, A. F.; Kauzlarich, S. M.; Snyder, G. J. Traversing the metal-insulator transition in a Zintl phase: Rational enhancement of thermoelectric efficiency in Yb₁₄Mn_{1-x}Al_xSb₁₁. *Adv. Funct. Mater.* **2008**, 18, 2795–2800.
- (398) Cox, C. A.; Toberer, E. S.; Levchenko, A. A.; Brown, S. R.; Snyder, G. J.; Navrotsky, A.; Kauzlarich, S. M. Structure, heat capacity, and high-temperature thermal properties of Yb₁₄Mn_{1-x}Al_xSb₁₁. *Chem. Mater.* **2009**, 21, 1354–1360.
- (399) Star, K.; Zevalkink, A.; Huang, C.-K.; Dunn, B.; Fleurial, J.-P. Synthesis and thermoelectric properties of doped Yb₁₄MnSb_{11-x}Bi_xZintl. *MRS Online Proceedings Library (OPL)* **2010**, 1267 (1267), DD1203–1205.
- (400) Yi, T.; Abdusaljamova, M. N.; Makhmudov, F.; Kauzlarich, S. M. Magnetic and transport properties of Te doped Yb₁₄MnSb₁₁. *J. Mater. Chem.* **2012**, 22, 14378–14384.
- (401) Ribeiro, R. A.; Hadano, Y.; Narazu, S.; Suekuni, K.; Avila, M. A.; Takabatake, T. Low-temperature thermoelectric properties of Yb₁₄MSb₁₁ ($M = \text{Mn, Zn}$). *J. Phys.: Condens. Matter* **2007**, 19, 376211.
- (402) Akrap, A.; Barišić, N.; Forró, L.; Mandrus, D.; Sales, B. C. High-pressure resistivity and thermoelectric power in Yb₁₄MnSb₁₁. *Phys. Rev. B* **2007**, 76, 085203.
- (403) Hu, Y.; Wang, J.; Kawamura, A.; Kovnir, K.; Kauzlarich, S. M. Yb₁₄MgSb₁₁ and Ca₁₄MgSb₁₁ – New Mg-containing Zintl compounds and their structures, bonding, and thermoelectric properties. *Chem. Mater.* **2015**, 27, 343–351.
- (404) Perez, C. J.; Qi, X.; Chen, Z.; Bux, S. K.; Chanakain, S.; Li, B.; Liu, K.; Dhall, R.; Bustillo, K. C.; Kauzlarich, S. M. Improved power factor and mechanical properties of composites of Yb₁₄MgSb₁₁ with iron. *ACS Appl. Energy Mater.* **2020**, 3, 2147–2159.
- (405) Perez, C. J.; Chen, Z.; Beeson, W. B.; Chanakian, S.; Liu, K.; Bux, S. K.; Kauzlarich, S. M. Chemical route to Yb₁₄MgSb₁₁ composites with nanosized iron inclusions for the reduction of thermal conductivity. *ACS Appl. Energy Mater.* **2021**, 4, 3748–3756.
- (406) Hu, Y.; Kauzlarich, S. M. Yb₁₄MgBi₁₁: structure, thermoelectric properties and the effect of the structure on low lattice thermal conductivity. *Dalton Trans.* **2017**, 46, 3996–4003.
- (407) Gascoin, F.; Ottensmann, S.; Stark, D.; Haile, S. M.; Snyder, G. J. Zintl phases as thermoelectric materials: tuned transport properties of the compounds Ca_xYb_{1-x}Zn₂Sb₂. *Adv. Funct. Mater.* **2005**, 15, 1860–1864.
- (408) Shuai, J.; Wang, Y.; Liu, Z.; Kim, H. S.; Mao, J.; Sui, J.; Ren, Z. Enhancement of thermoelectric performance of phase pure Zintl compounds Ca_{1-x}Yb_xZn₂Sb₂, Ca_{1-x}Eu_xZn₂Sb₂, and Eu_{1-x}Yb_xZn₂Sb₂ by mechanical alloying and hot pressing. *Nano Energy* **2016**, 25, 136–144.
- (409) Takagiwa, Y.; Sato, Y.; Zevalkink, A.; Kanazawa, I.; Kimura, K.; Isoda, Y.; Shinohara, Y. Thermoelectric properties of EuZn₂Sb₂ Zintl compounds: zT enhancement through Yb substitution for Eu. *J. Alloys Compd.* **2017**, 703, 73–79.
- (410) Zhang, X.; Peng, K.; Guo, L.; Yan, Y.; Zhan, H.; Lu, X.; Gu, H.; Zhou, X. Effects of lanthanum substitution on thermoelectric properties of YbZn₂Sb₂. *J. Electron. Mater.* **2017**, 46, 2611–2615.
- (411) May, A. F.; McGuire, M. A.; Ma, J.; Delaire, O.; Huq, A.; Custelcean, R. Properties of single crystalline AZn₂Sb₂ ($A = \text{Ca, Eu, Yb}$). *J. Appl. Phys.* **2012**, 111 (3), 033708.
- (412) Zhao, W.-Y.; Liang, Z.; Wei, P.; Yu, J.; Zhang, Q.-J.; Shao, G.-S. Enhanced thermoelectric performance via randomly arranged nanopores: Excellent transport properties of YbZn₂Sb₂ nanoporous materials. *Acta Mater.* **2012**, 60, 1741–1746.
- (413) Zevalkink, A.; Zeier, W. G.; Cheng, E.; Snyder, J.; Fleurial, J.-P.; Bux, S. Nonstoichiometry in the Zintl phase Yb_{1-δ}Zn₂Sb₂ as a route to thermoelectric optimization. *Chem. Mater.* **2014**, 26, 5710–5717.
- (414) Yang, X.; Gu, Y.; Li, Y.; Guo, K.; Zhang, J.; Zhao, J.-T. The equivalent and aliovalent dopants boosting the thermoelectric properties of YbMg₂Sb₂. *Sci. China Mater.* **2020**, 63, 437–443.
- (415) Yu, C.; Zhu, T. J.; Zhang, S. N.; Zhao, X. B.; He, J.; Su, Z.; Tritt, T. M. Improved thermoelectric performance in the Zintl phase compounds YbZn_{2-x}Mn_xSb₂ via isoelectronic substitution in the anionic framework. *J. Appl. Phys.* **2008**, 104 (1), 013705.
- (416) Zhu, T. J.; Yu, C.; He, J.; Zhang, S. N.; Zhao, X. B.; Tritt, T. M. Thermoelectric properties of Zintl compound YbZn₂Sb₂ with Mn substitution in anionic framework. *J. Electron. Mater.* **2009**, 38, 1068–1071.
- (417) Wang, X.-J.; Tang, M.-B.; Chen, H.-H.; Yang, X.-X.; Zhao, J.-T.; Burkhardt, U.; Grin, Y. Synthesis and high thermoelectric efficiency of Zintl phase YbCd_{2-x}Zn_xSb₂. *Appl. Phys. Lett.* **2009**, 94 (9), 092106.

- (418) Zhang, X.; Gu, H.; Zhang, Y.; Guo, L.; Yang, J.; Luo, S.; Lu, X.; Chen, K.; Chai, H.; Wang, G.; Zhang, X.; Zhou, X. Enhanced thermoelectric properties of $\text{YbZn}_2\text{Sb}_{2-x}\text{Bi}_x$ through a synergistic effect via Bi-doping. *Chem. Eng. J.* **2019**, *374*, 589–595.
- (419) Zhang, Z.; Yan, Y.; Li, X.; Wang, X.; Li, J.; Chen, C.; Cao, F.; Sui, J.; Lin, X.; Liu, X.; Xie, G.; Zhang, Q. A dual role by incorporation of magnesium in YbZn_2Sb_2 Zintl phase for enhanced thermoelectric performance. *Adv. Energy Mater.* **2020**, *10* (29), 2001229.
- (420) Zhou, T.; Feng, Z.; Mao, J.; Jiang, J.; Zhu, H.; Singh, D. J.; Wang, C.; Ren, Z. Thermoelectric properties of Zintl phase YbMg_2Sb_2 . *Chem. Mater.* **2020**, *32*, 776–784.
- (421) Zhou, T.; Mao, J.; Jiang, J.; Song, S.; Zhu, H.; Zhu, Q.; Zhang, Q.; Ren, W.; Wang, Z.; Wang, C.; Ren, Z. Large reduction of thermal conductivity leading to enhanced thermoelectric performance in p-type Mg_3Bi_2 – YbMg_2Bi_2 solid solutions. *J. Mater. Chem. C* **2019**, *7*, 434–440.
- (422) May, A. F.; McGuire, M. A.; Singh, D. J.; Ma, J.; Delaire, O.; Huq, A.; Cai, W.; Wang, H. Thermoelectric transport properties of CaMg_2Bi_2 , EuMg_2Bi_2 , and YbMg_2Bi_2 . *Phys. Rev. B* **2012**, *85*, 035202.
- (423) Kundu, A. K.; Roy, T.; Pakhira, S.; Wu, Z.-B.; Tsujikawa, M.; Shirai, M.; Johnston, D. C.; Pasupathy, A. N.; Valla, T. Topological electronic structure of YbMg_2Bi_2 and CaMg_2Bi_2 . *npj Quantum Mater.* **2022**, *7* (1), 67.
- (424) Nikiforov, V. N.; Pryadun, V. V.; Morozkin, A. V.; Irkhin, V. Y. Anomalies of transport properties in antiferromagnetic YbMn_2Sb_2 compound. *Phys. Lett. A* **2014**, *378*, 1425–1427.
- (425) Guo, K.; Cao, Q.-G.; Feng, X.-J.; Tang, M.-B.; Chen, H.-H.; Guo, X.; Chen, L.; Grin, Y.; Zhao, J.-T. Enhanced thermoelectric figure of merit of Zintl phase $\text{YbCd}_{2-x}\text{Mn}_x\text{Sb}_2$ by chemical substitution. *Eur. J. Inorg. Chem.* **2011**, *2011*, 4043–4048.
- (426) Dolyniuk, J.-A.; Owens-Baird, B.; Wang, J.; Zaikina, J. V.; Kovnir, K. Clathrate thermoelectrics. *Mater. Sci. Eng.: R: Rep.* **2016**, *108*, 1–46.
- (427) Liu, L.; Li, F.; Wei, Y.; Chen, N.; Bi, S.; Qiu, H.; Cao, G.; Li, Y. Synthesis and thermoelectric properties of rare earth Yb-doped $\text{Ba}_{8-x}\text{Yb}_x\text{Si}_{30}\text{Ga}_{16}$ clathrates. *J. Alloys Compd.* **2014**, *588*, 271–276.
- (428) Tang, X.; Li, P.; Deng, S.; Zhang, Q. High temperature thermoelectric transport properties of double-atom-filled clathrate compounds $\text{Yb}_x\text{Ba}_{8-x}\text{Ga}_{16}\text{Ge}_{30}$. *J. Appl. Phys.* **2008**, *104* (1), 013706.
- (429) Chen, C.; Zhang, L.; Dong, J.; Xu, B. Thermoelectric performance of Yb-doped $\text{Ba}_8\text{Ni}_{0.1}\text{Zn}_{0.54}\text{Ga}_{13.8}\text{Ge}_{31.56}$ type-I clathrate synthesized by high-pressure technique. *J. Electron. Mater.* **2017**, *46*, 2860–2866.
- (430) Tsujii, N. Preparation and thermoelectric properties of Yb-doped Si clathrates. *J. Jpn. Soc. Powder Powder Metall.* **2020**, *67*, 529–535.
- (431) Koga, K.; Anno, H.; Akai, K.; Matsuura, M.; Matsubara, K. First-Principles Study of Electronic Structure and Thermoelectric Properties for Guest Substituted Clathrate Compounds $\text{Ba}_6\text{R}_2\text{Au}_6\text{Ge}_{40}$ (R = Eu or Yb). *Mater. Trans.* **2007**, *48*, 2108–2113.
- (432) Shen, L.; Chen, J.; Li, D.; Liu, W.; Ge, W.; Deng, S. Preparation and thermoelectric properties of Yb doped type-VIII $\text{Ba}_{8-x}\text{Yb}_x\text{Ga}_{16}\text{Sn}_{30}$ clathrate. *Mater. Rep.* **2020**, *34*, 8136–8140.
- (433) Jeitschko, W.; Braun, D. $\text{LaFe}_4\text{P}_{12}$ with filled CoAs_3 -type structure and isotypic lanthanoid-transition metal polyphosphides. *Acta Crystallogr.* **1977**, *B33*, 3401–3406.
- (434) Braun, D. J.; Jeitschko, W. Preparation and structural investigations of antimonides with the $\text{LaFe}_4\text{P}_{12}$ structure. *J. Less-Common Met.* **1980**, *72*, 147–156.
- (435) Braun, D. J.; Jeitschko, W. Ternary arsenides with $\text{LaFe}_4\text{P}_{12}$ -type structure. *J. Solid State Chem.* **1980**, *32*, 357–363.
- (436) Braun, D. J.; Jeitschko, W. Thorium-containing pnictides with the $\text{LaFe}_4\text{P}_{12}$ structure. *J. Less-Common Met.* **1980**, *76*, 33–40.
- (437) Sales, B. C.; Mandrus, D.; Williams, R. K. Filled Skutterudite Antimonides: A New Class of Thermoelectric Materials. *Science* **1996**, *272*, 1325–1328.
- (438) Fleurial, J.-P.; Borshchevsky, A.; Caillat, T. High Figure of Merit in Ce-Filled Skutterudites. In *Proceedings of 15th International Conference on Thermoelectrics*, Pasadena, CA, USA, 1996; pp 91–95.
- (439) Sales, B. C. Filled Skutterudites. In *Handbook on the Physics and Chemistry of Rare Earths*, Gschneidner, K. A.; Bünzli, J. C. G.; Pecharsky, V. K., Eds.; Elsevier, 2003; Vol. 33, pp 1–34.
- (440) Uher, C. Skutterudites: Prospective novel thermoelectrics. In *Semiconductors and Semimetals*, Tritt, T. M., Ed.; Elsevier: Amsterdam, 2001; Vol. 69, pp 139–253.
- (441) Dilley, N. R.; Freeman, E. J.; Bauer, E. D.; Maple, M. B. Intermediate valence in the filled skutterudite compound $\text{YbFe}_4\text{Sb}_{12}$. *Phys. Rev. B* **1998**, *58*, 6287–6290.
- (442) Leithe-Jasper, A.; Kaczorowski, D.; Rogl, P.; Bogner, J.; Reissner, M.; Steiner, W.; Wiesinger, G.; Godart, C. Synthesis, crystal-structure determination and physical properties of $\text{YbFe}_4\text{Sb}_{12}$. *Solid State Commun.* **1999**, *109*, 395–400.
- (443) Dilley, N. R.; Bauer, E. D.; Maple, M. B.; Dordevic, S.; Basov, D. N.; Freibert, F.; Darling, T. W.; Migliori, A.; Chakoumakos, B. C.; Sales, B. C. Thermoelectric and optical properties of the filled skutterudite $\text{YbFe}_4\text{Sb}_{12}$. *Phys. Rev. B* **2000**, *61*, 4608–4614.
- (444) Kuznetsov, V. L.; Rowe, D. M. High temperature electrical transport properties of the $\text{EuFe}_4\text{Sb}_{12}$ and $\text{YbFe}_4\text{Sb}_{12}$ filled skutterudites. *J. Phys.: Condens. Matter* **2000**, *12*, 7915.
- (445) Hiroaki, A.; Jiro, N.; Kakuei, M. Electronic and thermoelectric properties of $\text{Yb}_y\text{Fe}_{4-x}\text{Ni}_x\text{Sb}_{12}$ filled skutterudites. *Proceeding of the 21th International Conference on the Thermoelectrics*, Long Beach, CA, USA, 2002; pp 56–59.
- (446) Bauer, E.; Galatanu, A.; Michor, H.; Hilscher, G.; Rogl, P.; Boulet, P.; Noël, H. Physical properties of skutterudites $\text{Yb}_x\text{M}_4\text{Sb}_{12}$, M = Fe, Co, Rh, Ir. *Eur. Phys. J. B* **2000**, *14*, 483–493.
- (447) Dilley, N. R.; Bauer, E. D.; Maple, M. B.; Sales, B. C. Thermoelectric properties of chemically substituted skutterudites $\text{Yb}_y\text{Co}_4\text{Sn}_x\text{Sb}_{12-x}$. *J. Appl. Phys.* **2000**, *88*, 1948–1951.
- (448) Yang, J.; Morelli, D. T.; Meisner, G. P.; Chen, W.; Dyck, J. S.; Uher, C. Effect of Sn substituting for Sb on the low-temperature transport properties of ytterbium-filled skutterudites. *Phys. Rev. B* **2003**, *67*, 165207.
- (449) Shi, X.; Kong, H.; Li, C. P.; Uher, C.; Yang, J.; Salvador, J. R.; Wang, H.; Chen, L.; Zhang, W. Low thermal conductivity and high thermoelectric figure of merit in n-type $\text{Ba}_x\text{Yb}_y\text{Co}_4\text{Sb}_{12}$ double-filled skutterudites. *Appl. Phys. Lett.* **2008**, *92*, 182101.
- (450) Elsheikh, M. H.; Sabri, M. F. M.; Said, S. M.; Miyazaki, Y.; Masjuki, H. H.; Shnawah, D. A.; Naito, S.; Bashir, M. B. A. Rapid preparation of bulk $\text{Al}_x\text{Yb}_{0.25}\text{Co}_4\text{Sb}_{12}$ ($x = 0, 0.1, 0.2, 0.3$) skutterudite thermoelectric materials with high figure of merit $ZT = 1.36$. *J. Mater. Sci.* **2017**, *52*, 5324–5332.
- (451) Yang, J.; Hao, Q.; Wang, H.; Lan, Y. C.; He, Q. Y.; Minnich, A.; Wang, D. Z.; Harriman, J. A.; Varki, V. M.; Dresselhaus, M. S.; Chen, G.; Ren, Z. F. Solubility study of Yb in n-type skutterudites $\text{Yb}_x\text{Co}_4\text{Sb}_{12}$ and their enhanced thermoelectric properties. *Phys. Rev. B* **2009**, *80*, 115329.
- (452) Hanus, R.; Guo, X.; Tang, Y.; Li, G.; Snyder, G. J.; Zeier, W. G. A chemical understanding of the band convergence in thermoelectric CoSb_3 skutterudites: Influence of electron population, local thermal expansion, and bonding interactions. *Chem. Mater.* **2017**, *29*, 1156–1164.
- (453) Li, W.; Wang, J.; Xie, Y.; Gray, J. L.; Heremans, J. J.; Kang, H. B.; Poudel, B.; Huxtable, S. T.; Priya, S. Enhanced thermoelectric performance of Yb-single-filled skutterudite by ultralow thermal conductivity. *Chem. Mater.* **2019**, *31*, 862–872.
- (454) Ryll, B.; Schmitz, A.; de Boor, J.; Franz, A.; Whitfield, P. S.; Reehuis, M.; Hoser, A.; Müller, E.; Habicht, K.; Fritsch, K. Structure, phase composition, and thermoelectric properties of $\text{Yb}_x\text{Co}_4\text{Sb}_{12}$ and their dependence on synthesis method. *ACS Appl. Energy Mater.* **2018**, *1*, 113–122.
- (455) Qin, D.; Cui, B.; Zhu, J.; Shi, W.; Qin, H.; Guo, F.; Cao, J.; Cai, W.; Sui, J. Enhanced thermoelectric and mechanical performance in n-type Yb-filled skutterudites through aluminum alloying. *ACS Appl. Mater. Interface* **2020**, *12*, 12930–12937.